

## **MEMS Micropropulsion**

### **Design, Modeling and Control of Vaporizing Liquid Microthrusters**

de Athayde Costa e Silva , M.

**DOI**

[10.4233/uuid:57f725e1-b3f3-455c-83ce-9156b2123c88](https://doi.org/10.4233/uuid:57f725e1-b3f3-455c-83ce-9156b2123c88)

**Publication date**

2018

**Document Version**

Final published version

**Citation (APA)**

de Athayde Costa e Silva , M. (2018). *MEMS Micropropulsion: Design, Modeling and Control of Vaporizing Liquid Microthrusters*. [Dissertation (TU Delft), Delft University of Technology].  
<https://doi.org/10.4233/uuid:57f725e1-b3f3-455c-83ce-9156b2123c88>

**Important note**

To cite this publication, please use the final published version (if applicable).  
Please check the document version above.

**Copyright**

Other than for strictly personal use, it is not permitted to download, forward or distribute the text or part of it, without the consent of the author(s) and/or copyright holder(s), unless the work is under an open content license such as Creative Commons.

**Takedown policy**

Please contact us and provide details if you believe this document breaches copyrights.  
We will remove access to the work immediately and investigate your claim.

# **MEMS MICROPROPULSION**

DESIGN, MODELING AND CONTROL OF VAPORIZING LIQUID  
MICROTHRUSTERS



# **MEMS MICROPROPULSION**

**DESIGN, MODELING AND CONTROL OF VAPORIZING LIQUID  
MICROTHRUSTERS**

## **Proefschrift**

ter verkrijging van de graad van doctor  
aan de Technische Universiteit Delft,  
op gezag van de Rector Magnificus prof. dr. ir. T.H.J.J. van der Hagen,  
voorzitter van het College voor Promoties,  
in het openbaar te verdedigen op  
woensdag 12 december 2018 om 12:30 uur

door

**Marsil de ATHAYDE COSTA E SILVA**

Mestre em Ciências  
Instituto Tecnológico de Aeronáutica, Brasil  
geboren te São Gabriel do Oeste, Brazilië.

Dit proefschrift is goedgekeurd door de promotoren.

Samenstelling promotiecommissie bestaat uit:

Rector magnificus  
Prof. dr. E. K. A. Gill  
Dr. A. Cervone

voorzitter  
Technische Universiteit Delft, promotor  
Technische Universiteit Delft, copromotor

*Onafhankelijke leden:*

Prof. dr. L. Sarro  
Dr. H. van Zeijl  
Prof. dr. K. H. Kienitz  
Prof. dr. M. Tajmar  
Dr. G. Saccochia

Technische Universiteit Delft  
Technische Universiteit Delft  
Instituto Tecnológico de Aeronáutica, Brazilië  
Technische Universität Dresden  
ESA-ESTEC



*Keywords:* Vaporizing Liquid Microthruster, Micro Electro-Mechanical Systems, spacecraft, control

*Printed by:* IPSKAMP Printing

*Front & Back:* M.A.C. Silva

Copyright © 2018 by M.A.C. Silva

ISBN 978-94-028-1311-1

An electronic version of this dissertation is available at

<http://repository.tudelft.nl/>.

*As pessoas boas devem amar seus inimigos.  
Good people must love their enemies.*

Seu Madruga



# CONTENTS

<b>Summary</b>	<b>xi</b>
<b>Samenvatting</b>	<b>xiii</b>
<b>1 Introduction</b>	<b>1</b>
1.1 Motivation . . . . .	2
1.1.1 Objective. . . . .	3
1.2 Micropropulsion Overview . . . . .	5
1.2.1 Conventionally manufactured micropropulsion systems . . . . .	5
1.3 Thesis Outline . . . . .	7
<b>2 Review of MEMS micropropulsion</b>	<b>9</b>
2.1 Introduction . . . . .	10
2.1.1 Theoretical background . . . . .	10
2.2 MEMS micropropulsion . . . . .	12
2.2.1 Resistojets . . . . .	12
2.2.2 Cold-gas microthrusters – CG . . . . .	15
2.2.3 Solid propellant – SP . . . . .	16
2.2.4 Liquid propellant – LP . . . . .	16
2.2.5 Electro spray thrusters – ES . . . . .	18
2.3 Analysis and discussion . . . . .	18
2.3.1 Future developments . . . . .	23
2.4 Concluding remarks . . . . .	25
<b>3 Design of Vaporizing Liquid Microthrusters</b>	<b>27</b>
3.1 Introduction . . . . .	28
3.2 Design description . . . . .	29
3.2.1 Requirements . . . . .	29
3.2.2 Design . . . . .	29
3.2.3 Propellant selection . . . . .	31
3.2.4 Performance parameters. . . . .	32
3.3 Manufacturing . . . . .	32
3.4 Experiment Description. . . . .	33
3.4.1 Mechanical characterization. . . . .	36
3.4.2 Electrical characterization . . . . .	37
3.4.3 Operational characterization. . . . .	37
3.5 Results and discussion . . . . .	40
3.5.1 Mechanical characterization. . . . .	40
3.5.2 Electrical characterization . . . . .	41
3.5.3 Operational characterization. . . . .	42

3.6	Concluding remarks . . . . .	46
<b>4</b>	<b>Modeling of Vaporizing Liquid Microthrusters</b>	<b>47</b>
4.1	Introduction . . . . .	48
4.2	Modeling Approach . . . . .	48
4.2.1	Boundaries and Requirements . . . . .	49
4.2.2	Vaporizing Liquid Microthruster . . . . .	50
4.2.3	Valve . . . . .	54
4.2.4	Tank . . . . .	56
4.3	Model Analysis . . . . .	56
4.3.1	Sensitivity Analysis: Thruster . . . . .	57
4.3.2	Sensitivity Analysis: Valve . . . . .	58
4.4	Model Validation . . . . .	58
4.5	Simulation Setup . . . . .	60
4.5.1	Spacecraft Parameters . . . . .	60
4.5.2	Controller Design . . . . .	60
4.6	Simulation Results . . . . .	61
4.7	Concluding remarks . . . . .	63
<b>5</b>	<b>Control of Vaporizing Liquid Microthrusters</b>	<b>65</b>
5.1	Introduction . . . . .	66
5.2	Sample mission description . . . . .	67
5.2.1	Control allocation . . . . .	69
5.3	Proposed approach . . . . .	69
5.4	Simulation settings and analysis . . . . .	71
5.4.1	Controller design . . . . .	72
5.4.2	Simulation cases . . . . .	74
5.4.3	Case 1: 4 thrusters with ideal shooting . . . . .	75
5.4.4	Case 2: 4 thrusters with experimental data . . . . .	76
5.4.5	Case 3: 6 thrusters with experimental data and failure . . . . .	78
5.4.6	Monte Carlo analysis . . . . .	79
5.5	Conclusions . . . . .	81
<b>6</b>	<b>Applications and Scenarios of VLM systems</b>	<b>83</b>
6.1	Introduction . . . . .	84
6.2	Spacecraft and micropropulsion requirements . . . . .	84
6.3	VLM Applications . . . . .	86
6.4	Concluding remarks . . . . .	88
<b>7</b>	<b>Conclusions</b>	<b>89</b>
7.1	Summary . . . . .	90
7.2	Research findings . . . . .	91
7.3	Innovations . . . . .	94
7.4	Future research . . . . .	95

---

<b>References</b>	<b>97</b>
<b>Acknowledgements</b>	<b>107</b>
<b>A Thrust direction control using MEMS actuators</b>	<b>109</b>
A.1 Description . . . . .	109
<b>List of Publications</b>	<b>111</b>



# SUMMARY

In recent years, there has been an increase in the number of small multi-mission platforms such as CubeSats, in an attempt to reduce costs of space missions. CubeSats have been used for different purposes including Earth observation, research and technology demonstration.

However, a key technology that is still under development is the micropropulsion system that has the potential to significantly increase the capabilities of CubeSat missions. Micropropulsion has been recognized as one of the key development areas for the next generation of highly miniaturized spacecraft such as CubeSats and PocketQubes. It will extend the range of applications of this class of satellites to include missions that require, for example, orbital maneuvering or drag compensation.

An interesting option for CubeSats and PocketQubes is the Vaporizing Liquid Microthruster (VLM) which has received increasing attention due to its ability to provide high thrust levels with relatively low power consumption. The thruster uses the vapor generated in the vaporization of the propellant to produce thrust using a nozzle. The vaporization is usually done by applying power to resistive heaters that could be integrated into the device or externally attached to it. The nozzle is usually a convergent-divergent nozzle that can accelerate the propellant to supersonic velocities.

This thesis aims to develop modeling and control concepts for micropropulsion systems to allow the spacecraft to perform maneuvers of position and attitude control. The Vaporizing Liquid Microthruster has been selected due to its characteristics that suit the needs of very small spacecraft.

The first part of the research is dedicated to an in-depth literature study of the currently available micropropulsion systems. Those that are manufactured with silicon and MEMS (Micro Electro-Mechanical Systems) technologies have been analyzed and compared in terms of their thrust, specific impulse, and power. A classification in terms of complexity is introduced in an attempt to identify the suitability of the devices for the current trend towards simplifying architectures. The analysis of development levels of different types of micropropulsion systems revealed that although the actual thrusters are significantly developed, the interfacing and integration to other components of the system are still to be further developed.

The second part of the research focuses on the characterization and modeling of VLM systems. This is an extremely important step in the development of such systems since a proper model, i.e., one that sufficiently represents the dynamics of the system, is required during the design phase to help, for example, in designing controllers, and also during the operational phase to help reproducing the events happening when the satellite is in orbit. A comprehensive model has been developed using theoretical and empirical relations.

The third part of the research addresses the problem of controlling multiple redundant devices allowing failures to occur. This is very important to guarantee the success-

ful operation of VLM systems with many thrusters while performing combined attitude-position maneuvers. A fuzzy control system was developed introducing an automatic rule generation algorithm that allows the fuzzy controller to solve control allocation problems.

Finally, the last part of the research investigates the possible applications of VLM systems. An example scenario is considered to analyze the performance required to execute different maneuvers and missions.

The key contributions of the work presented in this thesis are related to the modeling and control of Vaporizing Liquid Microthrusters. A comprehensive model of the complete system has been proposed and used to develop control algorithms for individual thrusters and for a set of thrusters. A fuzzy control system has been developed to solve the problem of controlling multiple devices with redundant outputs. Finally, an in-depth literature study and an analysis on the possible applications allowed to put VLM systems into perspective offering a glimpse into the future development of such systems.

# SAMENVATTING

De laatste jaren is het aantal kleine multi-missieplatforms zoals CubeSats toegenomen in een poging de kosten van ruimte missies te reduceren. CubeSats worden voor verschillende doeleinden gebruikt inclusief aardobservatie, onderzoek, en technologie-demonstratie.

Toch is er een belangrijke technologie die nog in ontwikkeling is: het microvoortstuwingsysteem dat de potentie heeft om de prestatiemogelijkheden van CubeSat missies sterk te verhogen. Microvoortstuwings is erkend als een van de belangrijkste ontwikkelingsgebieden voor de volgende generatie sterk geminiaturiseerde ruimtevaartuigen zoals CubeSats en PocketQubes. Microvoortstuwings gaat het toepassingsgebied van deze klasse van satellieten uitbreiden voor missies waarbij bijvoorbeeld baanmanoeuvres of weerstandscompensatie benodigd zijn.

Een interessant alternatief voor CubeSats en PocketQubes is de Vaporizing Liquid Microthruster (VLM), die meer aandacht heeft gekregen dankzij de hoge stuwkracht die opgewekt wordt met relatief laag elektrisch vermogen. De raketmotor gebruikt waterdamp, geproduceerd bij het verdampen van de brandstof, om stuwkracht via een straalbuis te genereren. De verdamping wordt meestal veroorzaakt door elektrische stroom door een weerstandsverwarming te leiden die of geïntegreerd in het apparaat of extern bevestigd kan worden. De straalbuis is meestal een convergente-divergente straalpijp die de brandstof tot supersonische snelheden kan versnellen.

In dit proefschrift worden concepten voor het regelen en modelleren van microvoortstuwingsystemen onderzocht om de positie en oriëntatie van het ruimtevaartuig te regelen. De Vaporizing Liquid Microthruster is gekozen door zijn eigenschappen die passen bij de behoeften van zeer kleine ruimtevaartuigen.

Het eerste deel van het onderzoek is toegewijd aan een grondig literatuuronderzoek over de verkrijgbare microvoortstuwingsystemen. Systemen vervaardigd met silicium en MEMS (Micro Electro-Mechanical Systems) technologie zijn geanalyseerd en hun stuwkracht, specifieke stoot, en vermogen zijn vergeleken. Een classificatie in termen van complexiteit is ingevoerd in een poging om de geschiktheid van de apparaten voor de huidige trend naar meer eenvoudige systemen te identificeren. De analyse van het ontwikkelingsniveau van microvoortstuwingsystemen maakte het duidelijk dat, terwijl de raketmotoren inmiddels goed doorontwikkeld zijn, de interfaces met andere onderdelen van het systeem meer ontwikkeling vereisen.

Het tweede deel van het onderzoek is gericht op het karakteriseren en modelleren van VLM-systemen. Dit is een heel belangrijke stap in de ontwikkeling van deze systemen omdat een goed model, namelijk een die voldoende is om de dynamica van het systeem toereikend te modelleren, nodig is om bijvoorbeeld regelaars te ontwerpen, maar ook gedurende de operationele fase om het gedrag van de satelliet te reproduceren. Een uitgebreid model is ontwikkeld op basis van theoretische en empirische relaties.

Het derde deel van het onderzoek gaat in op het probleem meervoudige redundante apparaten te besturen rekening houdend met defecten. Dit is zeer belangrijk om een succesvolle werking van VLM-systemen met meervoudig raketmotoren te garanderen bij gecombineerde positie en houding manoeuvres. Een fuzzy regelaar is ontwikkeld waarbij een algoritme voor geautomatiseerde regelgeneratie geïntroduceerd is. Dit algoritme staat de controller toe om het probleem van control allocation op te lossen.

Tot slot dekt het laatste deel van het onderzoek de mogelijk toepassingen van VLM-systemen. Een voorbeeldscenario is gebruikt om de prestatie van de systemen in verschillende manoeuvres en missies te beoordelen.

De belangrijkste bijdragen van dit werk zijn gerelateerd aan het modelleren en de regeltechniek van Vaporizing Liquid Microthrusters. Een uitgebreid model van het complete systeem is geïntroduceerd en gebruikt om regeltechnische algoritmen voor een enkele of een verzameling van raketmotoren te ontwikkelen. Een fuzzy regelaar is ontwikkeld om het probleem van het regelen van meervoudige redundante apparaten op te lossen. Tot slot werden VLM-systemen in perspectief gezet door een grondig literatuuronderzoek en een analyse van de mogelijke toepassingen, en een blik op de toekomstige ontwikkeling van deze systemen is gegeven.

# 1

## INTRODUCTION

*There is a freedom that everyone deserves.*

From the song *The lost boy* by Greg Holden

*The use of propulsion systems in nano- and pico-satellites has gained increasing attention due to its potential to improve the performance related to mission lifetime and mission capabilities. Size, mass, and power are important constraints that set a great challenge for developing micropropulsion systems for these classes of spacecraft. Such a system will significantly improve the functionality of the satellite by allowing the execution of attitude and position maneuvers creating the possibility to perform applications such as station keeping, orbit transfers or even enabling deep space missions. This chapter introduces the research context in which the work of this thesis was developed. The motivation and goals for studying and researching control aspects of micropropulsion systems are presented as well as a brief literature review and theoretical background.*

### 1.1. MOTIVATION

THE space sector is currently following a trend towards miniaturization to reduce costs and the development time of space missions. The mass is usually used to classify artificial satellites. In this work the definitions below are used to categorize very small satellites:

Table 1.1: Small satellites categories.

Category	Range of mass
Nanosatellite	1–10 kg
Picosatellite	0.1–1 kg

The concept of miniaturization also involves standardization and use of commercial off-the-shelf components. Such features are extensively used in the development of a class of small satellites called CubeSats. These spacecraft are composed of one or more cubic units (abbreviated as 1U, 2U, etc.) with volume equal to  $10 \times 10 \times 10 \text{ cm}^3$  and a mass of less than 1.33 kg. A similar concept that has recently been developed is the PocketQube which also embraces the miniaturization idea however in an even smaller form factor of  $5 \times 5 \times 5 \text{ cm}^3$  in volume and 180 g in mass per unit. A CubeSat unit typically produces about 2 W of power in low Earth orbits (Silva et al., 2018) whereas a PocketQube, which has an area four times smaller than that of a CubeSat, can produce around 0.5 W on average.

An important feature to improve the capabilities of these categories of satellite is the propulsion system which will increase the range of applications where they can be used enabling new kinds of missions to be executed. For this small scale, the thrust levels are desired to be in the range of micro- to milli-Newton (Silva et al., 2018). Such systems are called micropropulsion systems and they are designed to generate thrust in the mentioned range and also to fit within the constraints of nano- and picosatellites in terms of size, mass, and power consumption.

A micropropulsion system may significantly increase the capabilities of a micro- or nanosatellite. It gives the satellite the ability to perform attitude maneuvers for applications such as reaction wheel desaturation, attitude control, or compensation of small perturbations. Also, the propulsion system might provide the ability to change the orbit in which the satellite was inserted. This can be used in a wide range of applications that need station keeping or orbit transfers such as removal of space debris and formation flying.

In order to be able to fully perform the described functionalities and applications, a required feature of micropropulsion systems still needs to be developed is the thrust control which is important to allow the satellite to perform precise orbital and attitude maneuvers where precisely regulated forces and torques are necessary. Thrust control encompasses the ability of controlling the magnitude and the direction of the thrust vector. These two features are required to be very precise in order to effectively allow the execution of the mentioned applications. The magnitude control is different for each type of thruster depending on the type of the thruster and its propellant, however, it is always related to the propellant mass flow and exit velocity. The direction control can

be achieved in several ways, and for spacecraft it is usually realized by using an array of thrusters or a gimbal assembly in which the thruster is fixed. Also, such system is expected to keep its whole functionality until the end of the mission which can be affected by improper use of propellant or even improper design.

### 1.1.1. OBJECTIVE

The objective of this thesis is to investigate concepts of thrust control in a way to improve the performance of micropropulsion systems that use green propellants. The use of green propellants has received increasing attention over the last few decades in an effort to reduce the use of toxic materials that are hazardous to the environment and requires increased efforts in handling (Gohardani et al., 2014). The choice of green propellants is also crucial to the development of miniaturized spacecraft because it helps in reducing costs related to handling these dangerous substances.

This thesis aims to develop modeling and control concepts for micropropulsion systems in order to allow the spacecraft to perform maneuvers of position and attitude control. The major focus is given to the thrust control problem, i.e. controlling the magnitude and direction of the thrust-vector, considering the constraints imposed by the size of the satellites. The magnitude control is concentrated in the control of the propellant flow. In contrast, the direction control is focused on the control allocation of a set of thrusters and also on the control by means of altering the shape of the nozzle.

The Vaporizing Liquid Microthruster (VLM) has been selected for developing the concepts presented here. The VLM is very interesting for very small spacecraft due to its ability to provide high thrust levels with relatively low power consumption. The thruster uses the gases generated in the vaporization to produce thrust using a nozzle. The vaporization is usually done by applying power to resistive heaters that could be integrated into the device or externally attached to it.

### METHODOLOGIES

In order to achieve the proposed objective, the work described in this thesis was structured in such a way to address different parts of a conceptual VLM system (Fig. 1.1). Water is used as the propellant and this choice will be further discussed in Chapter 3.

The magnitude control can be achieved by changing the main parameters of the propellant flow that relate to the thrust: pressure, temperature, and mass flow rate. These parameters are related to the valve and the resistive heaters. The direction control can be achieved by actively changing the flow direction at the nozzle exit or by controlling a set of thrusters.

These points have been investigated with an approach combining theoretical and practical development in order to create a solid basis for the development of models and control algorithms. This method is important as it supports with facts the assumption making process and the creation of novel theories. Most importantly, the experiments help to better understand the dynamics of the system. The experiments were performed with VLM chips which have been manufactured in the Else Kooi Laboratory (EKL) of Delft University of Technology (TU Delft). The chips are made out of silicon wafers that are processed in one of the cleanrooms (class 100) of EKL.

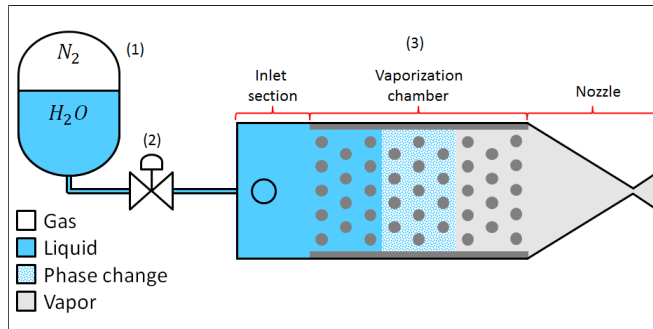


Figure 1.1: Concept of the microresistojet considered in this work. It contains a tank (1), a solenoid valve (2), and a thruster (3).

The work of this thesis can be divided into four strongly connected parts. The first part is an extensive analysis of the state-of-the-art literature regarding MEMS (Micro Electro-Mechanical Systems) microthrusters that is aimed at positioning the chosen system, i.e. VLM, with respect to other technologies. The second part regards the design, manufacturing, and experimental characterization of VLM chips. The third part is focused on the development of a complete model of the VLM system. The last part is dedicated to the development of control systems for the fine regulation of the thrust levels as well as the allocation of actuation efforts in a multi-thruster configuration.

The experimental data are combined with fundamental theory to arrive at a hybrid model of the complete system which allows the simulation of the system dynamics and its use in the design of controllers to precisely operate the thrusters or in the modeling of the complete spacecraft for a multitude of purposes. The models and controllers developed are tested in simulation scenarios to assess the performance of the system in missions with very small satellites.

This thesis is structured around the following research questions that were proposed in order to achieve the main objective. **What are the aspects that bound the state-of-the-art MEMS micropropulsion systems?** This question aims at defining the current development status and comparing the different types of micropropulsion systems. It is focused on MEMS devices which are the most promising in terms of miniaturization and applicability to very small spacecraft. More than just defining the current status, this question also focuses on the future developments regarding features or technologies that are still missing and could advance the development of miniaturized space missions.

In order to approach the problem of controlling the thrust magnitude of a microthruster, another question was formulated: **What is the best way of controlling the mass flow of a microthruster?** This question treats the challenges of controlling a liquid flow in a micro-scale environment where friction forces play a major role in the dynamics of the system. It aims at developing mathematical models that represent the behavior and are used in the design of controllers to regulate the mass flow rate. This question has been developed using the hybrid approach combining experimental data and theoretical models.

A third research question has been formulated to address the specific characteristics

of a VLM system: **How can we describe the dynamic behavior of a Vaporizing Liquid Microthruster?** This question is intended to guide the development of a mathematical model that can reproduce the dynamics of a VLM system. The experiments with the prototype devices are crucial to the success of this modeling due to the stochastic nature of the main process taking place in a VLM which is the vaporization. This question focuses as well on the analytical modeling of the thruster where it is possible to derive such a model. It is also intended to lead to recommendations to future designs including those for real missions.

The last question approaches the problem of controlling the direction of the thrust: **What are characteristics of controlling the thrust direction of microthrusters?** It covers the aspects related to actively changing the direction of the flow exiting the thruster and also the control allocation problem in systems with more than one thruster.

As the focus of this thesis is on MEMS micropropulsion, the next section is dedicated to a short overview of other systems that are suitable of very small spacecraft.

## 1.2. MICROPROPULSION OVERVIEW

Micropropulsion is defined here and throughout this thesis as any system that generates thrust in the range from micro- to milli-Newton and satisfies the constraints related to nano- and picosatellites in terms of size, mass, and power. Fig. 1.2 presents the classification used in this thesis to differentiate the types of micropropulsion systems. These systems are all suitable for at least nanosatellites in all aspects (mass, size, and power consumption). A secondary classification separates the systems that can be manufactured (in their totality or the most important component) using MEMS and silicon technologies from the ones that are made using conventional methods. In principle, all the systems might be manufactured with conventional methods however some systems gain a lot of advantages by using MEMS while others, e.g. solar sail, have little to gain from the use of such advanced technologies.

As mentioned before, this thesis focuses on MEMS thrusters as these are the most promising in terms of miniaturization and applicability to nano- and picosatellites. The following sub-sections discuss the conventionally manufactured systems that are suitable for very small spacecraft. A complete review of MEMS thrusters is presented in the next chapter.

### 1.2.1. CONVENTIONALLY MANUFACTURED MICROPROPULSION SYSTEMS PULSED PLASMA THRUSTERS

This type of thruster contains two electrodes that generate a spark close to the propellant that is heated creating a plasma. This plasma is accelerated by the Lorentz force and expelled with high velocity creating thrust. Due to the generation of a spark, it cannot be operated continuously, thus the name pulsed.

PPT is highly suitable for CubeSat missions due to its simplicity in manufacture and good reliability. It has been tested and successfully operated in space since 1964 and recently has been developed for CubeSat missions (Ciaralli et al., 2016, 2015; Coletti et al., 2015, 2011) and for micro-satellite missions (Kisaki et al., 2013; Tanaka et al., 2012).

The most common devices use solid propellant (Teflon) that is pushed towards the

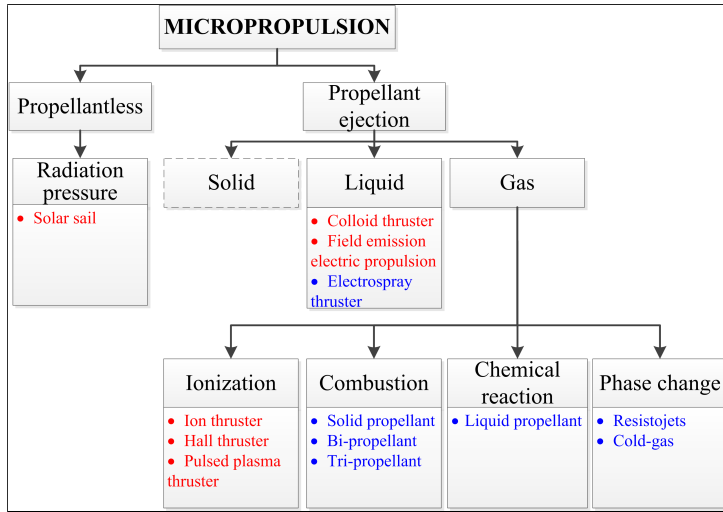


Figure 1.2: Classification of micropropulsion concepts. The concepts highlighted in red are manufactured with conventional methods whereas the ones in blue are made using MEMS and silicon technologies.

ignition place by a set of springs. In this case, the devices suffer from the lack of control in the amount of propellant used in each shot which might cause differences in the levels of thrust during its operational life. The use of liquid propellant, as in [Szelecka et al. \(2015\)](#), might reduce this issue but, on the other hand, bring other issues as the intrinsic complexity of flow control and propellant storage schemes.

### FIELD EMISSION ELECTRIC PROPULSION

Devices that operate by ejecting liquid propellant have to use high-density substances in order to maximize the efficiency of the thruster. The most common types are the Field Emission Electric Propulsion (FEEP) and the colloid thruster which uses liquid metal as the propellant that is ionized and ejected in very small droplets accelerated by an electric field ([Mitterauer, 2004](#); [Rudenauer, 2007](#); [Tajmar et al., 2004](#)).

This type of propulsion has already been used in space missions and is able to provide thrust in the range suitable for CubeSat missions. Thus, miniaturization is the key point to develop in order to use it as the main propulsion system for CubeSats.

### ION THRUSTERS

This type of device produces thrust by ejecting ions at very high velocities. Generally, they produce small thrust levels but with high specific impulse. There are mainly two different types: Hall thruster and ion-thruster. The first uses the Hall effect to trap electrons in a ring and then ionize the propellant which is accelerated due to an electric field and exhausted producing thrust. The second uses two charged grids to accelerate the ionized propellant ([Leiter et al., 2009](#); [Polzin et al., 2007](#); [Smirnov et al., 2002](#)).

### 1.3. THESIS OUTLINE

This thesis is split into seven Chapters (including introduction) that approach different parts of the work. Following the introduction in Chapter 1, the second Chapter is dedicated to a deep review of micropropulsion systems that are manufactured using MEMS and silicon technologies. The review embraces aspects of the development and the theory related to different types of MEMS micropropulsion systems. It also compares the different categories using data collected from the literature and analyzes the complexity of each system which is very important when it comes to miniaturization. The third chapter presents the design details of the micropropulsion system used in this work and also the results of an extensive experimental campaign that was carried out in order to characterize the devices. The fourth chapter shows the modeling of Vaporizing Liquid Microthrusters. The developed model combines theoretical with empirical relations derived from the characterization of the thrusters. The fifth chapter presents an approach to solve the control allocation problem for thrusters on board of a spacecraft. The control allocation approach is applied to an example mission of active space debris removal. The sixth chapter presents an analysis on the possible applications of Vaporizing Liquid Microthruster systems. The seventh chapter ends this thesis presenting the conclusions and the outlook on future development of micropropulsion systems.



# 2

## REVIEW OF MEMS MICROPROPULSION

*People hate what they don't understand – Martha Kent*

*From the movie *Batman v Superman: Dawn of Justice**

*CubeSats have been extensively used in the past two decades as scientific tools, technology demonstrators and for education. Recently, PocketQubes have emerged as an interesting and even smaller alternative to CubeSats. However, both satellite types often lack some key capabilities, such as micropropulsion, in order to further extend the range of applications of these small satellites. This chapter reviews the current development status of micropropulsion systems fabricated with MEMS (micro electro-mechanical systems) and silicon technology intended to be used in CubeSat or PocketQube missions and compares different technologies with respect to performance parameters such as thrust, specific impulse, and power as well as in terms of operational complexity. More than 30 different devices are analyzed and divided into seven main categories according to the working principle. A specific outcome of the research is the identification of the current status of MEMS technologies for micropropulsion including key opportunities and challenges.*

---

Parts of this chapter have been published in:

Silva, M. A. C., Guerrieri, D. C., Cervone, A., Gill, E., *A review of MEMS micropropulsion technologies for CubeSats and PocketQubes*, Acta Astronautica 143 (February 2018), 234-243, 2017.

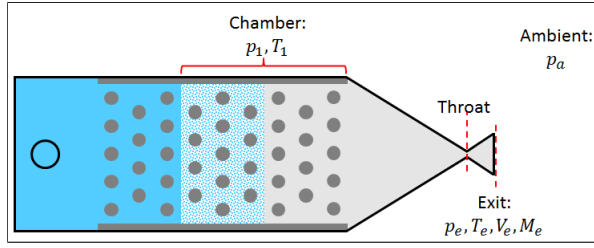


Figure 2.1: Diagram of a VLM showing the variables and their indexes.

## 2.1. INTRODUCTION

This chapter is dedicated to an extensive review of MEMS micropropulsion systems that are suitable for nano- and picosatellites. As mentioned in the previous chapter, the use of MEMS represents a promising way to develop highly miniaturized spacecraft as it fabrication of very small features and integration of electronics. The next section presents the theoretical background, used throughout this thesis, regarding the equations related to propulsion and to spacecraft dynamics.

### 2.1.1. THEORETICAL BACKGROUND PROPULSION

The performance of micropropulsion systems can generally be analyzed using ideal rocket conditions. However, it is important to note that those conditions are based on a set of assumptions that might not be applicable to micropropulsion systems as, for example, the assumption of negligible friction forces (Sutton and Biblarz, 2010). A deeper analysis on this point will be done in chapter 4. Thus, the following set of equations (the indexes correspond to those shown in Fig. 2.1) are used only to give insights into the ideal performance of such micropropulsion systems. In this case, two parameters are of major interest when analyzing the performance of the thruster: specific impulse and thrust. The thrust ( $F$  in equation 2.1) is the force generated by the gas accelerated and expelled through the nozzle.

$$F = \dot{m}V_e + (p_e - p_a)A_e \quad (2.1)$$

where  $\dot{m}$  is the mass flow rate,  $V_e$  is the exhaust velocity,  $p_e$  and  $p_a$  the exit and ambient pressures, and  $A_e$  is the exit area. The exhaust velocity can be calculated by 2.2 where  $M_e$  is the Mach number at the exit,  $\gamma$  is the ratio of the specific heat at constant pressure and constant volume,  $T_e$  is the exit temperature, and  $R_s$  is the specific gas constant

$$V_e = M_e \sqrt{\gamma R_s T_e}. \quad (2.2)$$

The mass flow rate can be written as a function of the chamber (stagnation) pressure and temperature ( $p_1$  and  $T_1$ ) and the area of the throat  $A_t$ :

$$\dot{m} = \frac{A_t p_1}{\sqrt{T_1}} \sqrt{\frac{\gamma}{R_s} \left( \frac{2}{\gamma + 1} \right)^{\frac{\gamma+1}{\gamma-1}}}. \quad (2.3)$$

Equations 2.4 to 2.6 are used to calculate the Mach number, temperature, and pressure at the exit as follows

$$\frac{A_e}{A_t} = \left( \frac{\gamma + 1}{2} \right)^{-\frac{\gamma+1}{2(\gamma-1)}} M_e^{-1} \left( 1 + \frac{\gamma-1}{2} M_e^2 \right)^{\frac{\gamma+1}{2(\gamma-1)}} \quad (2.4)$$

$$T_e = T_1 \left( 1 + \frac{(\gamma-1)}{2} M_e^2 \right)^{-1} \quad (2.5)$$

$$p_e = p_1 \left( 1 + \frac{(\gamma-1)}{2} M_e^2 \right)^{\frac{-\gamma}{\gamma-1}}. \quad (2.6)$$

The specific impulse  $I_{sp}$  is a measure of efficiency regarding the propellant consumption:

$$I_{sp} = \frac{\int_0^t F dt}{g \int_0^t \dot{m} dt} \quad (2.7)$$

where  $g = 9.80665 \text{ m/s}^2$  is the gravitational acceleration on Earth at sea level. Although the unit is given in seconds, it does not represent a measure of time but a measure of thrust per unit weight of propellant and it should be as high as possible for best propellant consumption efficiency.

Equations 2.1-2.7 are used to estimate the performance of the thrusters given the conditions of the experiments and the mechanical characterization of the devices.

### SPACECRAFT DYNAMICS

The spacecraft is modeled as a rigid body with constant mass, i.e. the mass of propellant ejected is considered negligible compared to the mass of the body. Then the angular and linear accelerations, with respect to the body reference frame located at the geometric center of the spacecraft, can be calculated based on the conservation of momentum. The angular acceleration is calculated by:

$$\dot{\boldsymbol{\omega}} = \mathbf{I}^{-1} [ -(\boldsymbol{\omega} \times \mathbf{I}\boldsymbol{\omega}) + \mathbf{T}_{ext} ] \quad (2.8)$$

where  $\boldsymbol{\omega}$  is the rotation rate of the body,  $\mathbf{I}$  is the inertia matrix, and  $\mathbf{T}_{ext}$  is any external torque. The linear acceleration is calculated as follows:

$$\dot{\mathbf{V}} = \frac{1}{m} \mathbf{U}_{ext} - \boldsymbol{\omega} \times \mathbf{V} \quad (2.9)$$

where  $\mathbf{V}$  is the linear velocity,  $m$  is the mass, and  $\mathbf{U}_{ext}$  is any external force.

In this thesis, the external torque and external force are composed by any disturbance (indicated with index  $d$ ) and the thrust generated by the thrusters

$$\mathbf{T}_{ext} = \mathbf{T} + \mathbf{T}_d \quad (2.10)$$

$$\mathbf{U}_{ext} = \mathbf{U} + \mathbf{U}_d. \quad (2.11)$$

Finally, the attitude of the spacecraft with respect to any arbitrary reference frame can be represented using quaternions. Using the angular velocity defined in (2.8) we can calculate the change in the attitude represented in quaternions  $\mathbf{q}$  (Wie and Barba, 1985):

$$\dot{\mathbf{q}} = \begin{bmatrix} 0 & -\omega_x & -\omega_y & -\omega_z \\ \omega_x & 0 & \omega_z & -\omega_y \\ \omega_y & -\omega_z & 0 & \omega_x \\ \omega_z & \omega_y & -\omega_x & 0 \end{bmatrix} \mathbf{q} \quad (2.12)$$

where  $\omega_x$ ,  $\omega_y$ , and  $\omega_z$  are the components of the vector  $\boldsymbol{\omega}$ . By knowing the initial attitude of the spacecraft one can integrate (2.12) in order to have the time evolution of the attitude.

## 2.2. MEMS MICROPROPULSION

This category consists of systems that use MEMS and silicon technologies in the production of the thruster component of the system. Other systems might have other MEMS components (e.g. sensors) which do not qualify the entire system as MEMS micropropulsion. The systems that do fall into this category and will be analysed in the following sections are: resistojets, cold-gas thrusters, solid propellant thrusters, liquid propellant thrusters, and electrospray thrusters.

The term MEMS refer to systems that have feature sizes in terms of micro-meters and integrates mechanical and electrical parts into a single device. In the case of micropropulsion, features such as fluidic channels and structural components are in the mechanical side whereas components such as resistive heaters, sensors, etc. are in the electrical side. However, the boundaries between mechanical and electrical components in MEMS are often hard to set due to the nature of the processes taking place in the device.

The manufacturing processes used in MEMS are often derived from those used in the production of silicon microelectronics. The fabrication of such devices often involves a series of repeated steps, starting from a silicon wafer, of the following processes:

- Deposition: used to deposit thin layers of materials on the surface of the wafer.
- Patterning: used to transfer a pattern to the surface in order to protect some parts while exposing other to form the features of the device.
- Etching: used to remove material from the exposed areas either isotropically or anisotropically.

These three basic processes are used to create a multitude of devices that have applications in many different areas. A specific example will be shown later in Chapter 3 describing the manufacturing of the microthrusters.

### 2.2.1. RESISTOJETS

The working principle of this type of micropropulsion is based on heating the gaseous propellant with a resistance and then accelerating and expelling it to space. Some devices use propellants stored in liquid or solid phase, therefore phase-change accompanies the heating of the gas. The phase-change is done by heating a resistance in contact

with a part or all the propellant that is kept in certain conditions of pressure and temperature to allow the specific process (sublimation or vaporization) to occur.

Considering the type of phase-change within the devices we can identify two main types of micro-resistojets which also differ regarding the governing flow regime: Vaporizing Liquid Microthruster (VLM) and Low-Pressure Microresistojet (LPM also known as Free Molecule Micro-Resistojet). The VLM accelerates the vaporized gas by means of adiabatic expansion in a convergent-divergent nozzle. In this case the flow can be modeled in the continuum flow range (Knudsen number  $Kn \leq 0.1$ ) although [Ivanov et al. \(1999\)](#) suggest that a statistical method such as DSMC (Direct Simulation Monte-Carlo) is better than the usual approach using Navier-Stokes equations for the flow in the nozzle exit because the Knudsen number in that region is high. Thus, for simulations, a combination of methods is apparently the most suitable approach to help and guide the design. The LPM works in a very low range of pressure and high Knudsen number ( $0.1 < Kn \leq 10$ ) in which the flow has to be modeled in the transitional flow regime. Usually, these devices use nitrogen as the propellant to evaluate the performance of the nozzle and water to prove the concept in terms of vaporization or even as the actual propellant ([Lee et al., 2008](#)).

#### VAPORIZING LIQUID MICROTHRUSTER – VLM

This is one of the most frequently found microresistojet concepts generally manufactured using MEMS technologies in silicon or ceramic wafers. It consists of an inlet channel through which the propellant is fed, a chamber where the propellant is vaporized by a heating element, and a convergent-divergent nozzle to accelerate the gases to supersonic velocities. Most of the work concerning this device has been focused on the numerical analysis of flow in micro-nozzles and in the design of the chamber that contains the heating element ([Cheah and Chin, 2011](#); [Haris and Ramesh, 2014](#)). However, the boiling process in the chamber is a complex and important factor to be analyzed in order to optimize the design of the chamber thus improving performance ([Cen and Xu, 2010](#); [Chen et al., 2012, 2010](#)).

The geometry and material of the heating element are one of the key features towards performance improvement since this is where most of the energy is converted and is usually a low-efficiency process ([Cheah and Chin, 2011](#); [Haris and Ramesh, 2014](#); [Kundu et al., 2014](#); [Mukerjee et al., 2000](#)). Most of the devices are tested with water due to its safety of handling and ease of acquiring but it can also be used as the actual propellant as it can be stored as a liquid with the conditions of temperature and pressure considered for CubeSats and PocketQubes ([Guerrieri et al., 2017](#)). The main drawback of water as a propellant is its high heat of vaporization that represents high power consumption to operate the thruster, however water has the best  $\Delta v$  (velocity change) per volume of propellant and specific impulse when compared to other substances that are suitable for CubeSats and PocketQubes ([Guerrieri et al., 2017](#)).

There are two different designs that arise from differences in the manufacturing process chosen (Fig. 2.2). The etching process can be tuned together with the type of wafer to create cavities with walls inclined around  $54.7^\circ$  which are used to create the nozzle perpendicular (out-of-plane) to the plane of the wafer ([Mukerjee et al., 2000](#); [Maurya et al., 2005b,a](#); [Ye et al., 2001](#)). This might simplify the manufacturing but it reduces the

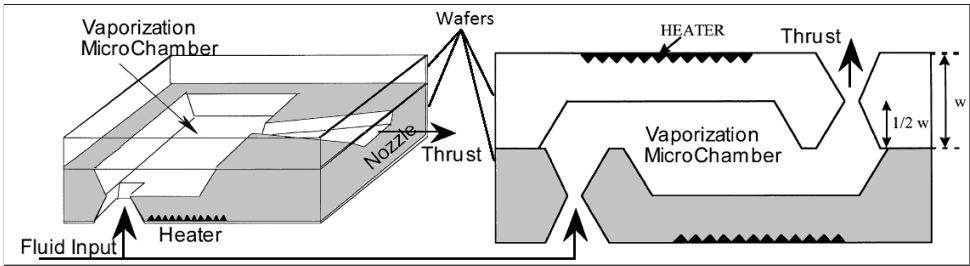


Figure 2.2: Comparison between two different designs (figure adapted from Mukerjee et al. (2000)): in-plane thrust design (left) and out-of-plane thrust design (right).

freedom of the design and perhaps degrading performance. Another option is to use a more elaborated etching step that uses the Bosch process in order to create out-of-plane nozzles with more complex shapes (Gad-el Hak, 2001).

In the in-plane design, the shape of the nozzle (and the chamber) is etched on the surface of the wafer to create a pseudo-two-dimensional feature (Mukerjee et al., 2000; Kundu et al., 2012; Mihailovic et al., 2011; Silva, 2017). The freedom in the design in this case, in contrast to the out-of-plane design, is slightly better while the simplicity in the manufacturing may be lost depending on the types of features one wants to fabricate.

Concerning the material used for fabrication and the process itself, silicon is the main choice but low temperature co-fired ceramic (LTCC) is an interesting choice for being simpler to manufacture and cheaper (Cheah and Low, 2015; Karthikeyan et al., 2012).

Current devices are able to deliver thrust in the range from around 1 mN to around 7 mN while consuming from 1 to 10 W which might be high depending on the type mission in consideration.

### LOW-PRESSURE MICRO-RESISTOJET – LPM

The low-pressure micro-resistojet, or Free Molecule Micro Resistojet (FMRR), works in the transitional flow regime due to the low pressure, i.e.  $0.1 < Kn \leq 10$ . Therefore, statistical methods based on the gas kinetic theory have to be used to model and simulate the operation of this microthruster (Ahmed et al., 2006; Ketsdever et al., 1998). The devices, see 2.3, are usually composed of an inlet section, a plenum where the gas is injected with low pressure typically below 1000 Pa, and a heater chip with slots or microchannels through which the gas is accelerated to space. The heater chip, usually fabricated with MEMS manufacturing, contains a resistance to increase the temperature of the channels thus the energy of the particles in contact with the walls. Therefore, the geometry of the channels is a very important point to consider in the design in order to enhance the efficiency of the heat transfer to the gas and the overall efficiency of the thruster (Guerrieri et al., 2016a, 2017). The type of resistance and the manufacturing approach is also important to ensure an optimal conversion of electrical to thermal energy.

Although this propulsion concept has been investigated numerically and experimentally, it still needs to overcome some issues in the design such as propellant choice and storage. The level of pressure needed in the plenum, in particular, poses a challenge for

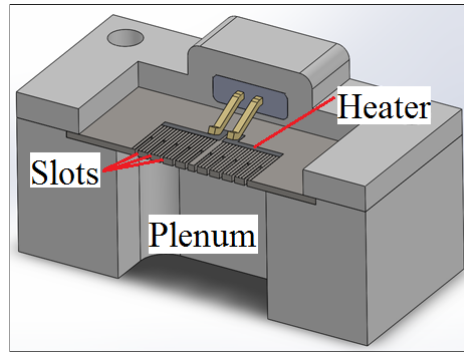


Figure 2.3: Cross section of a LPM indicating the parts of the thruster; the flow goes in the direction indicated by the red arrow.

the design of the valve and the tank for example.

In general, these devices are simulated or tested with inert gases, such as helium or nitrogen, or water but other propellants might be also considered (Lee et al., 2008; Ahmed et al., 2006; Blanco and Roy, 2013; Palmer et al., 2013).

An interesting advantage of this type of micropropulsion system is the scalability of the design which can be extended or shrunk by changing the number of channels in the heater chip. Each channel provides a certain amount of thrust so that the total thrust can be adjusted in the design for the particular mission by choosing the correct number of channels for the desired levels of thrust.

### 2.2.2. COLD-GAS MICROTHRUSTERS – CG

This type of micropropulsion system uses a pressurized gas as the propellant stored either in liquid, gaseous, or solid phase. The gas passes through a nozzle and it is accelerated to high velocities producing thrust. In general, the leakage levels of cold gas systems is the main challenge to overcome since the contamination with microscopic particles poses a threat to the sealing of valves, for example, which has to be taken into account when designing the system and estimating its performance. Depending on how long the satellite is stored waiting for launch (which in the case of CubeSats might be very long) leaks might consume much of its propellant if not treated with caution. The leak rate in the system presented by Kohler et al. (2002), for example, is below  $10^{-5}$  ssc/s which is acceptable for that system.

These systems are at an advanced level of development for CubeSats as they are simple to build and operate. Some of them, e.g. the one shown in 2.4, have already integrated control circuits to interface with the satellite bus and all fitting in 1U or less (Kohler et al., 2002; Kvell et al., 2014; Louwerse, 2009; Rangsten et al., 2013; Stenmark and Eriksson, 2002). Integrated sensors and control valves might be the next milestone for these engines.

Some differences arise in the method of storing the propellant that can be stored in the gaseous phase, liquid phase, or solid phase. The latter usually ignites a propellant pellet to generate a certain amount of gas in the plenum or tank; just as with solid pro-

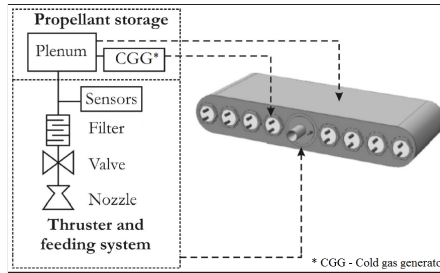


Figure 2.4: Example of cold-gas thruster (adapted from Louwerse (2009)) designed for the Delfi-N3xt mission.

pellant engines, the control and efficiency of the ignition are crucial for the performance of the thruster. Inert gases are a common choice due to safety concerns but other options, such as butane or other gasses with low boiling points, might be interesting since efficiency might improve when using liquid propellant.

### 2.2.3. SOLID PROPELLANT – SP

Solid propellant microthrusters consist of a chamber containing a small amount of propellant, an igniter (usually a heater), and a nozzle to accelerate the gasses after combustion (Fig. 2.5). These devices are among the most compact ones since there is no need of a feeding system or a pressurized container. Also, a good advantage brought by the compactness is the possibility to put many engines in a single chip as in Lewis et al. (2000); Rossi et al. (2001, 2005, 2002); Seo et al. (2012); Lee et al. (2010); Lee and Kim (2013), for example.

The main concerns in the development of SPs are in the design of the igniter and the chamber to assure an optimal combustion of the propellant in order to avoid the exhaust of unburned propellant grains (Chaalane et al., 2015; Oh et al., 2017; Wu et al., 2009). The disadvantages of these devices are the lack of control after ignition and that they are not able to restart. For repetitive ignitions, several stages would have to be used which increases the system complexity.

The efficiency of the combustion might be limited by the placement of the igniter which can be either on top or on the bottom of the propellant grain (Rossi et al., 2001; Briand et al., 2008; Koninck et al., 2011; Ru et al., 2016). The placement of the propellant grain might be also a challenge depending on the size of the igniter and amount of propellant since they can be on the micrometer scale. These facts are determinant since the efficiency of this type of micropropulsion system can be as low as 10% (Lewis et al., 2000) and the repeatability in terms of thrust is degraded by these circumstances and is very important for precision applications (Zhang et al., 2005, 2007).

### 2.2.4. LIQUID PROPELLANT – LP

This category comprises the MEMS micropropulsion systems which uses some liquid as a propellant that, when catalyzed, decomposes into hot gasses. The gasses are then accelerated through a nozzle to generate thrust. Common propellant choices for these systems are hydrazine and hydrogen peroxide which, when properly catalyzed,

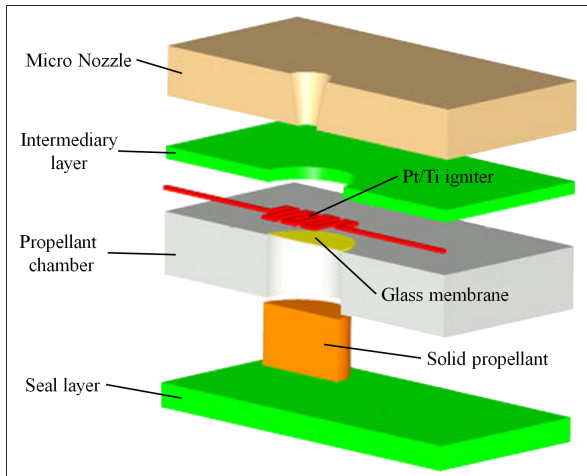


Figure 2.5: Example of a solid propellant microthruster (adapted from [Lee and Kim \(2013\)](#)).

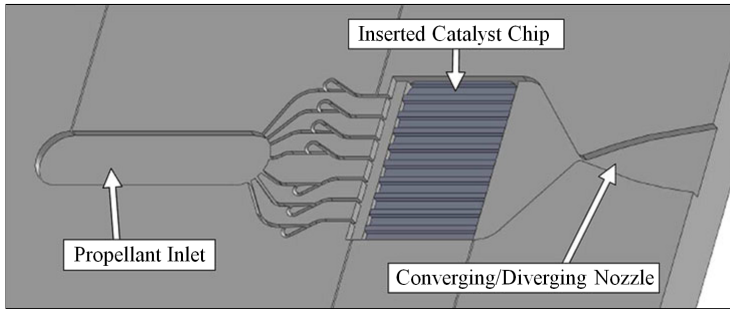


Figure 2.6: Example of liquid propellant thruster ([Miyakawa et al., 2012](#)).

decompose generating hot gasses. However, other alternatives are also interesting, for example using bipropellant concepts such as in [London et al. \(2001\)](#). The devices are composed of an inlet section, a catalyst chamber, and a nozzle as seen in Fig. 2.6.

Hydrazine thrusters have been developed and used as primary propulsion and attitude control for large spacecraft due to the medium level performance regarding specific impulse. However, due to its high toxicity and flammability, it needs special procedures and equipment to handle it on ground which represents an increase in the overall development cost for CubeSats and PocketQubes ([Patel et al., 2008](#)).

Hydrogen peroxide is an interesting alternative since it does not need the level of precaution in handling it ([Hitt et al., 2001](#); [Kundu et al., 2013](#)). One of its disadvantages is that organic materials are very likely to serve as a catalyst for its decomposition, therefore it might slowly decompose in the propellant tank due to minimum contact to undesired substances present in the storage. In the case of CubeSats that might be stored for long periods waiting for launch, a significant amount of propellant might be lost due to this fact.

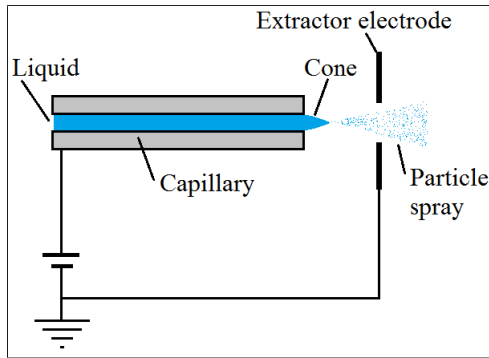


Figure 2.7: Schematic of an electro spray thruster.

### 2.2.5. ELECTROSPRAY THRUSTERS – ES

Electro spray thrusters are devices that produce thrust by emitting a spray of particles created by what is called a Taylor cone (Taylor, 1964). This effect occurs when an electric potential is applied to an ionic liquid in a capillary. Once a threshold voltage is applied the liquid at the tip of the capillary sharpens and forms a cone emitting particles that can be either single ions, droplets or both. A schematic is shown in Fig. 2.7.

Each emitter depending on the design and type of propellant generates a thrust in terms of nano- to micro-Newtons (Courtney et al., 2016; Xiong et al., 2005). The number of emitters can be chosen depending on the type of satellite and mission and it usually is in the order of thousands of emitters per thruster in order to achieve reasonable thrust levels to perform maneuvers (Courtney et al., 2015; Dandavino et al., 2014; Krejci et al., 2017; Krpoun and Shea, 2009). The propellant can be either an ionic liquid or mixture or a liquid metal and the emitters can be incremented with an accelerator grid after the extractor to further increase the exit velocity of the particles (Berg and Rovey, 2016; Berg et al., 2015).

The levels of thrust and specific impulse of these devices are aligned with the needs of PocketQubes and CubeSats and the modularity of the design and possibility of linearly changing the thrust by choosing the right number of emitters makes them an interesting choice for a propulsion system.

## 2.3. ANALYSIS AND DISCUSSION

In this chapter, the performance of the micropropulsion systems is analyzed in terms of thrust, specific impulse, and power consumption. The first two are important performance parameters to be chosen depending on the type of mission and the size of the spacecraft. Only the thrust may have a maximum boundary, which, in the case of very small spacecraft, can be set by the maximum disturbances the attitude control system can handle, to assure a safe operation of the spacecraft. The power consumption is particularly important for small satellites, since CubeSats and PocketQubes have strict limitations on available power. Therefore, it is especially important for electric propulsion, e.g. resistojets or electro spray thrusters, and in other cases, such as liquid propellant

thrusters, serves the only purpose of powering the control electronics which is needed for any system. Considering that each CubeSat unit typically produces about 2 W of power in low Earth orbits (Silva et al., 2018), then a 3U CubeSat would generate up to 6 W on average. A PocketQube has an area four times smaller than that of a CubeSat, then the power generated by 1U PocketQube can be considered up to 0.5 W, and a 3U PocketQube would generate up to 1.5 W on average. The average power of a spacecraft is, however, different from the power required by the propulsion system, because the thruster might not work continuously. However, this is also strictly connected to the thrust level. For low thrust systems, the thruster would need to be operated for a very long time in order to provide the same total impulse, which can be considered the same order of magnitude of the actual orbital lifetime of the spacecraft. For systems where the thrust level is higher one can operate the thruster for a much shorter time, meaning that the required power is close, or higher, than the average power produced by the spacecraft. In this analysis we suggest some boundaries for these parameters in order to help the reader in selecting a propulsion system for their mission.

In the following, we elaborate on a case of a 3U CubeSat to derive the maximum thrust suggested for a safe operation of the spacecraft. Considering a 3U CubeSat with an attitude control system using reaction wheels that can provide up to 0.2 mNm of torque (Candini et al., 2012; CubeSatShop.com, 2017) and a misalignment of the center of mass of the spacecraft of around 2 cm (Silva et al., 2015), we can derive the maximum disturbance torque that the thruster can generate while being counteracted by the attitude control. This represents a thrust of about 10 mN which can be considered a maximum for safe operation of the spacecraft. As the mass of a PocketQube is eight times smaller than that of an equivalent CubeSat, the maximum thrust for that category can be divided by the same factor resulting in a maximum thrust of around 1.25 mN. These values are shown in Fig. 2.8 to 2.10 suggesting maximum boundaries for 3U satellites. It is noted that these boundaries might be larger in case of more advanced systems for power and stability control.

We present in Fig. 2.8 to 2.10 an analysis of the average values of the mentioned parameters (thrust, specific impulse and power) collected from existing literature to provide an assessment of the current placement of each type of MEMS micropropulsion system. In Fig. 2.8 to 2.10, the centers of the ellipses represent the average values for the parameters while the eccentricity of the ellipses represent their standard deviation. The actual values of the parameters analyzed are presented in Table 2.4 along with other important aspects to consider, such as pressure and temperature. The estimated values of Technology Readiness Level (TRL) <sup>1</sup> are also given in order to position the different systems in terms of development. The average and standard deviation values are presented in Table 2.1.

In terms of thrust the solid-propellant thrusters are those with the highest values that might be interesting for missions of space debris removal or where fast orbital maneuvers are needed, but the lack of control in the operations renders them less interesting for applications requiring precision maneuvers for example. In this case, systems using liq-

<sup>1</sup>The TRL is in the range from 1 to 9. It is important to note that the analysis presented here is mostly based on scientific publications which explains the levels of TRL found. Higher levels might be found in commercial systems that due to the lack of public information were not included.

uid propellant are more suitable since the propellant flow can be controlled with valves. This comes, however, with a downside as the complexity of the system would increase in contrast to solid-propellant engines.

2

Table 2.1: Average values of thrust, specific impulse and power of MEMS from existing literature not considering the power used by the electronics. The standard deviation is given in brackets.

	$F$ [N]	$I_{sp}$ [s]	$P$ [W]
VLM	9.58E-4 (1.79E-3)	5.28E+1 (4.62E+1)	3.62E+0 (3.34E+0)
LPM	9.45E-4 (8.51E-4)	7.08E+1 (2.72E+1)	2.36E+0 (2.78E+0)
CG	6.08E-4 (8.00E-4)	5.77E+1 (1.04E+1)	2.18E+0 (2.02E-1)
LP	5.07E-1 (1.13E+0)	1.18E+2 (1.06E+2)	-
SP	9.99E-1 (1.63E+0)	5.93E+1 (3.87E+1)	5.77E-1 (6.75E-1)
ES	5.45E-5 (3.96E-5)	2.97E+3 (1.72E+3)	8.34E-1 (8.51E-1)

In terms of specific impulse, the electro spray thrusters perform very well due to the high velocity the propellant particles are expelled. The thrust produced by these engines, however, is relatively low which makes them an attractive option for propulsion systems dedicated to, for example, attitude control or for long duration operation in case of orbit transfers.

As seen in Fig. 2.9 and 2.10, the power used by solid-propellant thrusters is low since they only require it for ignition of the propellant grain. Other devices, such as resistojets, need continuous power to ensure that the propellant is fully vaporized which requires higher energy consumption. Note that the power usually presented in references does not take into account the electronic circuits necessary to operate the engines. The reason is that most of them are in an early stage of development and the electronics are not designed for the flight model.

Figure 2.8 shows a clear division in three sectors: high thrust, high specific impulse, and low thrust and specific impulse. This provides helpful insights into selecting the proper propulsion system for a specific mission. It also shows that there are regions not covered but could be achieved by, for example, design optimization or using hybrid technology that combines the characteristics of two or more types. Table 2.2 presents the suggested applications of thrusters in the regions identified. This is, however, a rough classification, with the exact applicability of specific propulsion systems depending on the specific mission and spacecraft characteristics.

Table 2.2: Suggested applications for the different regions on Fig. 2.8.

Thrust	Specific impulse	Suggested application
High	Low	space debris removal, fast orbital transfer/maneuvers (when spacecraft stability is not an issue)
Low	High	precise pointing, slow orbital transfer/maneuvers
Low	Low	attitude control, small orbit corrections (max. in the order of a few m/s)

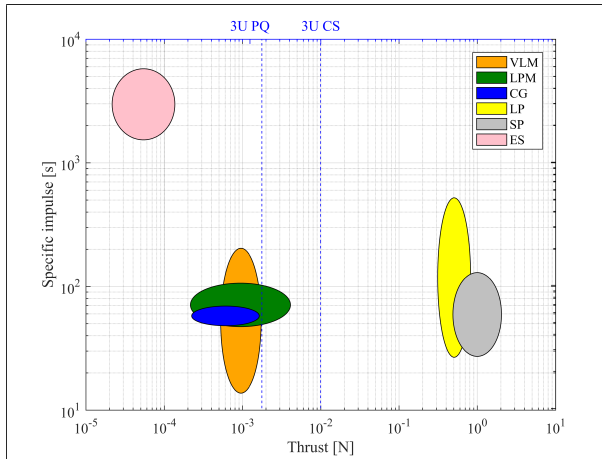


Figure 2.8: Comparison of specific impulse and thrust of the different types of micropropulsion systems. The centers of the ellipses are the average values and the minor and major axes are proportional to the standard deviation. The dashed lines represent the maximum (suggested) thrust for 3 units PocketQubes (PQ) and CubeSats (CS).

As mentioned, the power is a special constraint for the classes of satellites analyzed here (also for other classes) and, as Fig. 2.9 and 2.10 illustrate, there are no significant gaps in the range of power. However, the top values as indicated with the dashed lines are high for the limits of 3U CubeSats and PocketQubes.

Figure 2.8 clearly shows two different trends for chemical propulsion (i.e. liquid- and solid-propellant, and for electrical propulsion. Furthermore, the area covered by resistojets (orange and green ellipses) can fit within both trends, thus showing the hybrid nature of this concept where the propellant is heated electrically, but accelerated thermodynamically in a nozzle. In Fig. 2.9, looking at the centers of the ellipses (the averages) a relationship between power and thrust for all electric propulsion concepts is evident. This is expected, since in electric propulsion the thrust is power-driven. It can also be observed that chemical propulsion is not part of this trend. Finally, in Fig. 2.10, a close relationship between power and specific impulse for all the concepts considered. Again, this is to be expected, since specific impulse is a measure of the energy delivered by the system.

Looking at the boundaries suggested, if the boundary line falls in the middle of an ellipse, that type of propulsion is probably feasible since there might be a way of scaling it down to the desired power level levels of power or thrust. If the entire ellipse lies higher than the maximum level, then we can conclude that the current technology does not allow the use of that type of propulsion in that type of satellite. Thus, it can be concluded that in terms of power, most of the devices fit into the maximum for 3U CubeSats but if we increase this threshold, then we can consider all of the types for a possible propulsion system. For a 3U PocketQube, however, the situation is more difficult since the limitation in the power affects all types analyzed. In terms of thrust, solid and liquid propellant engines generate more thrust than the suggested maximum. This problem can be over-

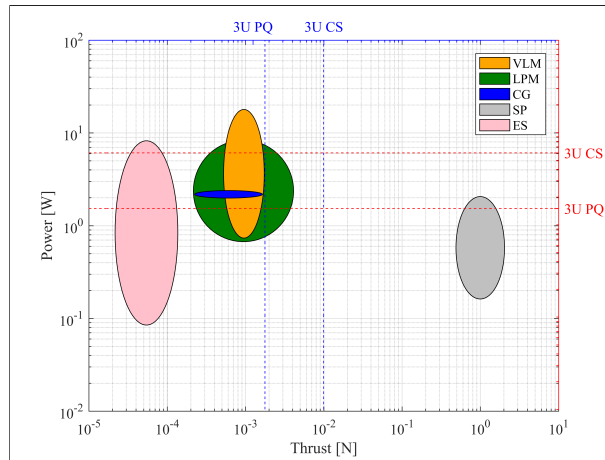


Figure 2.9: Comparison of power and thrust of the different types of micropropulsion systems. The centers of the ellipses are the average values and the minor and major axes are proportional to the standard deviation. The devices using liquid propellant usually use electric power only for control electronics, so they are not present in the graph. The dashed lines represent the maximum (suggested) thrust for 3 units PocketQubes (PQ) and CubeSats (CS).

come with a more advanced attitude control system to compensate for disturbances or by reducing uncertainties in the position of the center of mass.

One important aspect when comparing or selecting a micropropulsion system is the complexity of the system in terms of integration and operation characteristics. The former regards additional constraints to the design, such as fluidic fittings and connections, and the latter relates to, e.g., scheduling constraints in the communication link that have to be considered in the actuation of the thrusters, since control of the input parameters might not be realizable with CubeSats and PocketQubes due to data link limitations for example. An automatic controller may be considered to avoid this issue but will require more effort in the development. Here, to characterize complexity, we select four parameters characterizing each system: the minimum number of additional components that are needed in the system on top of the actual thruster and control electronics; the number of control parameters for the system; and the start-up and shut-down times which are respectively the times needed to achieve steady state full thrust and to completely shut down the engine, i.e. achieve zero thrust, from the moment when the command is sent. These last two parameters are important if one wants to perform precise maneuvers that need a specific total impulse. Then the time needed to achieve steady state and to shut the engine down have to be taken into account.

The number of components and the number of control parameters are given quantitative values from 1 to 3 representing the count of that criterion and the start-up and shut-down times are given qualitative scores from low to high corresponding to short and long times respectively. The complexity is then calculated as the average of these parameters (taking the numbers 1 to 3 for the qualitative values) and if the result is from 0 to 1 we consider it low complexity, from 1 to 2 medium, and from 2 to 3 high. Table 2.3

lists the 4 parameters for each type of system and provides the resulting complexity.

As we can see, the complexity increases with number of components and parameters. But on the other hand, a more controllable operation of the thruster may be achieved therefore increasing the performance and optimal use of propellant.

Table 2.3: Assessment of complexity of the types of MEMS micropropulsion.

Type	Complexity	Min. num. components	Num. control param.	Start-up time	Shut-down time	Comment
VLM	High	3 (heater, valve, tank)	2 (power, flow rate)	high	high	Liquid left in the path from the valve to the thruster gives high shut down time.
LPM	Medium	2 (valve, tank)	1 (flow rate)	low	medium	Number of control parameters and components increase if applying temperature to the gas or using liquid propellant.
CG	Medium	2 (valve, tank)	1 (flow rate)	low	medium	Number of control parameters and components increase in warm gas mode.
LP	Medium	2 (valve, tank)	1 (flow rate)	medium	high	May require power to accelerate the start up. Same issue with liquid and shut down time as for VLM.
LP	Medium	2 (valve, tank)	1 (flow rate)	medium	high	May require power to accelerate the start up. Same issue with liquid and shut down time as for VLM.
SP	Low	1 (igniter)	1 (power)	medium	-	Shut down is not controllable.
ES	Medium	2 (tank, energy storage)	1 (power)	low	low	Number of control parameters increases if using an accelerator grid

### 2.3.1. FUTURE DEVELOPMENTS

Although there has been a significant effort in developing micropropulsion systems, there are still challenges to be addressed. For highly miniaturized satellites, the devices may be so small that interfacing them to other larger components of the system becomes more and more difficult. In some cases, the electronics might be integrated into the fabrication process, which is one of the advantages of using MEMS, to incorporate sensors and control circuits into “smart thrusters”. This integration can also be extended to, for example, valves or pumps (Shoji and Esashi, 1994; Zhang et al., 2007) that can be manufactured in wafers with similar processes leading to a complete “propulsion on a chip” system which is very interesting for extremely miniaturized satellites.

The integration of the components of a propulsion system is one of the main challenges since traditionally these parts come separately (e.g. valves, tanks, etc.). However, with the advance of MEMS technology, more integrated devices can be accommodated

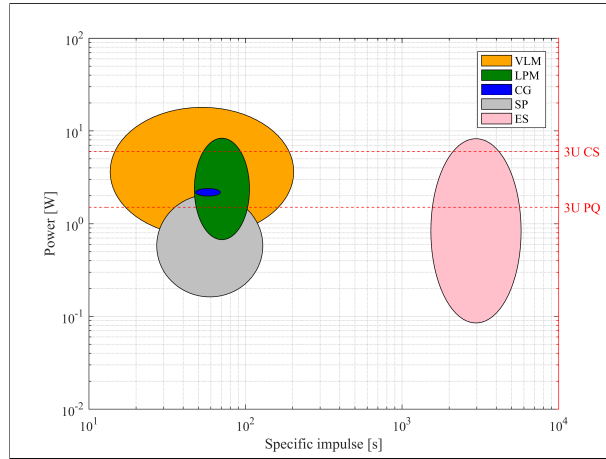


Figure 2.10: Comparison of power and specific impulse of the different types of micropropulsion systems. The centers of the ellipses are the average values and the minor and major axes are proportional to the standard deviation. The devices using liquid propellant usually use electric power only for control electronics, so they are not present in the graph. The dashed lines represent the maximum (suggested) thrust for 3 units PocketQubes (PQ) and CubeSats (CS).

Table 2.4: Data of micropropulsion systems for comparison extracted from the references in the first column.

Ref.	Type	$P_{min}$ [W]	$P_{max}$ [W]	$F_{min}$ [N]	$F_{max}$ [N]	$I_{sp_{min}}$ [s]	$I_{sp_{max}}$ [s]	$P_{min}$ [Pa]	$P_{max}$ [Pa]	$T_{min}$ [K]	$T_{max}$ [K]	TRL
Kohler et al. (2002)	CG	n/a	n/a	0.00E+00	2.00E-03	4.50E+01	4.50E+01	0.00E+00	5.00E+05	n/a	n/a	3
Kvell et al. (2014)	CG	2.35E+00	2.35E+00	0.00E+00	1.00E-03	6.80E+01	6.80E+01	2.00E+05	5.00E+05	n/a	n/a	3
Rangsten et al. (2013)	CG	2.00E+00	2.00E+00	0.00E+00	6.50E-04	6.00E+01	6.00E+01	2.00E+05	5.00E+05	n/a	n/a	5
Dandavino et al. (2014)	ES	5.53E-01	2.50E+00	3.12E-05	9.98E-05	4.74E+02	5.93E+03	n/a	n/a	n/a	n/a	3
Courtney et al. (2015)	ES	6.50E-01	4.00E-01	2.00E-05	3.00E-05	3.00E+03	3.00E+03	n/a	n/a	n/a	n/a	3
Courtney et al. (2016)	ES	1.00E-01	8.00E-01	5.00E-06	5.00E-05	1.50E+03	3.26E+03	n/a	n/a	n/a	n/a	3
Krpoun and Shea (2009)	ES	n/a	n/a	1.00E-04	1.00E-04	2.00E+03	4.60E+03	n/a	n/a	n/a	n/a	3
London et al. (2001)	LP	n/a	n/a	0.00E+00	1.00E+00	0.00E+00	1.50E+02	0.00E+00	1.20E+06	n/a	n/a	3
Wu and Lin (2010)	LP	n/a	n/a	2.00E-04	1.97E-03	2.92E+00	1.34E+01	n/a	n/a	n/a	n/a	3
Blanco and Roy (2013)	LPM	1.16E+00	1.16E+00	1.70E-03	1.70E-03	5.60E+01	5.60E+01	n/a	n/a	n/a	n/a	2
Ahmed et al. (2006)	LPM	n/a	n/a	1.00E-04	1.00E-03	4.00E+01	8.00E+01	5.00E+01	2.00E+02	3.00E+02	5.73E+02	3
Cervone et al. (2015)	LPM	8.00E-01	5.60E+00	1.00E-03	1.60E-03	7.00E+01	7.00E+01	4.90E+01	4.90E+01	5.74E+02	1.17E+03	2
Guerrieri et al. (2016b)	LPM	1.46E+00	9.68E+00	2.80E-04	2.72E-03	6.37E+01	1.11E+02	5.00E+01	3.00E+02	3.00E+02	9.00E+02	2
Ketsdever et al. (2005)	LPM	1.00E+00	3.40E+00	1.00E-04	1.70E-03	4.00E+01	1.40E+02	3.50E+01	1.20E+02	3.00E+02	5.00E+02	3
Lee et al. (2008)	LPM	0.00E+00	2.50E+00	1.29E-04	1.29E-04	7.92E+01	7.92E+01	n/a	n/a	3.00E+02	5.80E+02	3
Palmer et al. (2013)	LPM	0.00E+00	1.60E+00	0.00E+00	1.07E-03	5.20E+01	5.40E+01	2.55E+02	9.00E+02	2.74E+02	5.44E+02	3
Briand et al. (2008)	SP	1.60E+00	1.60E+00	4.00E-03	1.00E-02	1.00E+02	1.00E+02	n/a	n/a	n/a	n/a	3
Lee et al. (2010)	SP	3.40E-01	3.40E-03	3.62E+00	3.62E+00	6.23E+01	6.23E+01	n/a	n/a	n/a	n/a	4
Rossi et al. (2001)	SP	0.00E+00	7.50E-01	4.00E-02	5.10E-02	n/a	n/a	n/a	n/a	1.53E+03	1.53E+03	3
Zhang et al. (2005)	SP	1.60E-01	1.60E-01	5.00E-02	6.00E-01	2.68E+00	2.83E+01	n/a	n/a	n/a	n/a	3
Cen and Xu (2010)	VLM	n/a	n/a	2.00E-03	6.50E-03	1.10E+02	1.10E+02	1.00E+05	2.60E+05	4.54E+02	5.74E+02	3
Cheah and Low (2015)	VLM	0.00E+00	5.00E+00	2.50E-04	6.34E-04	3.10E+01	3.10E+01	n/a	n/a	3.24E+02	6.83E+02	3
Chen et al. (2010)	VLM	n/a	n/a	1.00E-03	6.00E-03	3.07E+01	3.07E+01	1.00E+05	2.00E+05	4.23E+02	5.73E+02	3
Karthikeyan et al. (2012)	VLM	7.10E+00	9.20E+00	3.36E-05	6.77E-05	3.42E+00	6.90E+00	1.04E+05	1.04E+05	4.00E+02	4.22E+02	3
Kundu et al. (2010)	VLM	1.60E+00	3.60E+00	1.50E-04	1.01E-03	5.00E+01	1.05E+02	1.00E+05	1.00E+05	3.74E+02	4.74E+02	3
Kundu et al. (2013)	VLM	2.00E+00	2.20E+00	3.00E-04	1.08E-03	8.00E+01	1.80E+02	n/a	n/a	4.23E+02	4.23E+02	3
Maurya et al. (2005b)	VLM	1.00E+00	2.40E+00	5.00E-06	1.60E-04	2.04E+01	2.04E+01	n/a	n/a	3.75E+02	3.76E+02	3
Maurya et al. (2005a)	VLM	1.00E+00	2.40E+00	5.00E-06	1.20E-04	1.75E+01	1.75E+01	n/a	n/a	n/a	n/a	3
Mihailovic et al. (2011)	VLM	n/a	n/a	2.00E-05	9.60E-04	6.53E+01	6.53E+01	0.00E+00	6.00E+05	2.74E+02	6.24E+02	2
Mukerjee et al. (2000)	VLM	7.80E+00	1.08E+01	3.10E-04	4.60E-04	8.85E+01	8.85E+01	n/a	n/a	n/a	n/a	3
Ye et al. (2001)	VLM	9.00E-01	9.70E-01	7.10E-07	2.86E-06	1.91E+00	7.68E+00	n/a	n/a	n/a	n/a	3

in very small spacecraft. This requires a good and reliable interface between mechanical, electrical, and fluidic parts. The integration of the system and interfaces between the macro- and micro-systems, and components, such as microvalves to control the mass flow rate, the electronic circuits, and the propellant management, are some of the engineering challenges that can be facilitated with the use of MEMS.

Regarding the manufacturing processes, new technologies and materials such as membranes, thin metal layers, or composites will allow for designing and building ultra-light components, for example tanks, that currently consume most of the dry mass budget. With the development of additive manufacturing methods, the emerging 3D printing technology is an interesting option that might facilitate the integration and interfacing of mechanical, electrical, and fluidic parts (Arestie et al., 2012; Imken et al., 2015; Stevenson and Lightsey, 2016). Other conventional manufacturing approaches also allow the development of advanced systems that may be compatible with CubeSat standards (Carroll et al., 2015; Ciaralli et al., 2016, 2015; Coletti et al., 2015, 2011, 2009; Hejmanowski et al., 2015; Khaji et al., 2016; Kisaki et al., 2013; Leiter et al., 2009; Liu et al., 2015; Polzin et al., 2007; Sathiyathan et al., 2011; Smirnov et al., 2002; Szelecka et al., 2015; Tanaka et al., 2012; Tsay et al., 2016a,b). Also, innovative propellants, especially green ones, might open the path to new concepts of thrusters or new ways of using them.

Concerning the operation of thrusters, there are challenges related to disturbances generated by the thruster in combination with a possibly movable center of mass. This might require a more sophisticated system with micro-gimbaled nozzles or arrays of microthrusters in order to allow thrust direction control. The use of MEMS pumps for avoiding pressurization of the propellant may also be considered an option to facilitate the operation by having a more controlled pressure system and reducing the total mass of the system in exchange of complexity and power consumption.

## 2.4. CONCLUDING REMARKS

This chapter presented and analyzed the status of development of micropropulsion systems that are candidates for CubeSat and PocketQube missions. We have analyzed more than thirty devices regarding performance aspects and assessed them in relation to needs and limitations imposed by these types of satellites.

A simple way of comparing the complexity of the systems has been introduced in order to help in choosing an appropriate propulsion system for the mission. Moreover, the comparison also shows where interesting operational characteristics can be found on each type of device and where new methods could be developed.

It has been shown that the systems analyzed can be grouped and separated according to the performance parameters evaluated and also the operational complexities can be used to identify which approach is the most appropriate for certain missions. Moreover, the TRL of the systems indicate that most of them are in a research/development stage.



# 3

## DESIGN OF VAPORIZING LIQUID MICROTHRUSTERS

*Cause hate is all the world has even seen lately.*

From the song *Take a look around* by Limp Bizkit

*This chapter presents the design, manufacturing and characterization of Vaporizing Liquid Microthrusters (VLM) with integrated molybdenum heaters and temperature sensing. The devices were used in an extensive experimental campaign aimed at providing insights into the challenges in developing this technology. The thrusters use water as the propellant and are designed for use in CubeSats and PocketQubes. The devices are manufactured using silicon based MEMS (Micro Electro Mechanical Systems) technology and include resistive heaters to vaporize the propellant. The measurements of the heaters' resistances are used to estimate the temperature in the vaporizing chamber. The manufacturing process is described as well as the characterization of the thrusters' structural and electrical elements. In total, 12 devices with different combinations of heaters and nozzles have been assessed and four of them have been used to demonstrate the successful operation of the thrusters. Results, used to validate the thrusters, show a performance close to the design parameters and comparable to other devices found in the literature. Also, the results were extensively used in the development of the models that will be presented in the next chapters.*

---

Parts of this chapter have been published in:

Silva, M. A. C., Guerrieri, D. C., van Zeijl, H., Cervone, A., Gill, E., *Vaporizing Liquid Microthrusters with integrated heaters and temperature measurement*, Sensors and Actuators A: Physical 265, Pages 261-27, 2017.

### 3.1. INTRODUCTION

WITHIN micropropulsion systems, microresistojets are a very interesting choice, especially for CubeSats, since it is one of the few types of such systems currently able to achieve a thrust level in the range 0.1–10 mN while still meeting all the constraints posed by extremely miniaturized spacecraft especially in terms of power. The principle of microresistojets is based on heating a gaseous propellant with a resistance and then accelerating it to space. Some devices use propellants stored in liquid or solid phase, hence a phase-change process is required prior to the heating of the gas. The phase-change is done by heating a resistance in contact with the propellant that is kept in certain conditions of pressure and temperature to allow the phase change (sublimation or vaporization) to occur. Devices that use liquid propellants are called Vaporizing Liquid Microthrusters (VLM) and has been investigated by different research groups.

Different designs can be found in the literature reporting the development of microresistojets. [Cheah and Low \(2015\)](#) present a microthruster consisting of layers of ceramic. The microthruster is built by combining three layers of ceramic material: the combustion chamber, the inlet channel, and the nozzle are cut in the inner layer and a micro-heater is attached to the third layer. Tests were performed using water as propellant and it was found that the ceramic thruster is slightly more efficient than some silicon thrusters with respect to power consumption and delivered thrust. [Karthikeyan et al. \(2012\)](#) present the details of fabrication and test of a low temperature co-fired ceramic (LTCC) microthruster. They analyze the results for pressure, temperature, power and thrust and also present some comments about the relation between the temperature of the chamber and the vaporization of the propellant.

[Kundu et al. \(2012\)](#) show the design, simulation, fabrication and test of a VLM. The design of the chamber is based on basic calculations with temperature and residence time. The inlet channel is designed to reduce the pressure drop caused by the friction (which is high for diameters below 500  $\mu\text{m}$ ).

[Maurya et al. \(2005a\)](#) describe the fabrication and test of a vaporizing liquid microthruster whose nozzle points in the direction normal to the chip plane. They built and tested two devices with different nozzle exit areas and tested them under different power conditions to characterize the thrust level per applied power.

The analytical modeling of a vaporizing liquid microthruster is shown by [Maurya et al. \(2005b\)](#). The thruster is the same presented by [Maurya et al. \(2005a\)](#). They focus on the formulation of the equations to calculate the power necessary to vaporize the liquid.

[Ye et al. \(2001\)](#) describe the design of four micro resistojets that were fabricated using MEMS technology and silicon wafers. The main differences among them are the type of nozzle (convergent or divergent) and the chamber volume (300 $\mu\text{m} \times 750\mu\text{m}$  and 600 $\mu\text{m} \times 1500\mu\text{m}$ ).

[Mihailovic et al. \(2011\)](#) present the design and manufacturing techniques used to construct a micro resistojet consisting of an inlet portion, a heating section with one or more long channels, and a nozzle. Some tests were performed with three different devices: two with only one channel between the inlet and the nozzle and one with 3 channels.

The devices found in literature often make use of complicated experimental setups including high performance data acquisition systems that might be incompatible with

the limitations imposed by very small satellites such as CubeSats specially due to budgetary constraints since usually these satellites make extensive use of commercial-off-the-shelf components. Also, interfacing such a system to external components is a challenge since these complex devices integrate fluidic, electrical, and mechanical characteristics into a very small device that also needs a reliable way of sensing the important parameters such as pressure and temperature.

In this chapter, the design of VLMs with integrated heating and sensing capabilities is presented. The design allows the easy operation of the microthrusters using standard commercial-off-the-shelf equipment. The devices are designed to meet the strict requirements of nano- and pico-satellites such as CubeSats and PocketQubes and operate using water as the propellant (Cervone et al., 2017). It has been shown that water is an interesting choice for micropropulsion applications as it can provide a very high velocity change ( $\Delta v$ ) per volume of propellant when compared to other green propellants (Guerrieri et al., 2017) making it very interesting for applications where orbital maneuvers are required. The heaters are made out of molybdenum which is a metal that can withstand very high temperatures (melting point 2693 °C) and can be patterned with standard dry or wet etching methods (Mele et al., 2012). The resistivity of molybdenum is linearly proportional to the temperatures up to 700 °C allowing the design of heaters that also need precise temperature measurements as in the case of the VLMs. The structural design of the thrusters is based on previous work done by Poyck et al. (2014). A special interface combining fluidic, electric, and mechanic connections has been developed to facilitate the operations of the thrusters right after dicing. The results of manufacturing and characterization of the VLMs are presented demonstrating the operations including feedback use of measurements of pressure and temperature. The devices have been manufactured with silicon wafers and tested under conditions close to operational in terms of pressure, mass flow, and power.

## 3.2. DESIGN DESCRIPTION

### 3.2.1. REQUIREMENTS

The thrusters have been designed to be used in the next generation of miniaturized spacecraft such as CubeSats and PocketQubes. These spacecraft have strict limitations in size, mass, and more importantly power which might be very limited depending on the spacecraft design. Table 3.1 show the requirement values considered for the design. The requirements related to performance, are not as strict as those of size, mass, and power as the devices are still under development and those values can be seen as target performance values instead of a strict limitation.

### 3.2.2. DESIGN

The microresistojets are composed of three main parts: a nozzle, a vaporizing chamber, and a heater. Each of these parts have different designs (Cervone et al., 2016). The mask used during manufacturing containing all the needed features is presented in Fig. 3.1. The channels and the heaters are made in a modular manner such that a successive exposure of the slots is needed to make the complete chamber. Each module, defined as the block containing one heater, is designed to produce 1 W of power given a voltage

Table 3.1: Requirements considered in the design of the thrusters.

Requirement	Minimum	Maximum	Comment
Mass	n/a	0.1–1 kg	1U CubeSat or PocketQube
Size	n/a	cube of 5–10 cm	1U CubeSat or PocketQube
Power	n/a	4.5–10 W	1U CubeSat or PocketQube
Thrust	0.1 mN	3 mN	–
Specific Impulse	50 s	100 s	–

of 5 V. In this case, seven modules are used in order to produce 7 W of power with 5 V which is the middle between maximum and minimum power needed for the thrusters as we will see in the next sub-section. The details of the channels are shown in Fig. 3.1. The dimensions are expected to be slightly different in the manufactured devices due to isotropic etching of the walls that erode approximately by 20  $\mu\text{m}$ .

There are three types of nozzle:

- long nozzle, indicated in Fig. 3.1 as Nozzle 1. Area ratio  $A_r = 11$ .
- wide nozzle, Nozzle 2. Area ratio  $A_r = 17$ .
- bell nozzle, Nozzle 3. Area ratio  $A_r = 11$ .

The vaporizing chamber is divided into modules that have four designs:

- diamond pillars: can be large or small with a total surface area per module of  $7.09 \times 10^{-6} \text{ m}^2$  and  $2.27 \times 10^{-5} \text{ m}^2$ . Channel 2 and Channel 4 in Fig. 3.1.
- serpentine channels: can be large or small with a total surface area per module of  $5.40 \times 10^{-6} \text{ m}^2$  and  $5.16 \times 10^{-6} \text{ m}^2$ . Channel 1 and Channel 3 in Fig. 3.1

Finally, there are two types of heaters:

- One type with 21 lines per module divided into three sets of 7 lines.
- Another with 30 lines per module divided into sets of 2 lines.

In both configurations the lines are 12  $\mu\text{m}$  wide and 3000  $\mu\text{m}$  long. Considering a sheet resistance of around  $2 \Omega/\square$  (Mele et al., 2012) the total resistance of each heater should be 3.40  $\Omega$  and 2.38  $\Omega$  respectively according to the following equation:

$$R = R_{sh} \frac{L}{W} \quad (3.1)$$

where  $R$  is the resistance,  $R_{sh}$  is the sheet resistance,  $L$  is the length of the resistance, and  $W$  is the width of the resistance.

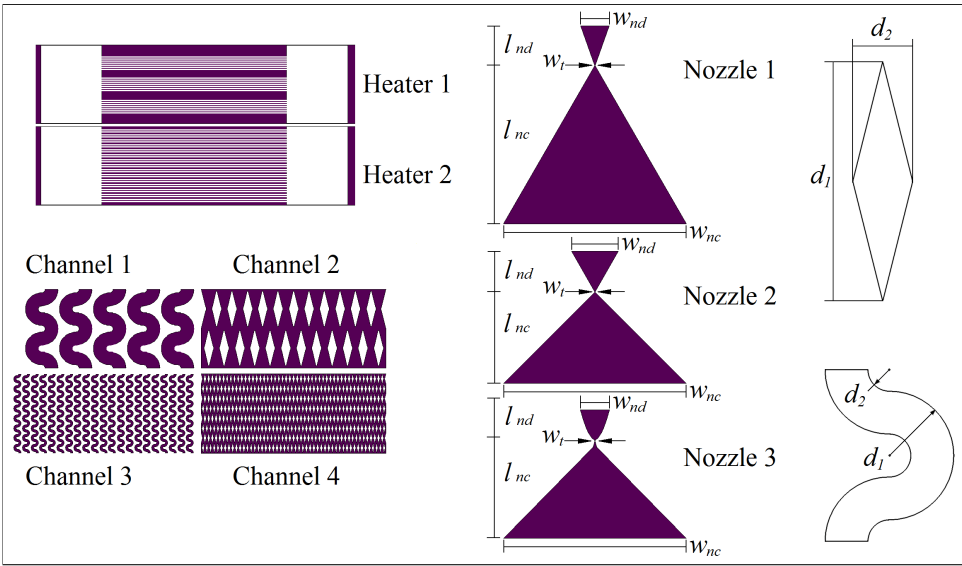


Figure 3.1: Masks used in the manufacturing of the thrusters. The indexes  $nc$  and  $nd$  stand for the convergent and divergent parts of the nozzle respectively and the index  $t$  stands for the throat part of the nozzle. Dimensions are shown in Table 3.6.

### 3.2.3. PROPELLANT SELECTION

Microresistojets can be designed to work with a variety of propellants in any state (gaseous, liquid, or solid) and the VLMs work with those that are stored as liquid. Considering the range of pressure and temperature required by CubeSats and PocketQubes (which is less than 10 bar), the number of propellant choices is significantly reduced and considering the safety of the substance it can be further reduced. In a previous study, [Guerrieri et al. \(2017\)](#) compared many substances that are applicable to microresistojets and the 10 most suitable propellants are listed in Table 3.2 with their respective performance values. The performance is evaluated for chamber pressures in the range of 2–5 bar, throat area of  $5 \times 10^{-9} \text{ m}^2$ , and nozzle expansion ratio equal to 11.

Considering the fourth parameter,  $\Delta v$  per volume of propellant, water is the best candidate meaning that it can accelerate the spacecraft to higher velocities using the same volume of propellant. This is due to the fact that water is the most dense among all the candidates in conditions considered. Considering the specific impulse, water has one of the highest values together with ammonia for the conditions analyzed. However, ammonia in its pure form is highly toxic which might not be suitable for use in CubeSats and PocketQubes. On the other hand, the power needed to vaporize water is the highest due to its high enthalpy of vaporization. Still, it is within reasonable range that can be provided by the electric power system of CubeSats and PocketQubes.

Therefore, water is the most suitable candidate for use in VLMs as it outperforms the other candidates in terms of specific impulse and  $\Delta v$  which compensates the drawback of the power consumption. Thus, it has been selected as the propellant in the characterization tests of the VLMs and as the propellant for a future in-flight demonstration.

Table 3.2: Comparison of different propellants that are suitable for use in VLMs (Guerrieri et al., 2017).

Propellant	Temperature [K]	Thrust [mN]	Sp. Impulse [s]	$\Delta v$ per volume [m/(s mL)]	Power [W]
Acetone	360–550	1.8–4.5	66.7–82.5	0.14–0.18	1.8–5.4
Ammonia	300–550	1.7–4.2	98.8–133.7	0.16–0.22	0.1–2.1
Butane	300–550	1.8–4.6	61.6–83.5	0.10–0.13	1.2–5.4
Cyclopropane	300–550	1.8–4.4	67.7–91.7	0.12–0.16	0.1–3.5
Decane	500–550	1.9–4.7	53.0–55.6	0.11–0.11	2.9–7.9
Ethanol	370–550	1.8–4.5	74.8–91.2	0.16–0.20	2.8–7.4
Isobutane	300–550	1.8–4.5	59.5–80.6	0.09–0.12	0.1–5.3
Methanol	360–550	1.7–4.3	83.2–102.8	0.18–0.22	2.7–7.1
Propene	300–550	1.8–4.5	69.5–94.1	0.10–0.13	0.1–2.6
Water	400–550	1.7–4.2	110.3–129.3	0.30–0.35	4.0–10.2

### 3.2.4. PERFORMANCE PARAMETERS

With the design parameters of the nozzles, one can estimate the values of thrust and specific impulse given the conditions in the chamber using the equations introduced in chapter 1. Assuming that the system is in the saturation point due to the boiling, the temperature in the chamber will vary in the range from 100 to 150°C with the pressure in the range 1–5 bar. Note, however, that it is still possible to heat the vapor to a higher temperature by providing more power to the heaters. With these conditions the thrust and specific impulse are calculated using the equations presented in chapter 1 using the saturation temperature and pressure. The thrust and specific impulse for the long nozzle and the bell nozzle are the same as they have the same area ratio, respectively 0.75–3.79 mN and 105–113 s. The wide nozzle is expected to have a slightly higher thrust 0.77–3.86 mN and specific impulse 107–115 s. As all nozzles have the same throat area, the mass flow rate is the same for all of them in the range 0.73–3.42 mg/s. The power  $P$  necessary to heat-up the water from room temperature of about 24°C to boiling point and vaporize it is calculated according to the following equation:

$$P = \dot{m}\Delta H \quad (3.2)$$

where  $\Delta H = H_V - H_L$ ,  $H_V$  is the enthalpy of water vapor at boiling temperature, and  $H_L$  is the enthalpy of liquid water at room temperature. For the given mass flow rates, the power lies in the range 1.87–9.01 W.

### 3.3. MANUFACTURING

The thrusters have been manufactured at the Else Kooi Laboratory (EKL) of TU Delft. The entire process is done in one of the cleanrooms (class 100) until the dicing step which is done in the MEMSLab. The specific process' steps are presented in the next paragraphs.

The starting material is a 100 mm double side polished silicon wafer with thickness of 300  $\mu\text{m}$ . A layer of 500 nm of LPCVD (low pressure chemical vapor deposition) silicon nitride is deposited on the wafer to isolate the substrate from the heaters. Then, a layer of 200 nm of molybdenum is deposited on the front side of the wafer by sputtering. To form a hard mask for patterning Mo, a layer of PECVD TEOS (Plasma-enhanced chemical vapor deposition tetraethoxysilane) is deposited. The mask for the heaters is made

with photoresist and the patterning is done first for TEOS (hard mask) by wet etching with buffered hydrofluoric acid (BHF) for approximately 2 min. Then, Mo is etched with aluminum etch at 35 °C for approximately 26 s. The complete diagram with all the steps and a schematic cross-section of the device are shown in Fig. 3.3.

After stripping off the photoresist with plasma cleaning and removing TEOS with BHF, a layer of 5  $\mu\text{m}$  of silicon dioxide is deposited on both sides to form the hard mask of the cavities (chamber and inlet hole). Photoresist is used to form the soft mask for  $\text{SiO}_2$  which is etched with plasma etching. The layer of silicon nitride is also etched in this step with a different recipe. The cavities of the chamber are etched in silicon using a combination of isotropic and anisotropic deep reactive ion etching (DRIE). The isotropic step is done in order to make sure that the narrow channels are successfully opened. The fluid inlets are isotropically etched with DRIE from the heater side after the deposition of a layer of silicon dioxide on the chamber side.

Following the cleaning and removal of the hard masks, the silicon wafer is bonded to a glass wafer with anodic bonding at 400 °C and 1000 V. The glass is intended to provide a good visualization of the flow inside the thruster. This helps to understand the dynamics of the two-phase flow inside the chamber. The last step of manufacturing is dicing. Then the thrusters are ready for tests. A sample diced wafer and a thruster are shown in Fig. 3.2. The flow is from the bottom to the top: the propellant enters by the inlet hole, passes by the chamber where it is vaporized and is expelled to the environment by the nozzle. The area after the nozzle is added in order to have a safe path for the cutting blade during dicing; as shown in section 3.2 the nozzles can have different lengths. Therefore this area is to make sure that the shorter nozzles are open.

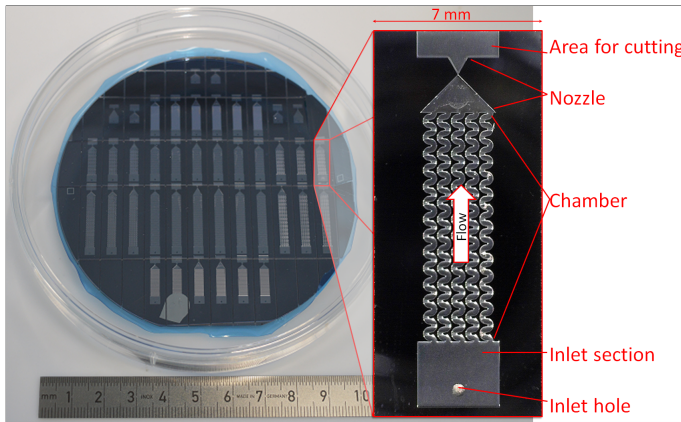


Figure 3.2: In total each processed wafer yields 36 different devices plus 6 nozzle-only thrusters. In the right, one of the thrusters installed in the interface.

### 3.4. EXPERIMENT DESCRIPTION

Two wafers have been processed using the steps described above. The first one was made without the inlet holes (to assess an intermediate step in the process) while the

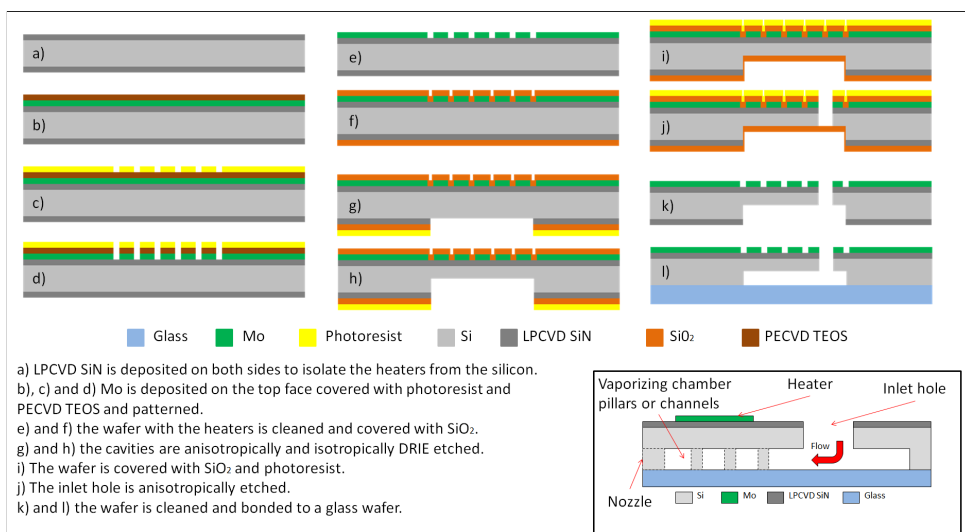


Figure 3.3: Process flow diagram showing the steps of the manufacturing. On the bottom right a schematic cross-section of the thrusters. The chamber can have either diamond pillars or serpentine channels.

Table 3.3: Codes used to identify the different thrusters.

Feature	Types		
Heater	1 - 21 lines	2 - 30 lines	
Nozzle	L - Long	W - Wide	B - Bell
Chamber	d - Diamond small	D - Diamond large	s - Serpentine small    S - Serpentine large

second was completely processed. The first wafer is intended to be used for electrical and mechanical tests only and was also used to first assess the bonding process. For these applications, the inlet hole is not needed. A single wafer yields 42 different devices that combine the different options described in chapter 1. For the mechanical and electrical experiments, 10 thrusters have been selected and 4 of them went through a further step of characterization to validate the devices in near-operational conditions. The complete list of thrusters is given in Table 3.4. Two devices (number 6 and 8) were found blocked, i.e. no flow can go from the inlet to the nozzle. This is probably due to incomplete etching or a defect caused by particles present during the manufacturing.

The thrusters received an identifier that describes the different design options. The code is in the form 'XX-ABx-*nn*' where 'XX' is the wafer number (00 or 01), 'A' is the type of nozzle (L - long, W - Wide, B - bell), 'B' is the type of chamber (d - diamond small, 'D' - diamond large, 's' - serpentine small, 'S' - serpentine large), 'x' is the type of heater (1 - 21 lines, 2 - 30 lines), and '*nn*' is the thruster number in case of repetition.

The test setup for the measurements is depicted in Fig. 3.4. It comprises a computer that controls the power supply for the heaters and the syringe pump used to pump water inside the thrusters at the desired flow rates. A list is presented in Table 3.5 with the ranges for each component and the respective accuracy. The biggest source of inaccu-

Table 3.4: List of selected thrusters. Test 1 is the mechanical test, test 2 is the electrical test, and test 3 is the operational test. The codes are presented according to the description given in Table 3.3

Thruster	Code	Test 1	Test 2	Test 3	Detail
1	00-LD1-01	×	×		no inlet
2	00-Ld1-01	×	×		no inlet
3	00-WD2-01	×	×		no inlet
4	00-Bd2-01	×	×		no inlet
5	01-LS1-01	×	×	×	
6	01-BD1-01	×	×		nozzle blocked
7	01-BS2-01	×	×	×	
8	01-WS2-01	×	×		nozzle blocked
9	01-Ld1-01	×	×	×	
10	01-WD2-01	×	×	×	
11	01-Ws1-01	×			
12	01-Bs2-01	×			

Table 3.5: List of equipment used in the tests with the respective ranges and accuracies.

Equipment	Function	Output
ES 030-10	Power supply	0–30V ± 5mV / 0–10A ± 6mA
NE-1000	Pump - 2.5 mL syringe	$2.5595 \times 10^{-3}$ –186.15mL/h
A35sc	Thermal camera	–40–160pm5°C
MS5837-30BA	Pressure/Temperature sensor	0–30bar ± 0.1bar / –20–85bar ± 4°C

racies is related to the mechanical movement of the pump that causes small variations in the flow rate that can be seen in the pressure measurements as reported by [Zeng et al. \(2015a,b\)](#); [Korczyk et al. \(2011\)](#). The data of temperature and pressure from the interface of the thruster is sent to the computer which also measures the voltage and current levels of the power supply. For the electrical characterization of the resistances, no water is injected into the thruster.

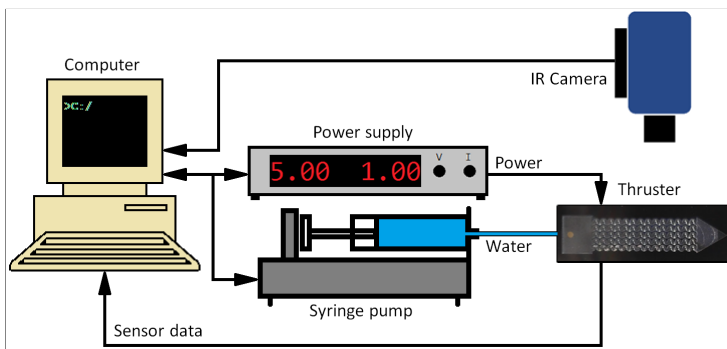


Figure 3.4: Test configuration for electrical and operational characterization. The infra-red camera is only used during the electrical characterization. The pressure/temperature sensor is attached to the thruster interface.

A special interface, shown in Fig. 3.5, has been designed made out of Teflon and aluminum to allow the easy operation of the thrusters. This interface provides the means for electrical connection to the heaters and also a leak-free connection for the propellant feeding line. Also, a digital sensor measures the pressure and temperature of the liquid being injected into the thruster. The sensor measures pressures in the range  $0\text{--}30 \pm 0.1$  bar and temperatures in the range from  $-20\text{--}85 \pm 4^\circ\text{C}$ .

3

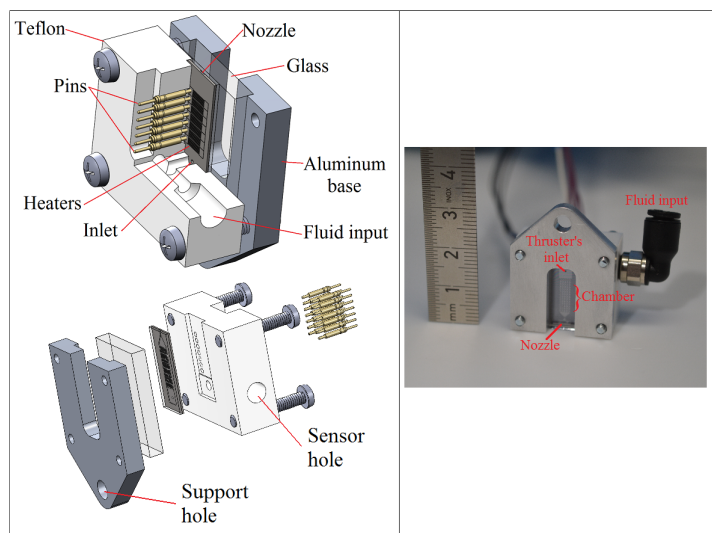


Figure 3.5: Interface for easy operation of the thrusters. Top left corner: a cut showing the details of the pins and the fluidic channels; bottom left corner: an exploded view of the 3D model; right side: a photo of the interface. The pressure and temperature sensor are on the side opposite to the fluid input. The spring loaded pins connect the heaters to the power supply.

### 3.4.1. MECHANICAL CHARACTERIZATION

All the devices have been subject to a mechanical characterization using an optical microscope in order to evaluate the dimensions of the features and compare them with the designed values. Table 3.6 presents the design parameters for the structures. The values  $d_1$  and  $d_2$  refer to the dimensions of the channels. In the case of diamond pillars, these are the sizes of the diamonds as indicated in Fig. 3.1; in the case of serpentine channels, these are the inner and outer radii of the semi-circles. The surface roughness is also characterized in order to evaluate the results of the last step of the etching process (isotropic etching). The effect of the surface roughness is an important parameter that affects the performance of microthrusters and has been reported by [La Torre et al. \(2010\)](#); [Cai et al. \(2017\)](#).

Table 3.6: Parameters used in the design of the thrusters. All dimensions are in  $\mu\text{m}$ . Type descriptions can be found in Table 3.3.

Type	Nozzles					Channels		
	$w_{nd}$	$l_{nd}$	$w_{nc}$	$l_{nc}$	$w_t$	Type	$d_1$	$d_2$
L	500	645	3000	2600	45	d	160	40
W	780	660	3000	1500	45	D	580	160
B	500	500	3000	1600	45	s	60	20
						S	266	54

### 3.4.2. ELECTRICAL CHARACTERIZATION

The devices were subject to a resistance test in order to characterize the temperature resistance coefficient  $\alpha$  given by:

$$\alpha = \frac{R - R_0}{R_0(T - T_0)} \quad (3.3)$$

where  $R$  is the resistance of the heaters,  $T$  is the current temperature, and  $R_0$  is the resistance measured at temperature  $T_0$ . The value of  $\alpha$  can be characterized for each device and later used to estimate the temperature of the heaters. As the devices are very small and made of silicon which is good thermal conductor, a zero gradient of temperature is assumed for the device. Therefore we can estimate that the temperature of the whole device is the same as the one estimated for the heaters. This approach has also been used to characterize similar devices made of molybdenum (Mele et al., 2012).

The test consists in applying a constant voltage to the heaters, measuring the current passing through them, and recording images with the thermal camera. Fig. 3.6 shows a sequence of images taken with the infra-red camera from the nozzle exit plane. The nozzle face of the thruster is in the middle of the image where we see the highest temperatures. Thus, the flow vector is normal to the plane of the picture. This approach provides a good estimation of the temperature, given the assumption that the whole thruster is at the same temperature.

The images of the thermal camera are then used to estimate the average temperature of the thruster over time. This average temperature is used to estimate  $\alpha$  for each thruster. The test starts with applying very low power to the heaters in order to measure the initial resistance. Then the power is increased in two steps applying first 5 V till the temperature stabilizes at a certain value (i.e. reaches steady state) and 7 V till it reaches steady state. Based on the measurements for each device, the value of  $\alpha$  is estimated using (3.3). In total, 10 devices have been characterized using this method.

### 3.4.3. OPERATIONAL CHARACTERIZATION

#### CONSTANT MASS FLOW RATE

In the last step of characterization, four devices have been tested in order to validate the devices in conditions close to operational. The test consists of injecting water into the thruster and applying power to the heaters to vaporize the water. The data from the sensors, i.e. pressure and temperature, and from the power supply is collected and also

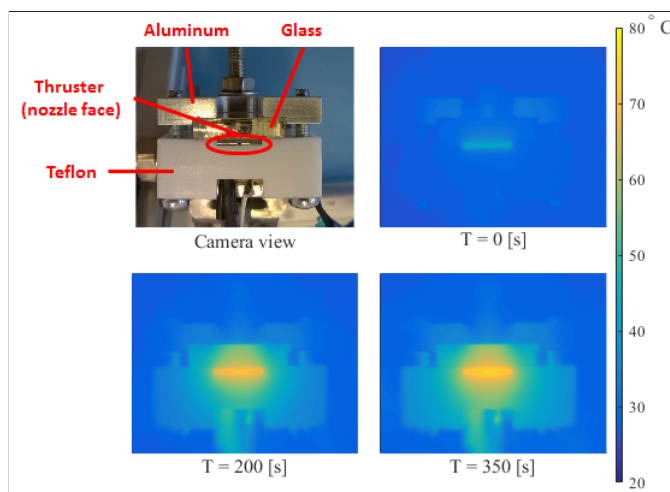


Figure 3.6: Thermal images of different moments of the test.

used during the tests as feedback information for manual control of the input variables (flow rate and power).

Water is pumped into the thrusters using the pump with a glass syringe of 2.5 mL to provide a constant mass flow rate sufficient to achieve a pressure of 5 bar in the vaporizing chamber. Although it is a reliable way of controlling the thrusters, it is only applicable for experimental testing since it does not represent the system as in the real application which will consist of a pressurized tank that provides the propellants to the thruster. Also, as already mentioned the syringe pump causes low frequency pressure fluctuations in the flow. These fluctuations might affect the stability of the two-phase flow inside the chamber (i.e. droplets can be ejected during the peaks in pressure).

The manual control is done based on the visual behavior of the vaporization. The power and mass flow rate are manually set to such values that correspond to a complete vaporization of the water without spotting any droplets coming out of the nozzle. The avoidance of droplets is very important because the heaters, made of Mo, can oxidize very easily when in contact with water at high temperatures. A video showing one of the tests is available at [Silva \(2017\)](#). Fig. 3.7 shows some snapshots at different moments of a test.

A steady state is achieved when the complete boiling is occurring at an arbitrary section of the chamber. At this operating state, the power and mass flow rate are adjusted to achieve a constant pressure in the chamber of approximately 5 bar.

#### VARIABLE MASS FLOW RATE

For this experiment, a digital microscope with frame rate of 20 fps and a resolution of  $640 \times 480$  pixels has been used. The aim of this experiment is to characterize the gas volume changes in the vaporization chamber that occur due to different pressures and different chip temperatures. This analysis will help in the development of the models in the next chapter.

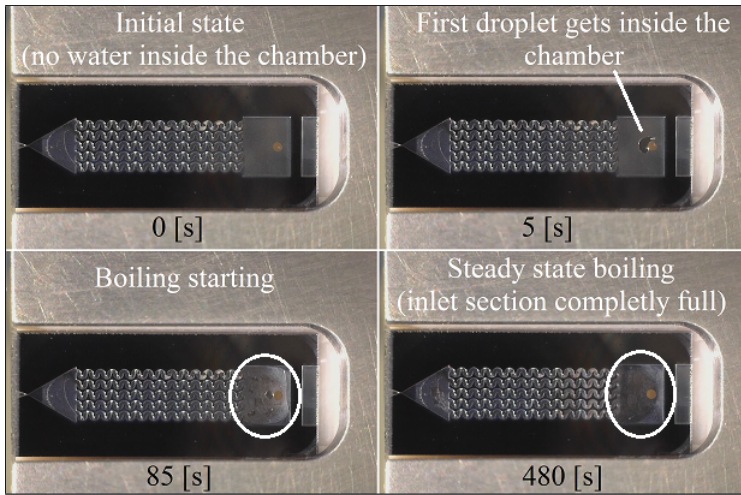


Figure 3.7: Water is pumped very slowly in the beginning in order to avoid instabilities. Top left corner: water has not yet come inside the chamber; top right corner: water just getting in the chamber; bottom left corner: chamber partially full and boiling; bottom right corner: complete boiling during steady state.

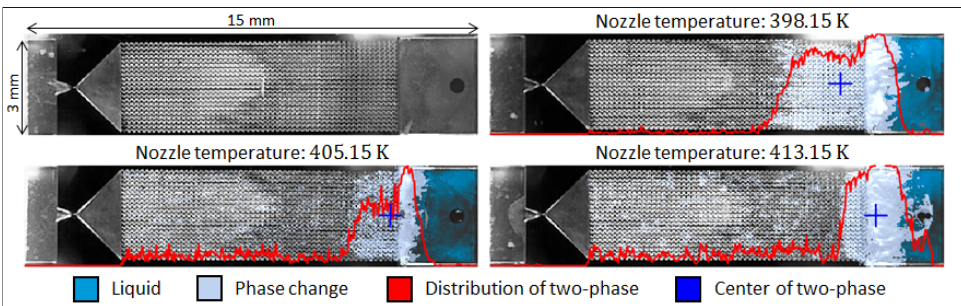


Figure 3.8: Snapshots used for the measurement of the volume. An empty thruster is shown on the top left corner for reference.

The movement of the two-phase part is the only visible part of the propellant and is used to determine the percentage of liquid or gas inside the chamber (see Fig. 3.8). The movement is detected by taking the difference between each pixel of a frame and the same pixel of a successive frame. Then, the two-phase part of the flow is where the difference between the successive frames is higher than a certain threshold. A threshold of 80% has been empirically identified as the best value when the detected movement is similar to the movement seen with the naked eye. We can see the linear fit of the volume and the temperature in Fig. 3.9 where the temperatures measured at the nozzle section were ranging from 398.15 K to 413.15 K for a pressure of 5 bar. Similarly, with a pressure of 3 bar the maximum and minimum volumes where observed at temperatures of 383.15 K and 408.15 K.

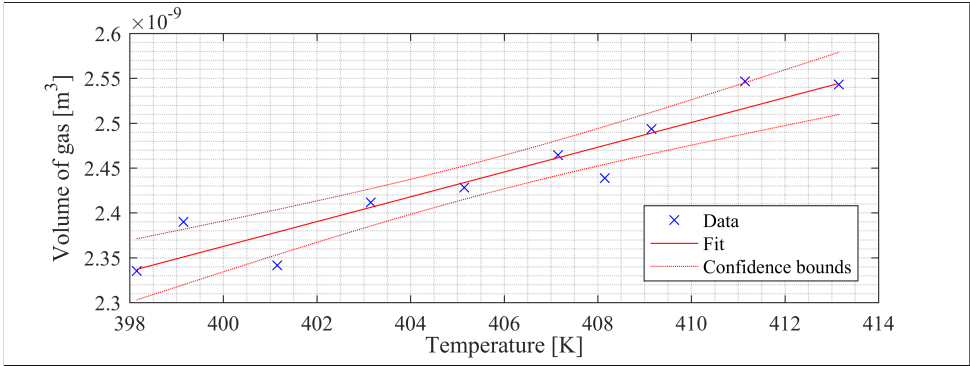


Figure 3.9: Linear fitting of the volume of vapor inside the chamber as a function of the nozzle temperature for a pressure of 5 bar.

### 3.5. RESULTS AND DISCUSSION

#### 3.5.1. MECHANICAL CHARACTERIZATION

The structural dimensions have been assessed as described in section 3.4 with an optical microscope. In Table 3.7 the average measured values are shown and the designed values are in brackets. In general, the averages are slightly smaller than what they were designed. Figure 3.10 shows the boxplot of the percentage of difference between designed and measured values. The heaters were also measured in order to compare with the designed values. On average each line of the heaters is around 11.3  $\mu\text{m}$ .

Table 3.7: Average measured values of the dimensions of the thrusters in  $\mu\text{m}$ . Design values are in brackets.

Type	Nozzles					Channels		
	$w_{nd}$	$l_{nd}$	$w_{nc}$	$l_{nc}$	$w_t$	Type	$d_1$	$d_2$
L	$489.2 \pm 2.7$ (500)	$626.0 \pm 4.2$ (645)	$2979.0 \pm 5.6$ (3000)	$2549.2 \pm 22.9$ (2600)	$25.1 \pm 3.5$ (45)	d	$10.3 \pm 0.3$ (160)	$2.8 \pm 0.1$ (40)
W	$777.7 \pm 1.5$ (780)	$643.6 \pm 2.9$ (660)	$2980.4 \pm 4.9$ (3000)	$1489.5 \pm 20.9$ (1500)	$26.0 \pm 2.8$ (45)	D	$547.7 \pm 4.9$ (580)	$144.3 \pm 4.7$ (160)
B	$492.6 \pm 4.5$ (500)	$486.9 \pm 2.3$ (500)	$2983.3 \pm 10.2$ (3000)	$1581.3 \pm 13.0$ (1600)	$20.1 \pm 3.2$ (45)	s	$76.6 \pm 0.1$ (60)	$8.2 \pm 0.9$ (20)
						S	$289.7 \pm 7.2$ (266)	$39.9 \pm 2.1$ (54)

The depth of the cavities has been measured with a Dektak Surface Profiler and on average they are 100  $\mu\text{m}$ . With these measurements, we can recalculate the performance parameters estimated in section 3.2. As it is seen in Table 3.8, the mass flow and the thrust are reduced almost by half due to the reduction in the throat width while the specific impulse remains the same. As a consequence the power needed also decreases. Although the differences seen are acceptable, this indicates the need for more precision in the manufacturing to reduce differences between the designed and manufactured devices.

The characterization of the surface roughness was done with AFM (Atomic Force Microscopy) using a nTEGRA Aura AFM with NSG10 tip (10 nm tip radius) and a 100  $\mu\text{m}$

Table 3.8: Comparison between the design parameters (in brackets) and the ones calculated with the measured values.

Nozzle	$\dot{m}$ [mg/s]	$F$ [mN]	$I_{sp}$ [s]	$P$ [W]
L	0.41-1.91 (0.73-3.42)	0.43-2.16 (0.75-3.79)	107.34-115.60 (105.22-112.89)	1.04-5.03 (1.87-9.01)
W	0.42-1.97 (0.73-3.42)	0.45-2.27 (0.77-3.86)	108.34-117.22 (106.98-115.09)	1.08-5.20 (1.87-9.01)
B	0.33-1.53 (0.73-3.42)	0.35-1.75 (0.75-3.79)	107.94-116.51 (105.22-112.89)	0.84-4.03 (1.87-9.01)

closed-loop sample scanner. The measurement was done in an area of  $40 \times 40 \mu\text{m}$  of a sample that has not been completed in terms of manufacturing since an open device is needed for the measurement. As the last step of the manufacturing is the isotropic etching, we can assume that the roughness of all the surfaces (including the nozzle throat) is similar to the measured roughness of the sample. Table 3.9 shows the average values of the measurement taken from the sample presented in the third column.

### 3.5.2. ELECTRICAL CHARACTERIZATION

In Fig. 3.11 the measurements recorded with the camera are plotted against the resistance measured for four devices. These measurements (done with 10 devices) are used to estimate the value of  $\alpha$  as shown in Table 3.10. The average value is  $\bar{\alpha} = 1.09 \times 10^{-3} / ^\circ\text{C}$  and standard deviation  $\sigma_\alpha = 1.79 \times 10^{-4}$  and can be used for other devices that have been manufactured together. An accurate measurement of the initial resistance at room temperature is very important to avoid discrepancies in the estimation of temperature. Fig. 3.12 shows the comparison between the measurements with the thermal camera and the estimation based on (3.3). The noise seen in the plots comes from the experimental setup that was built using standard equipment with limited precision. This is useful in order mimic the conditions in which the thruster will eventually operate, i.e. in a very small satellite with limited electronics in a harsh environment (i.e. space). As we can see, without considering the noise, the estimation matches very well with the measurements.

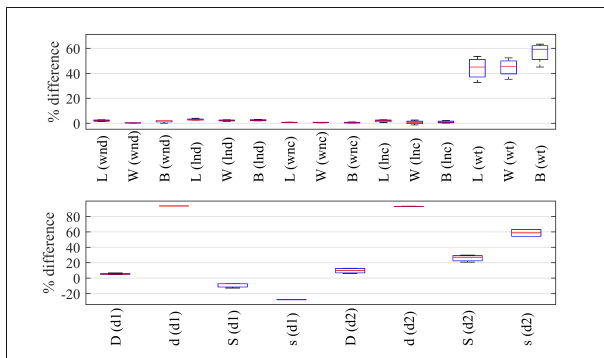
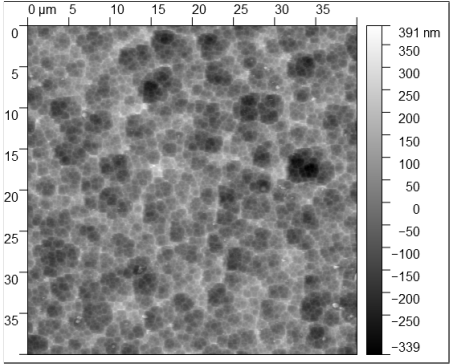


Figure 3.10: Boxplot of the difference between designed and measured values.

Table 3.9: Surface roughness statistical values.

Property	Value	Measurement sample
Minimum	-338.671 nm	
Maximum	391.408 nm	
Average value	11.412 nm	
Median	12.999 nm	
$R_a$ ( $S_a$ )	65.223 nm	
$R_{RMS}$ ( $S_q$ )	81.803 nm	
$R_{RMS}$ (grain-wise)	81.803 nm	
Skew	-0.152	
Kurtosis	0.1514	
Surface area	$1.67834 \times 10^{-9} \text{ m}^2$	
Projected area	$1.60157 \times 10^{-9} \text{ m}^2$	
Variation	$438.125 \mu\text{m}^2$	
Entropy	-14.903	
Entropy deficit	0.0029304	
Inclination $\theta$	0.03 deg	
Inclination $\phi$	165.26 deg	

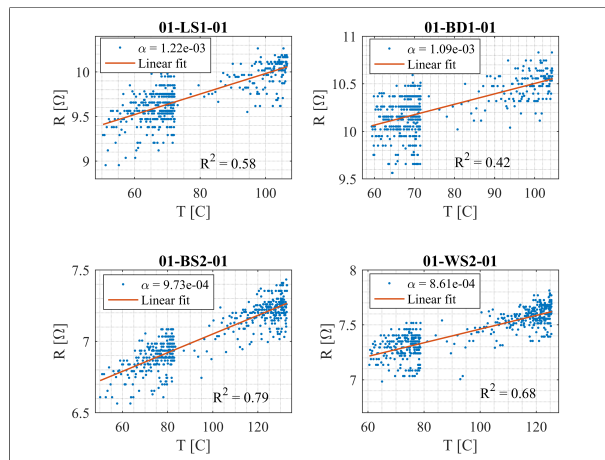


Figure 3.11: Resistance of the heaters as a function of the temperature for 4 devices. The concentration of points around different values (steady state values) is due to the two-level voltage increase.

### 3.5.3. OPERATIONAL CHARACTERIZATION

As mentioned earlier, four thrusters have been tested with water under conditions close to operational but with ambient pressure equal to atmospheric pressure. Water is pumped inside the thruster (very slowly in the beginning) and, after it reaches the inlet section, the power is increased to start the vaporization. When this happens the pressure increases and the power is manually controlled to allow full vaporization (visually) of the propellant. Then, the mass flow rate and the power are kept constant in order to

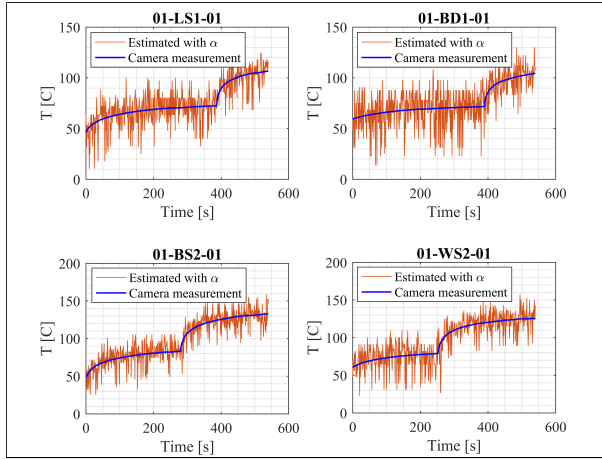


Figure 3.12: Comparison between measured temperature of four thrusters and the estimated values using (3.3).

Table 3.10: Average values of  $\alpha$  for all tested thrusters.

Thruster	Code	$\alpha$ [ $^{\circ}\text{C}^{-1}$ ]
1	00-LD1-01	$1.30 \times 10^{-3}$
2	00-Ld1-01	$1.33 \times 10^{-3}$
3	00-WD2-01	$1.28 \times 10^{-3}$
4	00-Bd2-01	$8.76 \times 10^{-4}$
5	01-LS1-01	$1.22 \times 10^{-3}$
6	01-BD1-01	$1.09 \times 10^{-3}$
7	01-BS2-01	$9.73 \times 10^{-4}$
8	01-WS2-01	$8.61 \times 10^{-4}$
9	01-Ld1-01	$9.55 \times 10^{-4}$
10	01-WD2-01	$1.01 \times 10^{-3}$
Average		$1.09 \times 10^{-3}$
Standard deviation		$1.79 \times 10^{-4}$

maintain the pressure in the chamber at approximately 5bar (as mentioned before the control is done manually and with visual feedback). In Fig. 3.13 the values of pressure, power, and mass flow rate during the steady state part of the experiment are plotted. We can see that the mass flow rate is not the same even though the nozzle throat area is not much different. The measured values for the throat width are 23.1, 16.5, 20.9 and 23.6  $\mu\text{m}$  for thrusters 5, 7, 9 and 10 respectively. This fact might be attributed to the efficiency in the vaporization which is dependent on the shape of the microchannels. In Table 3.11 we can see the difference in energy per milli-gram of water used in the process. It is clearly seen that the one with the small diamonds (thruster 9) is the most efficient due to its larger surface area (it is 3.5, 3.6, and 2.9 times larger than thrusters 5, 7, and 10 respectively). We can also see in Fig. 3.13 the variation in the pressure that is caused by the syringe pump as described in section 3.4. Although this effect is clearly visible in the

pressure measurements, no instability (i.e. no droplets coming out of the nozzle) was spotted during the steady state.

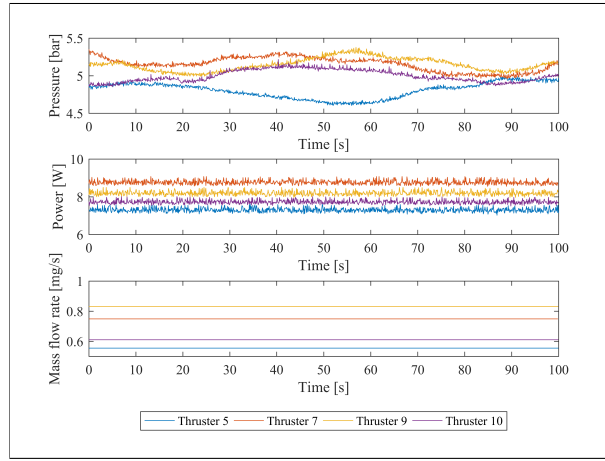


Figure 3.13: Measured pressure, power, and mass flow rate for the tested devices. The low frequency variation in the pressure is caused by mechanical oscillations in the pump.

Table 3.11: Average values measured during steady state.

Thruster	Pressure [bar]	Mass flow rate [mg/s]	Measured power [W]	Calculate power [W]	Energy [J/mg]	Efficiency [%]
5	4.80	0.55	7.29	1.47	13.16	20.2
7	5.15	0.75	8.76	1.99	11.71	22.7
9	5.15	0.83	8.19	2.21	9.84	27.0
10	5.00	0.61	7.72	1.62	12.66	21.0

Considering the applied mass flow rate, we can recalculate the power needed to heat-up and vaporize the water and subtract it from the measured power in order to estimate the losses to the structure and the environment which on average for all the tests is around  $P_{loss} = 6.17W$ . This represents an efficiency in the energy use of around 23% on average.

Fig. 3.14 shows the resistances measured during the steady state and the temperature estimated with these values. Given the pressure of water around 5 bar, the saturation temperature is around 151.83 °C. As the power is controlled such that full vaporization occurs, we can consider that this is the temperature that should be measured. This approach is valid for characterization, however in the real operations of the thrusters the power can be set higher to further increase the temperature of the vapor. We can see that the estimated temperature is slightly different for each thruster which can be attributed to differences in the measurements of the initial resistances and initial temperature.

Table 3.12 presents a comparison of the expected performance in terms of thrust, specific impulse and power of the devices tested with water and the results of other references found in the literature. The last column shows the thrust to power ratio which is

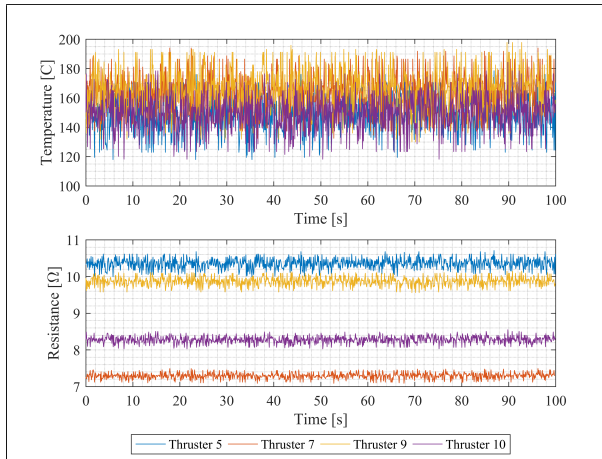


Figure 3.14: Estimated temperature derived from the measured resistance for the tested devices.

calculated dividing the thrust by the power. The level of thrust is in a range comparable to other devices but it needs to be experimentally measured. The power is the power needed to heat up not only the thruster and the propellant but also the complete interface which has not yet been optimized in terms of thermal isolation. Also, the tests were conducted under room conditions which means that a significant amount of power is lost to the environment. Therefore, the power consumption of an optimized system in vacuum is expected to be significantly lower than these values. However, looking at the parameter  $\tau$  we can see that the (calculated) delivered thrust per unit power is already in a range among the highest values.

Table 3.12: Comparison between the results of this work and other references. The values marked with \* are calculated or simulated.

Reference	$P$ [W]	$\dot{m}$ [mg/s]	$F$ [mN]	$I_{sp}$ [s]	$p$ [bar]	$T$ [K]	$\tau$ [mN/W]
Cen and Xu (2010)	n/a	2.33–8.33	2–6.5	65–105	1.0–2.6	454–574	n/a
Cheah and Low (2015)	4.01	1.0	0.634	31	n/a	n/a	0.16
Chen et al. (2010)	n/a	2.08–16.6 *	1–6 *	48.9–36.9 *	1.0–2.0	423–573	n/a
Karthikeyan et al. (2012)	7.1–9.2	1.0	0.034–0.07	3.42–6.9	1.0	400–422	0.005–0.007
Kundu et al. (2012)	1.6–3.6	0.2–2.04	0.15–1.01	50–105	1.0	374–474	0.09–0.28
Maurya et al. (2005b)	1–2.4	0.7	0.005–0.12	17.5 *	n/a	n/a	0.01–0.05
Mukerjee et al. (2000)	10.8	8.8	0.46	5.33 *	n/a	n/a	0.04
Ye et al. (2001)	30	0.038	0.003	7.78 *	n/a	n/a	0.0001
This work							
Thruster 5	7.29	0.55	0.67 *	124.02 *	4.80	423.03	0.09
Thruster 7	8.76	0.75	0.88 *	119.80 *	5.15	425.65	0.10
Thruster 9	8.19	0.83	0.98 *	120.20 *	5.15	425.65	0.12
Thruster 10	7.72	0.61	0.74 *	123.72 *	5.00	424.54	0.10

### 3.6. CONCLUDING REMARKS

This chapter presented the details of the design, manufacturing, and characterization of microresistojets with integrated heating and temperature measurement capabilities that operate by vaporizing water and accelerating the vapor with a convergent-divergent nozzle. In total, 12 devices have been assessed for their mechanical characteristics while 10 of those have undergone an electrical characterization to allow the estimation of temperature using measurements of resistance. Finally, four devices have been tested under near-operational conditions in order to validate the current thruster design and have a glimpse into the operational characteristics of such devices. The operations of the devices were successfully demonstrated using water as propellant and having online measurements of temperature that can be used for feedback control, for example. The results presented here serve to determine the fundamental operational and design characteristics of this kind of propulsion system and will be useful in future implementations.

The manufacturing process has been effective in the sense that most of the devices could be tested with water with the exception of two that have been found blocked. The use of a glass wafer to cover the cavities was very important since it provides a good visualization of the vaporization process and allows the visual control of the operation which would be much more difficult without it. Also, it provides valuable information for automatic control of temperature of the semi stochastic boiling process. However, this will not be necessary in the flight models where no flow visualization is required and a pure silicon wafer can be used together with an automatic controller.

The use of molybdenum heaters has proven to be a very effective design choice since it is very stable at the temperatures used and can also achieve very high temperatures up to 850 °C. However, the heaters need a protection, such as PECVD silicon oxide, to avoid oxidation at temperatures higher than 350°C. The measurements of temperature were used to control the process and keep the vaporization stable showing the reliability of this technique. The modularity of the design allows the measurement of temperature at different positions in the chamber and will be further investigated in the future.

The developed interface for testing the thrusters has proven to be very robust and easy to use. The thrusters can be tested right after dicing and they can be reconnected to the interface in a couple of minutes reducing testing time. It provides a good way of connecting the heaters to a power supply without the need of wire bonding and also a leak-free connection for the fluid inlet. The sensor included in the interface provides a measurement of pressure very close to the chamber such that it is safe to assume that the measured values are representative of the ones inside the chamber. This interface also facilitates the fast replacement of thrusters without damaging the devices.

Compared to other devices found in the literature, the tested thrusters have shown a performance close to the highest specially in terms of thrust to power ratio ( $\tau$ ) which is very interesting for nano- and pico-satellites that have limited capabilities in power generation. However, the values of thrust have been calculated based on the measurements of pressure, temperature, and mass flow. In order to validate these values, a direct measurement of the thrust has to be performed.

# 4

## MODELING OF VAPORIZING LIQUID MICROTHRUSTERS

*Let us die to make things cheap.*

From the song *Steer your way* by Leonard Cohen

*This chapter presents a comprehensive approach for the modeling of VLM systems. The model combines analytical and empirical relations derived from the extensive experimental analysis presented in the previous chapter and fundamental physical laws. This allows modeling of key parameters of the system, such as mass flow rate. The entire system comprises a tank to store the liquid propellant, a valve to control the mass flow, and a microthruster that vaporizes the propellant and accelerates it generating thrust. A sensitivity analysis is performed considering the boundaries of the modeling space.*

---

Parts of this chapter have been published in:

Silva, M. A. C., Silvestrini, S., Guerrieri, D. C., Cervone, A., Gill, E., *A Comprehensive Model for Control of Vaporizing Liquid Microthrusters*, IEEE Transactions on Control Systems Technology, manuscript accepted.

## 4.1. INTRODUCTION

ALTHOUGH the development of VLM systems has been quite significant, the literature regarding modeling of such system is limited to relations of power and thrust and cover only the steady state behavior (Maurya et al., 2005a; Bidabadi et al., 2010). A model that reproduces the dynamic behavior of the system is very important for the design of controllers to allow the proper operation of the thruster and also for the design of the entire spacecraft.

This chapter presents a comprehensive model of the VLM combining analytical and empirical relations and including models of all the components of a VLM system. The model allows the simulation of the complete system including particularities involved in the process such as temperature and pressure changes caused by the operation of the thruster. The system considered is composed by a tank to store the propellant, a valve to control the liquid flow, and a thruster to vaporize the liquid and generate thrust. The thruster is designed to work with water as the propellant since it has been shown that water is a very good candidate for this kind of propulsion system due to its density that results in a higher  $\Delta v$  (velocity change) per volume of propellant when compared to other safe substances (Guerrieri et al., 2017).

## 4.2. MODELING APPROACH

Fig. 4.1 shows the architecture of the micropropulsion system used in the modeling that comprises a tank (1) to store the liquid propellant (water) pressurized with nitrogen, a solenoid valve (2) to control the flow of liquid inside the thruster, a MEMS resistojet (3) with integrated heaters for the vaporization and temperature estimation, and sensors (4) for pressure and temperature measurement. The pressure sensors are placed in the tank and right before the thruster's inlet to measure the upstream and downstream pressures. The latter is the same as the chamber pressure. The temperature sensors are placed close to the nozzle which is the most suitable position due to the size of the thruster. Chapter 3 describes the design of the MEMS resistojet.

The dynamics of the system is basically governed by two factors: an unbalance between the three mass flow rates indicated in Fig. 4.1 that contributes to the pressure changes inside the vaporization chamber, and the power applied to the heaters that affects the vaporization process thus the vaporization rate and the vapor quality. As the

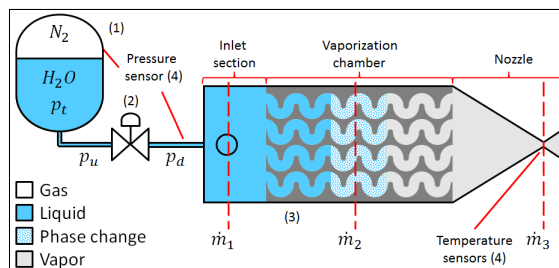


Figure 4.1: VLM system showing a tank (1), a valve (2), a thruster (3), and sensors (4). The mass flow rate  $\dot{m}_1$  is the liquid flow rate,  $\dot{m}_2$  is the vaporization rate, and  $\dot{m}_3$  is the mass flow of the nozzle.

mass flow rates considered are in terms of milligrams per second, it is assumed that the changes in the mass of propellant do not influence the spacecraft dynamics. The valve is used to control the mass flow rate  $\dot{m}_1$  affecting the pressure inside the thruster  $p_1 = p_d$  which, in turn, affects the mass flow rate  $\dot{m}_3$ . The vaporization rate  $\dot{m}_2$  is affected by changes in pressure that change the boiling point of the propellant and by changes in the applied power that change the temperature of the thruster affecting the heat transfer to the fluid.

In order to model this dynamics, the model of the microthruster has been divided into four parts:

- Nozzle model: provides the mass flow rate  $\dot{m}_3$  based on the pressure in the chamber.
- Vaporization model: calculates the volumetric fraction of vapor inside the chamber.
- Pressure model: calculates the pressure inside the chamber based on the density of the vapor part.
- Temperature model: relates the thruster temperature to the applied power.

The model of the solenoid valve combines models of three subsystems:

- Electromagnetic subsystem: models the electromagnetic force generated by the solenoid.
- Fluidic subsystem: models the flow through the valve.
- Mechanical subsystem: models the motion of the plunger.

Finally, the tank is modeled as a pressurized container that reduces its pressure with the ejection of liquid and expansion of the pressurant gas.

In the system considered in this analysis, as already mentioned, there are four identical thrusters and each one has a its own valve; the tank with the propellant, however, is shared by all the thrusters.

#### 4.2.1. BOUNDARIES AND REQUIREMENTS

The models presented in this chapter are developed to work within some operational boundaries set based on the requirements commonly applied to CubeSats and PocketQubes. Propulsion systems for these spacecraft usually are at a development stage that do not require strict performance parameters. Therefore the applicable requirements regard electrical and/or mechanical constraints, and safety constraints to not endanger the mission.

The maximum thrust has been estimated considering a scenario where the center of mass of the spacecraft is at most 2 cm off of the geometric center (Silva et al., 2018). Then the maximum thrust is calculated based on the maximum torque that the reaction wheels of the spacecraft can provide, and the torque generated by a thruster positioned at the center of the furthest face of the spacecraft and pointing towards the geometric center. For a 3 units CubeSat with a reaction wheel that can provide  $2 \times 10^{-3}$  Nm,



As the propellant is boiling inside the chamber, it is assumed that the temperature of the gas is the saturation temperature. With this assumption, the temperature of the vapor can be calculated based on the pressure using (4.1) known as the Antoine equation.

$$T = \frac{B}{A - \log_{10} p} + C \quad (4.1)$$

where  $A = 10.27$ ,  $B = 1810.94$ , and  $C = 28.67$  for pressure in Pa and temperature in the range 372.15–647.15 K (DDBST, 2018).

Considering the pressure in the range 1–5 bar, then we can replace the term  $\frac{p_1}{\sqrt{T_1}}$  in (2.3) with a function of the pressure:

$$\frac{p_1}{\sqrt{T_1}} = \frac{p_1}{\sqrt{\frac{B}{A - \log_{10} p_1} + C}} \approx \alpha_1 p_1 + \beta_1 \quad (4.2)$$

where  $\alpha_1$  and  $\beta_1$  are the coefficients of the first order Taylor series expansion and are functions of the parameters used in (4.1) and the linearization point  $p_s$ :

$$\alpha_1 = \frac{C \log_{10}(p_s)^2 - (2AC + B) \log_{10}(p_s) + A(AC + B) - \frac{B}{\ln(10)}}{\left(C + \frac{B}{(A - \log_{10}(p_s))}\right)^{\frac{3}{2}} (A - \log_{10}(p_s))^2} \quad (4.3)$$

$$\beta_1 = \frac{p_s}{\sqrt{C + \frac{B}{(A - \log_{10}(p_s))}}} - \alpha_1 p_s \quad (4.4)$$

Finally, we can rewrite (2.3) as follows:

$$\dot{m}_3 = (\alpha_1 p_1 + \beta_1) A_t \sqrt{\frac{k}{R_s} \left(\frac{2}{k+1}\right)^{\frac{k+1}{k-1}}} \quad (4.5)$$

Evaluating the expressions around the middle point in the range of pressure of interest, i.e.  $p_s = 3\text{bar}$ , we get  $\alpha_1 = 0.048\text{K}^{-\frac{1}{2}}$  and  $\beta_1 = 626.99\text{Pa K}^{-\frac{1}{2}}$ .

The resulting linear equation is faster to solve computationally and provides a good fitting for the pressure and temperature term. Fig. 4.3-a shows the comparison between the proposed linear approximation and the curve for  $\frac{p_1}{\sqrt{T_1}}$  with the temperature calculated using (4.1).

#### VAPORIZATION MODEL

The vaporization rate is related to several aspects of the two phase flow and the heat transfer which can be very difficult to measure. In order to overcome this challenge, an empirical model for the change in the volume of gas inside the chamber has been developed. One of the thrusters presented by Silva et al. (2017) was selected to undergo a series of tests to correlate the pressure and chip temperature to the volume of gas inside the chamber. Then a linear model for the volume of gas was identified using snapshots taken during the experiments as shown in Fig. 3.8. For this experiment, a digital microscope with frame rate of 20 fps and a resolution of  $640 \times 480$  pixels has been used.

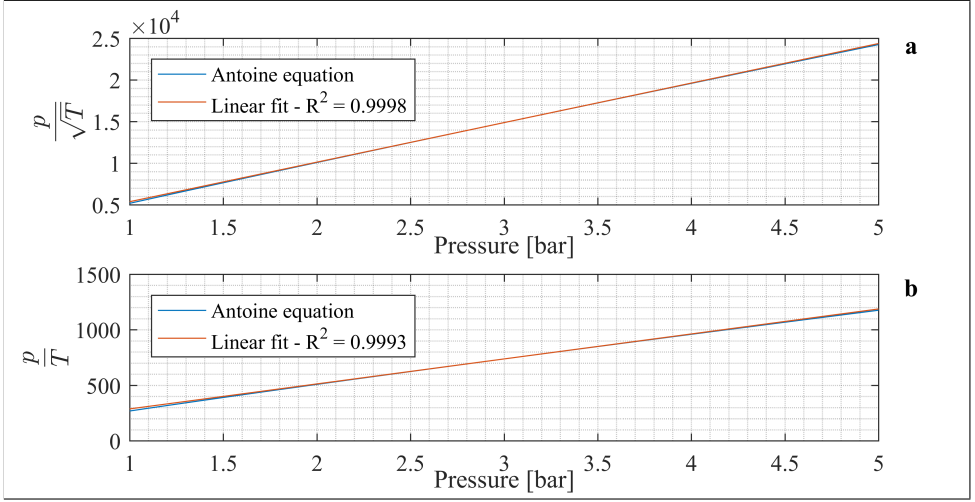


Figure 4.3: Linear approximation of the pressure and temperature terms used in the modeling considering 401 points calculated using (4.1).

In Chapter 3, an analysis of the volume changes caused by different pressures and chip temperature was presented. This analysis is used here to develop a model that relates the pressure inside the chamber and the temperature of the chip. Fig. 3.9 showed the linear fitting of data that is used to calculate the average volume of vapor  $V_{av}$  as a function of the temperature of the thruster and the pressure:

$$V_{av} = a_T T_n + a_p p + b \quad (4.6)$$

where  $a_T$ ,  $a_p$ , and  $b$  are the parameters of the linear regression and  $T_n$  is the temperature of the chip measured around the nozzle. In this analysis, the coefficients have been estimated as:  $a_T = 1.63 \times 10^{-11} \text{ m}^3/\text{K}$ ,  $a_p = -7.45 \times 10^{-15} \text{ m}^3/\text{Pa}$ , and  $b = -4.36 \times 10^{-10} \text{ m}^3$ .

In order to complete the model, we need an expression for the time derivative of the volume which in this analysis has been assumed to be a first-order linear system of the form:

$$\dot{V} = A(V_{av} - V) \quad (4.7)$$

where  $A = 75/\text{s}$  has been empirically chosen based on the image analysis already described. The rate of change in the volume is faster than the frame rate of the microscope indicating that the time constant  $\tau = \frac{1}{A}$  of a first-order system is less than 2 ms.

Then the vaporization rate  $\dot{m}_2$  can be calculated as follows:

$$\dot{m}_2 = \dot{m}_1 - \dot{V} \rho_l \quad (4.8)$$

where  $\rho_l$  is the density of the liquid.

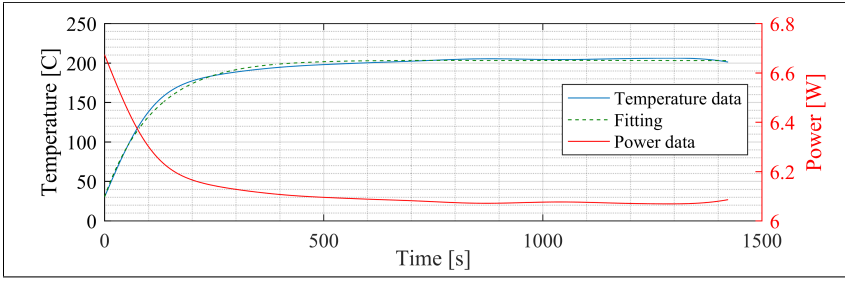


Figure 4.4: Fitting of temperature over time with a power input.

### PRESSURE MODEL

Considering the ideal gas law given by:

$$\frac{p}{T} V = mR_s \quad (4.9)$$

where  $m$  is the mass of gas. Following a similar approach as the linear approximation used in the nozzle model, we can approximate the term  $\frac{p}{T}$  by a linear relation reducing the equation to:

$$p = \frac{1}{\alpha_2} \left( \frac{mR_s}{V} - \beta_2 \right) \quad (4.10)$$

where:

$$\alpha_2 = \frac{C \log_{10}(p_s)^2 - (2AC + B) \log_{10}(p_s) + A(AC + B) - \frac{B}{\ln(10)}}{(B - C \log_{10}(p_s) + AC)^2} \quad (4.11)$$

$$\beta_2 = \frac{p_s}{\sqrt{C + \frac{B}{(A - \log_{10}(p_s))}}} - \alpha_2 p_s \quad (4.12)$$

Evaluating around the linearization point one gets  $\alpha_2 = 0.0023/\text{K}$  and  $\beta_2 = 62.17\text{Pa/K}$ . The results of this linearization are plotted in Fig. 4.3-b in comparison with the values calculated using (4.1).

### CHIP TEMPERATURE MODEL

The temperature of the thruster is modeled as a linear first-order system whose input is the applied power. The Laplace transfer function of the power-temperature system is given by (4.13):

$$\frac{T(s)}{P(s)} = \frac{K}{s + \frac{1}{\tau}} \quad (4.13)$$

where  $\tau = 119.5\text{s}$  and  $K = 28.5\text{K/(Ws)}$  have been experimentally estimated using data of power and temperature. Figure 4.4 shows the data used to fit the model.

As described in a previous research by Silva et al. (2017), the resistance used in the heaters is linearly dependent on the temperature. The change in resistance caused by changes in temperature is described by the following equation (Mele et al., 2012):

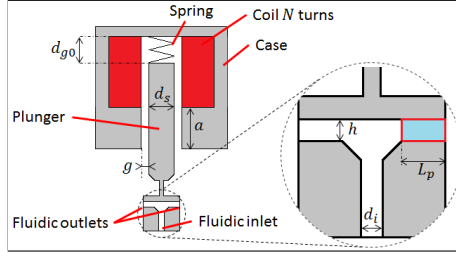


Figure 4.5: Reference geometry of the valve model. The part highlighted in blue is the parallel plates section used in the fluidic model. The top edge of the plunger moves up and down and the flow goes from left to right.

4

$$R = \alpha R_0 (T - T_0) + R_0 \quad (4.14)$$

where  $R$  is the resistance,  $T$  is the current temperature, and  $R_0$  is the resistance measured at temperature  $T_0$ . The value of  $\alpha$  has been experimentally characterized for many devices and on average is  $\alpha = 1.09 \times 10^{-3}/\text{K}$  (Silva et al., 2017).

### 4.2.3. VALVE

The analytical model of a solenoid-actuated microvalve is a complex system that can be described by interfacing three different physical systems: the electromagnetic, the fluidic and the mechanical system.

#### ELECTROMAGNETIC SYSTEM

The electromagnetic actuation of the valve takes place when a voltage is applied to the inner coil of the microvalve. The current flowing in the coil generates a magnetic field that pulls the magnetic plunger and consequently opens the microvalve. The equivalent electric circuit can be described by the following equation (Cheung et al., 1993):

$$v = R_c i + \dot{\lambda} \quad (4.15)$$

where  $v$  is the voltage,  $R_c$  is the coil equivalent resistance,  $i$  the electric current and  $\lambda$  is the flux linkage. The flux linkage is defined as  $N\Phi$  where  $\Phi$  is the magnetic flux. In order to express the flux linkage a simple representation of the magnetic circuit is required, assuming the solenoid is operating in the linear region. The electro-magnetic circuit can be represented as follows, according to Cheung et al. (1993):

$$Ni = \Phi \mathcal{R} \quad (4.16)$$

where  $N$  is the number of turns in the coil,  $\Phi$  is the magnetic flux, and  $\mathcal{R}$  is the global magnetic reluctance of the circuit. The latter can be determined by geometric considerations only, see Fig. 4.5, regardless of the material used in the valve, since the magnetic reluctance of the air gaps is prominent with respect to that of the metallic structure.

Rearranging (4.15) and (4.16), the flux linkage can be expressed as:

$$\lambda(x, i) = \frac{N^2 \mu_0 A_{sol} a}{a(d_{g0} - x) + \frac{d_{sol} g}{4}} i \quad (4.17)$$

where  $\mu_0$  is the air permeability constant,  $A_{sol}$  is the cross section area of the solenoid,  $a$  is the bottom iron strips length,  $d_{g0}$  is the initial air gap between the plunger and the iron core,  $d_{sol}$  is the solenoid diameter, and  $g$  is the side air gap between the plunger and the iron core.

The partial derivative of the flux linkage with respect to the electric current is the equivalent magnetic inductance  $L$  of the system, which depends on the position  $x$  of the plunger. The time derivative of the current can thus be expressed as:

$$\dot{i} = \frac{1}{L(x)} (v - i(R_c + \dot{x}L(x))) \quad (4.18)$$

which represents the first order differential equation of the transient behavior of the electric current. The magnetic force that is generated by the current can be derived from the co-energy, defined as the integral of the flux linkage against the current (Cheung et al., 1993):

$$F_{mag} = \frac{\partial}{\partial x} \left( \frac{L(x)}{2} i^2 \right) \quad (4.19)$$

where  $F_{mag}$  is the magnetic force and  $L$  is the inductance of the system.

#### FLUIDIC SYSTEM

The fluid flow within the microvalve is usually described by the orifice equation. Nevertheless, such equation is not appropriate to simulate correctly the transient behavior rapidly occurring during the microvalve actuation. For this reason, a novel approach has been developed to include the unsteady characterization of the fluid flow. Assuming the flow occurring between two infinite parallel plates, as shown in Fig. 4.5 by the section highlighted in blue, the Navier-Stokes equations can be rearranged to obtain the following equation describing the time derivative of the flow bulk velocity:

$$\dot{u} = -\frac{12\mu}{\rho h^2} u + \frac{\Delta p}{\rho_l L_p} \quad (4.20)$$

where  $u$  is the velocity of the fluid,  $\mu$  is the dynamic viscosity of the fluid,  $h$  is the height of the section (see Fig. 4.5), and  $L_p$  is the length of the section. The flow is considered incompressible, isothermal and unidirectional. It is important to note that the pressure drop is that of the parallel plates region, hence different from the pressure drop across the microvalve. The pressure loss can be calculated by geometrical considerations using a numerical analysis or by the discharge coefficient of the real hardware.

The outlet volumetric flow rate  $Q$ , and hence the mass flow rate, can be calculated from the outlet velocity  $u$  and area  $A_{out}$  which is a function of  $x$ :

$$Q = u A_{out}(x) \quad (4.21)$$

The inlet fluid flow is deviated by the plunger towards the outlet aperture; in turns, the fluid flow exerts a load on the plunger itself. The fluid force can be described using the momentum conservation of the Reynolds Transport Theorem:

$$F_{f,pl} = p_{in} A_{in} + \rho u^2 A_{in} - \rho_l \dot{Q}(x) (x + L_0) \quad (4.22)$$

where  $F_{f,pl}$  is the fluid force on the plunger,  $p_{in}$  is the inlet pressure,  $A_{in}$  is the inlet area, and  $L_0$  is the minimum height of the control volume. The first two terms represent the steady-state load, whereas the third term is linked to the transient load. Nevertheless, simulations showed that its influence is negligible.

### MECHANICAL SYSTEM

The motion of the plunger is driven by several external loads. The main contribution is certainly given by the electromagnetic force in (4.19). Its dynamics can be described by Newton's 2<sup>nd</sup> law as follows:

$$M\ddot{x} + c\dot{x} + k(x - x_0) = F_{mag} + F_{f,pl} - p_{out}A_{in} \quad (4.23)$$

where  $M$  is the mass of the plunger,  $c$  is the viscous coefficient,  $k$  is the elastic constant of the spring, and  $x_0$  is the spring pre-load.

### STATE-SPACE MODEL

Based on the equations developed in previous sections, the state space model can be expressed using the plunger position  $x = x_1$ , the plunger velocity  $\dot{x} = x_2$ , the electric current  $i = x_3$  and the fluid outlet velocity  $u = x_4$  as state variables, and  $y = \dot{m}_1$  the output of the system.

$$\begin{cases} \dot{x}_1 \\ \dot{x}_2 \\ \dot{x}_3 \\ \dot{x}_4 \end{cases} = \begin{cases} \frac{x_2}{M} (-cx_2 - k(x_1 - x_0) + F_{mag} + F_{f,pl} - p_{out}A_{in}) \\ \frac{1}{L(x_1)} (v - x_3 (R_c + x_2 \dot{L}(x_1))) \\ -\frac{12\mu}{\rho x_1^2} x_4 + \frac{\Delta p}{\rho L_p} \end{cases} \quad (4.24)$$

$$y = \rho x_4 A_{out}(x_1) \quad (4.25)$$

The presented state-space model fully describes the dynamics of the actuation of the solenoid actuated microvalve.

#### 4.2.4. TANK

The propellant tank is a pressurized tank containing a given fraction of liquid propellant, in our case water, with mass  $m_l$ . During operations, the propellant is ejected at a rate  $\dot{m}_1$  and the pressurant gas, in our case  $N_2$ , expands lowering the pressure of the tank  $p_t$ . As the expansion is quasi-static, it can be considered an isothermal process. From the ideal gas law, the time derivative of the pressure is calculated by:

$$\dot{p}_t = -p_t \frac{\dot{m}_1}{V_t \rho_l - m_l} \quad (4.26)$$

where  $V_t$  is the tank volume and  $\rho_l$  is the density of the liquid propellant.

### 4.3. MODEL ANALYSIS

A sensitivity analysis was performed in order to assess the impact of all the parameters in the response of the model. The performance parameters thrust  $F$  and specific

Table 4.1: List of input parameters for the sensitivity analysis.

Thruster model					
Par.	Description	Min.	Ref.	Max.	Scale/Unit
$a_T$	Vap. model	1.62	1.63	1.64	$10^{-11} \text{m}^3/\text{K}$
$a_p$	Vap. model	-7.56	-7.45	-7.33	$10^{-15} \text{m}^3/\text{Pa}$
$b$	Vap. model	-5.20	-4.36	-3.52	$10^{-10} \text{m}^3$
$A$	Vap. model	70	75	80	1 s
$\alpha_1$	Noz. model	0.046	0.048	0.05	$1 \text{K}^{-\frac{1}{2}}$
$\beta_1$	Noz. model	197.22	626.99	1075.32	$1 \text{PaK}^{-\frac{1}{2}}$
$\alpha_2$	Pres. model	0.0021	0.0023	0.0025	1/K
$\beta_2$	Pres. model	20.43	62.17	104.29	1 Pa/K
$\tau$	Temp. model	100	120	140	1 s
$K$	Temp. model	25	30	35	1 K/(Ws)
Valve model					
Par.	Description	Min.	Ref.	Max.	Scale/Unit
$L_p$	See Fig. 4.5	0.90	1.00	1.10	$10^{-3} \text{m}$
$d_i$	See Fig. 4.5	0.90	1.00	1.10	$10^{-3} \text{m}$
$d_s$	See Fig. 4.5	4.50	5.00	5.50	$10^{-3} \text{m}$
$N$	Num. of turns	27.9	31.0	34.1	1
$R_c$	Eq. coil res.	0.90	1.00	1.10	$10^3 \Omega$
$a$	See Fig. 4.5	3.60	4.00	4.40	$10^{-3} \text{m}$
$d_{g0}$	See Fig. 4.5	2.25	2.50	2.75	$10^{-3} \text{m}$
$g$	See Fig. 4.5	2.70	3.00	3.30	$10^{-4} \text{m}$
$M$	Plunger mass	7.20	8.00	8.80	$10^{-4} \text{kg}$
$c$	Viscous coef.	450.0	500.0	550.0	1 Ns/m
$k$	Spring coef.	12.15	13.50	14.85	$10^3 \text{N/m}$

impulse  $I_{sp}$  are the basis for the analysis. Here we focus on the parameters that cannot be tuned by design, e.g. the estimated parameters  $\alpha_1$  and  $\beta_1$ , but instead they depend on the operational range used or the experimental setup. Thus, as the propellant tank has been modeled using only an analytical expression to relate the mass flow rate and the pressure, it has not been covered by the sensitivity analysis because its parameters are dependent on the specific design choices.

#### 4.3.1. SENSITIVITY ANALYSIS: THRUSTER

The parameters of the thruster model are shown in Table 4.1. The sensitivity analysis has been carried out assessing all combinations of the maximum and minimum values for each parameter. These values are selected based on the boundaries defined for the model and the confidence intervals of the linearization. The outputs of the model for each set of parameters are compared to the reference outputs calculated with the reference values. The deviation of the output from the reference is the cost function of the analysis and the rank correlation values between the change in the output and the variable are given in Table 4.2.

Table 4.2: Results of the sensitivity analysis. Values correspond to the rank correlation between the parameter and the output.

Thruster			Valve	
Par.	Thrust	Specific impulse	Par.	Mass flow rate
$\beta_1$	0.625	0.747	$N$	0.055
$\beta_2$	0.115	0.088	$R_c$	-0.052
$\alpha_1$	0.108	0.048	$c$	-0.051
$\alpha_2$	-0.106	0.011	$d_{g0}$	-0.049
$\tau$	0.085	0.091	$k$	-0.046
$K$	0.075	0.092	$L_p$	-0.044
$b$	-0.066	-0.010	$g$	-0.039
$A$	-0.066	0.045	$d_s$	-0.038
$a_p$	0.018	0.042	$M$	-0.023
$a_T$	0.006	0.027	$d_i$	-0.011
			$a$	-0.008

As we can see in Table 4.2, the most influent parameter of the thruster model is  $\beta_1$  as it has the largest correlation to the thrust and the specific impulse. The difference in the response of the model using the worst set of parameters, i.e. the ones that give the response with the largest difference to the reference response, is around 2.8% for specific impulse and 0.1% for thrust.

#### 4.3.2. SENSITIVITY ANALYSIS: VALVE

An analysis similar to the one of the thruster has been done for the valve model using the parameters shown in Table 4.1. A more detailed analysis can be found in [Silvestrini \(2017\)](#) where an optimal set of parameters for the valve model has been identified comparing with experimental data. A range of  $\pm 10\%$  around the values presented in that reference has been used for each parameter in order to assess the influence on the mass flow rate (response of the model). All the combinations of the maximum and minimum values are used in the sensitivity analysis.

Table 4.2 shows the correlation between each parameter and the output of the valve model, i.e. the mass flow rate. For this model, the number of turns in the coil and the resistance, are the most influent. The response in the worst case changes 0.02%.

#### 4.4. MODEL VALIDATION

The model of the complete system includes empirical and theoretical relations to represent the dynamics of VLM systems. The empirical parts are related to either parameters of the thruster chip dependent on the design choices or to parameters that have no absolute theoretical models or are significantly complex. The chip temperature model, for example, depends strongly on the geometry and mass of the final chip, however, a complete theoretical/numerical model might only be achieved using the finite element method. The vaporization model also depends on the design choices, such as channel geometries and materials, and it has no definite theoretical model, i.e. only empirical

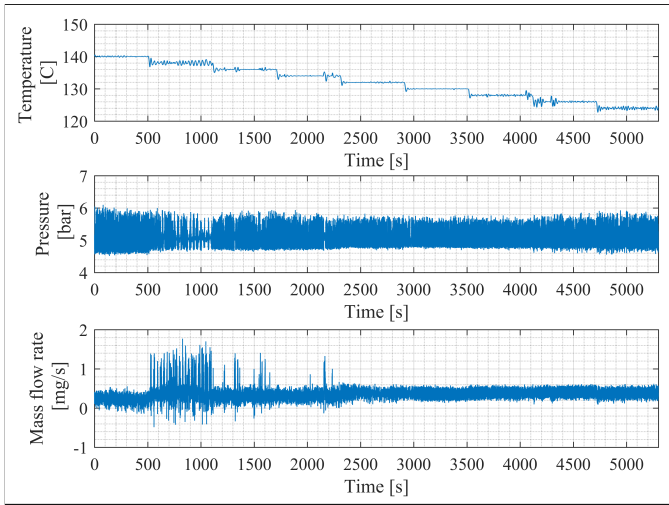


Figure 4.6: Temperature, pressure, and mass flow rate used in the validation of the model.

relations are currently available in the scientific literature (Karayiannis and Mahmoud, 2017; Thome, 2004). The chip temperature model and the vaporization model have been modeled as shown in Figs. 3.9 and 4.4.

The next point to be validated is the assumption that the temperature of the gas after boiling is significantly close to the saturation temperature. This assumption is used in 4.2 and 4.10. Measuring the temperature of a gas inside a microchannel is very difficult and, with the current design of the VLM chip, it is impossible as there is no sensor inside the chamber. Therefore, an indirect method is used to assess the changes in the temperature inside the vaporization chamber:

- Keep the pressure constant.
- Apply different temperatures to the thruster chip. From the temperature with which the boiling occurs at the beginning of the vaporization chamber (high temperature) to the temperature with which droplets escape through the nozzle (low temperature).
- If the temperature of the gas changes significantly, then the mass flow rate should change accordingly.

The pressure is kept constant at around 5 bar and the chip temperature is changed from 140 °C to 124 °C. The data collected during this test is shown in Fig. 4.6. Figure 4.7 shows the boxplot of mass flow rate and pressure as functions of the temperature. As we can see, the average mass flow rate changes slightly according to the average pressure changes, however, no significant change can be seen following the increase in temperature.

Therefore, it can be concluded that the chip temperature does not significantly affect the mass flow rate. The gas temperature might be changing with the chip temper-

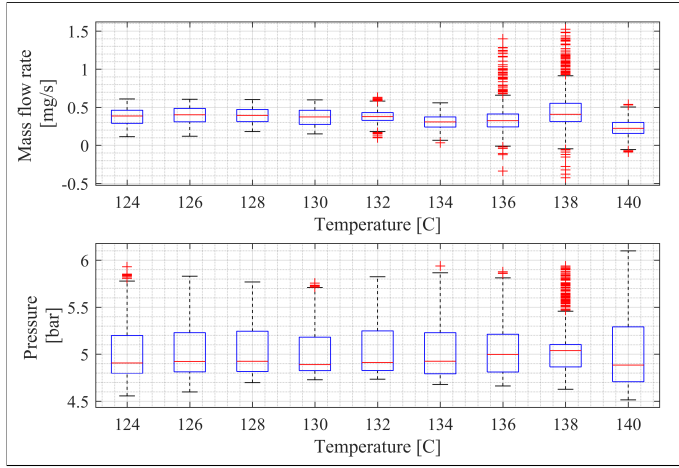


Figure 4.7: Boxplot of the pressure and mass flow rate for different temperatures.

ature, however, the pressure is the largest contributor to mass flow rate changes. Thus, assuming that the gas temperature is the saturation temperature might be a suitable approximation. The current design allows only a limited range of chip temperatures which might explain the no-changes in the mass flow rate.

## 4.5. SIMULATION SETUP

### 4.5.1. SPACECRAFT PARAMETERS

The complete model of the micropropulsion system has been used in a simulation loop to control the attitude of a micro-satellite. The satellite is a 3 units PocketQube consisting of three units of  $5 \times 5 \times 5$ cm with a mass of 0.5 kg. Considering the mass equally distributed in all dimensions, the components of the inertia matrix around the principal axis of the spacecraft are  $I_1 = 1.0 \times 10^{-3} \text{kgm}^2$ ,  $I_2 = 1.0 \times 10^{-3} \text{kgm}^2$ , and  $I_3 = 2.083 \times 10^{-4} \text{kgm}^2$ . The maximum thrust provided by each thruster is defined as 1.25mN. A complete list of the parameters used in the simulations is given by Table 4.3.

### 4.5.2. CONTROLLER DESIGN

In order to control the attitude of the spacecraft, two controllers have been implemented in the simulation loop: one to calculate the torque  $\vec{M}_{ref}$  necessary to execute the desired maneuver and one to control each thruster in order to produce the desired thrust  $F$ . The former also decides which of the four thrusters to use depending on the current and target attitude. A simple proportional-derivative control law is used to calculate  $\vec{M}_{ref}$  (Wie and Barba, 1985):

$$\vec{M}_{ref} = \mathbf{k}_p \hat{q}_e + \mathbf{k}_r \vec{\omega} \quad (4.27)$$

where  $\mathbf{k}_p$  and  $\mathbf{k}_r$  are the gains of the controller in  $x$ ,  $y$  and  $z$ , and  $\hat{q}_e$  is the vectorial part of the quaternion representing the error between the current and the target attitude de-

Table 4.3: Parameters used in the simulations.

Component	Par.	Value	Unit	Description
Valve	$M$	$8 \times 10^{-4}$	kg	Plunger mass
	$k$	$1.35 \times 10^4$	N/m	Spring constant
	$c$	500	Ns/m	Fluid visc. damp.
	$V$	12	V	Coil voltage
	$R_C$	31	$\Omega$	Coil resistance
	$d_{in}$	0.001	m	Inlet diameter
	$N$	1000	1	Number of turns
	$f_{PWM}$	200	Hz	PWM frequency
Tank	$p_{t0}$	5	bar	Initial pressure
	$m_{l0}$	$30 \times 10^{-3}$	kg	Init. mass of prop.
	$V_t$	$40 \times 10^{-6}$	m <sup>3</sup>	Volume
Thruster	$A_t$	$2 \times 10^{-9}$	m <sup>2</sup>	Throat area
	$V_{tot}$	$4 \times 10^{-9}$	m <sup>3</sup>	Chamber volume
	$\alpha$	$1 \times 10^{-3}$	/K	Temp. res. coef.
Spacecraft	$h$	0.15	m	Height
	$w$	0.05	m	Width
	$l$	0.05	m	Length
	$m$	0.5	kg	Mass
Fluid	$\gamma$	1.33	1	Ratio of spec. heat
	$R_s$	461.5	J/(kgK)	Spec. gas constant
	$\mu_{H_2O}$	0.001	Pas	Viscosity
	$\rho_l$	1000	kgm <sup>3</sup>	Propellant density

fined as  $q_e = q^{-1} \otimes q_t$  where  $q_t$  represents the target attitude and  $\otimes$  is the multiplication of two quaternions. Then,  $\vec{M}_{ref}$  is used to calculate the thrust of each thruster which is the reference input to the valve controller that actuates on the valve's input voltage  $v(t)$ :

$$v(t) = K_p e(t) + K_i \int_0^t e(\tau) d\tau \quad (4.28)$$

where  $K_p$  and  $K_i$  are the gains of the controller and  $e(t)$  is the error defined as the difference between the target and the actual thrust. In order to simulate the behavior of the real system, the voltage is converted into a PWM (pulse width modulation) input with frequency  $f_{PWM}$  and amplitude  $V$ .

## 4.6. SIMULATION RESULTS

The models were implemented in Simulink/Matlab and tested in a case with four thrusters used to control the attitude of a pico-satellite. The controllers were empirically tuned with the gains  $\mathbf{k}_p = [1 \ 3 \ 3] \times 10^{-4}$ ,  $\mathbf{k}_r = [5 \ 15 \ 15] \times 10^{-4}$ , for the spacecraft controller and  $K_p = 200$ , and  $K_i = 9500$  for the valve controllers. These gains have been selected based on the desired response time, less than 0.1 s for the valves and 20 s for the spacecraft, and on the maximum allowed overshoot of less than 20% for the valves and

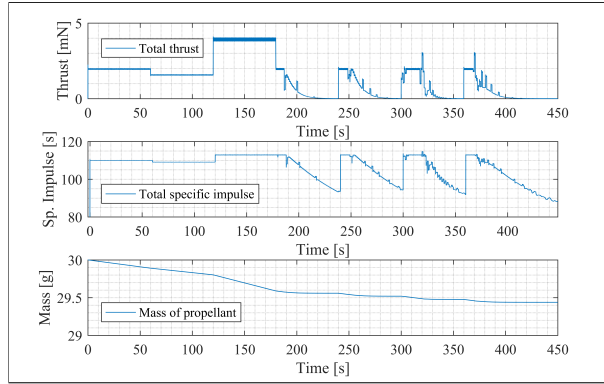


Figure 4.8: Total thrust generated by the all thrusters (top), total specific impulse (middle) and mass of propellant left in the tank (bottom). The attitude control starts after 180 s.

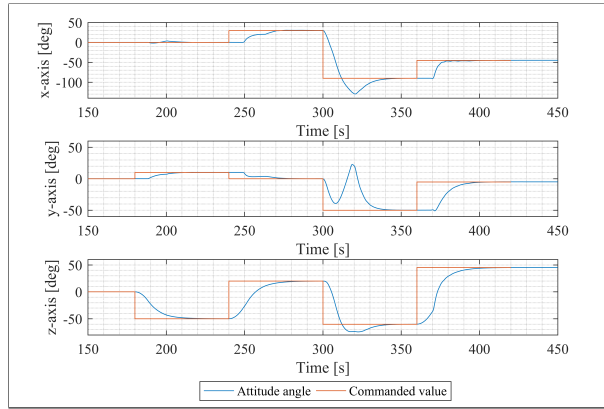


Figure 4.9: Angles of the spacecraft during the attitude control phase that starts after 180 s.

no-overshoot for the spacecraft.

The test is divided into two parts during the time of the simulation. In the first part, before 180 s, a sequence of thrust commands is sent to all the thrusters in order to assess the thrust level control. Then, after 180 s, a sequence of attitude commands is sent to the controller that calculates the necessary thrust for each of the thrusters to perform the maneuver.

Fig. 4.8 shows the thrust generated by all the thrusters, the total specific impulse and the mass of propellant in the tank. The attitude angles are plotted in Fig. 4.9 together with the commanded values shown in red.

As we see in Fig. 4.8, the mass of propellant in the tank drops very slowly meaning that the amount of propellant considered, i.e. 30 g, can be used for very long time before the pressure drops below a critical level where the maximum provided thrust is lower than the required maximum thrust  $F = 1.25\text{mN}$ .

## 4.7. CONCLUDING REMARKS

This chapter presented a comprehensive modeling approach for micropropulsion systems using Vaporizing Liquid Microthrusters. The model developed comprises all relevant elements of microresistojets and the necessary equations to simulate the dynamics of such system. The resulting model is hybrid comprising fundamental laws of physics as well as empirical relations. Some parts of the model are derived from well known relations, such as the ideal gas law, and some others are empirically derived from an extensive experimental campaign done with test models of the real propulsion system. The models of the thruster, the valve, and the tank have been tuned to work within the boundaries usually considered for miniaturized spacecraft, e.g. CubeSats and PocketQubes, in terms of operational parameters such as pressure and temperature. However, these boundaries can be changed in order to adapt and extend the model to other applications with different sets of requirements.

The model has been successfully applied in a simulation loop demonstrating the attitude control of a pico-satellite using an array of four thrusters. The model can be applied in other types of simulation that need a precise description of the system dynamics including optimization of the propulsion system's parameters as well as of the thruster's parameters.

As the current design only allows a small range of temperatures to be applied to the chip, an improvement to the thruster could be achieved by including a chamber separate from the vaporization chamber to further increase the gas temperature.



# 5

## CONTROL OF VAPORIZING LIQUID MICROTHRUSTERS

*The world is too crowded and it's lonely here.*

From the song *Fallen Angelz* by Special Teamz

*This chapter presents an innovative approach combining a fuzzy controller and a control allocation method to solve the control problem of allocating actuators' efforts in an over-actuated system. The controller is applied to a space debris removal mission using a deployable net on-board of a 3U CubeSat. The controller calculates the necessary effort of each thruster on-board the spacecraft to compensate disturbances or the perform a re-orientation/reposition maneuver. Two cases with four and six thrusters are analyzed in a simulation scenario. The simulation also covers the non-nominal situation of failure in one of the thrusters. A Monte Carlo simulation is performed in order to assess different scenarios considering failures and different simulation configurations. Results show that the proposed approach successfully controls the satellite after a disturbance.*

## 5.1. INTRODUCTION

**T**HRUST direction control can be done by controlling a set of thrusters. To achieve this, a control allocation method is often necessary if there is redundancy in the generation of torques and forces, i.e., there are multiple solutions for the problem. This chapter proposes a fault tolerant fuzzy control allocation method to control a set of microthrusters. The proposed approach uses a control allocation method to automatically generate the rules used by the inference system of the fuzzy controller that actuates the thrusters. Control allocation methods are necessary when the system is over-actuated, i.e., there is redundancy in the set of actuators that allows multiple solutions for the generation of control efforts. There are many applications for such methods including the attitude/position control of spacecraft with thrusters (Servidia and Pena, 2002, 2005; Pena et al., 2000). Many different methods exist to solve the control allocation problem in unconstrained or constrained spaces (Oppenheimer, 2011; Johansen and Fossen, 2013), however, they are often based on complicated calculations that are computationally expensive. In this case, the use of fuzzy logic might help in simplifying the implementation of a control allocation method (Tohidly and Sedigh, 2013; Fan et al., 2011; Chang et al., 2016).

The fuzzy controller utilizes linguistic variables and a set of rules to calculate its outputs. The process of transforming the inputs into linguistic values, such as “low” and “high”, is called fuzzification and it uses membership functions to determine how much a certain numerical value belongs to a given level, i.e., the probability of an input being, for example, “low” or “high” (Passino et al., 1998). The inference system then uses a set of rules to determine the outputs. An example rule using linguistic values can be:

- **IF** *temperature = high*
- **THEN** *gas valve = low*

The last step of the fuzzy logic is to convert the outputs from linguistic values to numerical values (defuzzification).

As the fuzzy controller is based on a set of rules, it is intended to help in reducing computational costs that are very important for such small systems as the case of CubeSats. The computational effort rises significantly when using traditional approaches of control allocation based on matrices calculations as they require matrix inversions that can be costly depending on the size of the system (Johansen and Fossen, 2013). With the approach presented here, the computational cost can be transferred from the operational phase to a design phase therefore reducing the computational effort specially in cases with a large number of actuators.

In the proposed approach, the rules of the fuzzy controller are automatically generated using a control allocation method, e.g., the redistributed pseudo inverse (Oppenheimer, 2011; Johansen and Fossen, 2013). The generation of the rules is usually done using expert’s knowledge of the system (Tohidly and Sedigh, 2013). However, when the system is over-actuated, there might be multiple solutions for the problem and a computational method might be needed to select the most appropriate configuration specially when a large set of actuators are to be used. Therefore, another advantage of the proposed approach is that it combines the intuitive part of the fuzzy system with the math-

ematically formal part of the control allocation method. This combination is important to comply with the needs of both simple and complex systems.

The proposed method is applied to a space debris removal mission using a deployable net. Two cases are analyzed: one with four thrusters and the other with six thrusters considering failure in one of them during operation. In this case, a failure is a situation in which one of the thrusters is not able to provide any thrust and it is assumed that the failure is instantaneously detected. Results show that the novel fuzzy controller is able to control the spacecraft, i.e., bring the relative angular and linear velocities back to zero, in the normal and in the faulty situation. A Monte Carlo simulation is performed to assess the influence of different input parameters (including experimental values) in the response of the controller.

## 5.2. SAMPLE MISSION DESCRIPTION

Space debris poses a big threat to operational satellites which form a crucial infrastructure for society and to astronauts' lives. According to the main source of information on space debris, the U.S. Space Surveillance Network (SSN), more than 18900 objects larger than 10 cm have been cataloged as of April 2018 (Anz-Meador, 2018). Among the total number of objects in orbit, only 1987 spacecraft are active, i.e., around 10% of the objects are operating in an environment where 90% of the other objects are space debris (Kelso, 2018).

Several space debris removal methods have been proposed in the past decades (Shan et al., 2016) including the net capturing method which is regarded as one of the most promising due to its compatibility with different target sizes, shapes and orbits. Additionally, it is flexible, lightweight, cost efficient and less likely to generate more space debris objects (Shan et al., 2017b,a). This method deploys a light-weight net using a set of bullets, attached to the corners of the net, that are fired in a diverging manner in the direction of the target spacecraft as depicted in Fig. 5.1. Once the net reaches the target, it will wrap itself around the body and allow the main satellite to move the target. The firing of the bullets generates forces and torques on the main satellite that need to be compensated in order to keep the stability of the chaser spacecraft and the safety of the mission.

This chapter analyses the performance of the proposed fuzzy controller when applied to a hypothetical CubeSat mission to remove space debris using a deployable net. The chaser satellite is a 3U CubeSat equipped with a set of microresistojets. The spacecraft's body is considered a cuboid of  $30 \times 10 \times 10$  cm form factor with mass uniformly distributed in order to simplify the modeling, i.e., it reduces the inertia matrix to a diagonal matrix.

The net deployment system is based on the one presented in Shan et al. (2017c) which deploys a net of  $1 \times 1$  m using four bullets with mass of 30 g each attached to the corners of the net. The bullets are fired with a velocity of 1.8 m/s at an angle of  $25^\circ$  to assure that the net is open when it reaches the target. However, due to uncertainties in the operations the velocities and shooting angles might vary. In the experiment reported in Shan et al. (2017c) these values vary with  $\pm 0.14$  m/s and  $\pm 4.21^\circ$  respectively.

The options of propulsion systems for such small spacecraft are not many as most of the CubeSats launched to this date do not have a propulsion system. As indicated

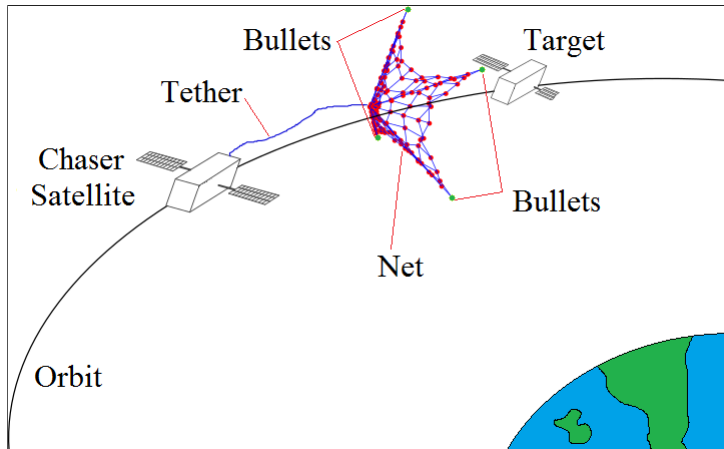


Figure 5.1: Representation of a space debris removal mission using the net capturing concept (Shan et al., 2017b).

5

previously, a space debris removal mission would require a set of microthrusters with relatively high thrust to compensate the disturbances generated by the firing of the bullets within a reasonable time.

In order to help quantifying the performance parameters of the candidate propulsion system, the following hypothetical scenario is considered. Suppose all four bullets are fired at the same velocity of 1.8 m/s and at the same angle  $25^\circ$ . If we want to compensate the linear momentum generated by the bullets within, as an example, 60 s after shooting them (this depends on the mission and the post-capturing operations), then the thrust generated by all thrusters should be at least around 3.3 mN. Similarly, to compensate the angular momentum generated by the bullets in a hypothetical case in which two bullets on the same side are fired and the other two are not fired, then the total thrust that should be generated is around 0.9 mN (if they are placed at the corners of the spacecraft). Considering a set of four thrusters on board the CubeSat (which is the minimum to achieve 3-axis attitude control (Pena et al., 2000)), then the maximum required thrust for each thruster might be set to 1 mN.

The Vaporizing Liquid Microthruster (VLM) is a very interesting option for space debris removal as it is able to generate thrust in the levels of 0.1–1 mN using pressures in the range 1–10 bar and low power consumption that fits within the assumed maximum power of 10 W (Silva et al., 2018). Due to the fact the VLM works with a liquid propellant, it presents a great advantage in terms of control since the flow of liquid can be controlled with a valve regulating the levels of thrust generated with a fast response time compared to gaseous flow. This is a very important feature that allows a more precise attitude control as compared to, for example, solid propellant microthrusters (see Chapter 2).

### 5.2.1. CONTROL ALLOCATION

The problem of control allocation is finding a set of actuators inputs  $\mathbf{u} \in \mathbb{R}^n$  that provides a desired output  $\tau \in \mathbb{R}^m$  written as:

$$\tau = \mathbf{C}\mathbf{u} \quad (5.1)$$

where  $\mathbf{C} \in \mathbb{R}^{m \times n}$  is a matrix of constant values (in case of linear systems) and it is called control effectiveness matrix. In case of an unconstrained system, the vector  $\mathbf{u}$  can be found by solving  $\mathbf{C}^{-1}\tau = \mathbf{u}$  where the superscript  $-1$  denotes the inverse of a matrix. However, in practice most of the systems are constrained by physical characteristics and the direct solution might be an unachievable state within the time frame considered. Therefore an approach that takes into account actuator's upper and lower boundaries and rate limits has to be considered (Johansen and Fossen, 2013).

### THRUST ALLOCATION

A thrust control system with  $n$  thrusters is a constrained type of system that can be written in the form (Pena et al., 2000):

$$\begin{cases} \vec{T} = \mathbf{A}\mathbf{F} \\ \vec{U} = \mathbf{B}\mathbf{F} \end{cases} \quad (5.2)$$

where  $\vec{T} \in \mathbb{R}^3$  is the torque,  $\mathbf{F} \in \mathbb{R}^{n \times 1}$  is a column matrix of  $n$  thrusters containing the amplitude of the force of each thruster,  $\vec{U} \in \mathbb{R}^3$  is the force,  $\mathbf{A} \in \mathbb{R}^{3 \times n}$  and  $\mathbf{B} \in \mathbb{R}^{3 \times n}$  represent the configuration of the thrusters given the vectors of position  $\vec{d}_i$  and orientation  $\vec{e}_i$  of the  $n$  thrusters with respect to the spacecraft body and  $i \in \{1, \dots, n\}$  and are defined as:

$$\mathbf{A} = \begin{bmatrix} \vec{d}_1 \times \vec{e}_1 & \dots & \vec{d}_n \times \vec{e}_n \end{bmatrix} \quad (5.3)$$

$$\mathbf{B} = [\vec{e}_1 \dots \vec{e}_n] \quad (5.4)$$

Each thruster  $i$  is bounded by lower and upper values  $F_{min} \leq F_i \leq F_{max}$ . The control allocation problem is to find the column matrix of thrust forces  $\mathbf{F} = [F_1, \dots, F_n]^T$ , where the superscript  $T$  denotes the transpose of a matrix, that generates the desired torques and/or forces on the spacecraft body in order to perform a maneuver or reject a disturbance.

As indicated by Pena et al. (2000), the minimum number of thrusters to allow 3-axis torque generation is four without considering failures in which case a minimum of six thrusters is necessary to tolerate failure in exactly one thruster.

## 5.3. PROPOSED APPROACH

The fuzzy controller determines, based on a set of rules, which thruster should be activated for the desired maneuver. The rules are defined according to the possible motion of the spacecraft, i.e., depending on which direction the body is rotating and/or translating with respect to the target's inertial frame. Therefore the number of rules depends on the number of degrees of freedom and the number of membership functions for each

degree of freedom. For example, considering six degrees of freedom and three membership functions for each one (e.g. negative, zero and positive) a total of  $3^6$  rules would apply to the controller in order to have a complete map of inputs. However, the number of outputs and the respective number of membership functions defines how many rules are possible and in case there are multiple rules with the same input, those rules can be combined into one.

The proposed fuzzy controller follows the algorithm shown in Fig. 5.2. The case of controlling thrusters on-board of a spacecraft is used as an example and the approach presented here can be used in any control allocation problem. The steps of the algorithm are explained in the following:

- **Start:** initialize all variables.
- **Check thrusters:** check the status of the thrusters looking for failures. A failure is assumed when the thruster does not provide any thrust, i.e.,  $F_i = 0$  for  $t \geq t_f$  where  $i$  indicates which thruster has failed at the instant  $t_f$ . The control system is assumed to always be able to detect the failures. The problem of detecting the failure is not approached in this thesis. However, an advanced method for fault detection might be used (Zolghadri, 2018).
- **Generate rules:** in case of failure or in the beginning of the routine, i.e.,  $t = 0$ s, the matrices **A** and **B** are updated zeroing the column corresponding to the faulty actuator if there is any. Then, the controller automatically generates the rules of the inference system. The inputs of the fuzzy controller are the target torques and forces to be generated by the thrusters ( $\tau$  in (5.1),  $\vec{T}$  and  $\vec{U}$  in (5.2)) and the output is the thrust that each thruster needs to generate ( $u$  in (5.1) and **F** in (5.2)). The outputs calculated by a standard control allocation method (it can be any method) is used as the consequent of the rules. For example, suppose that **F** =  $[1, 0, 0, 1]^T$  mN is the output calculated by the control allocation method for an input  $\vec{T} = [1, -1, 0]^T$  mNm, then a possible rule can be:

- **IF**  $T_x = \text{positive}$  **AND**  $T_y = \text{negative}$  **AND**  $T_z = \text{zero}$
- **THEN**  $\mathbf{F} = [\text{positive}, \text{zero}, \text{zero}, \text{positive}]^T$

- **Fuzzy control:** fuzzify the inputs, use the rules generated with the control allocation method to calculate the outputs, and defuzzify the outputs. The type of fuzzy controller can be any type including more advanced concepts such as adaptive fuzzy or hybrid neural/fuzzy approaches (Passino, 2011).
- **Stop control:** check the stopping criteria. In most cases this can be when the error between the reference inputs and the outputs of the system is less than a certain threshold.

The rules of the fuzzy controller can be generated using any control allocation method, e.g. redistributed pseudo inverse, daisy chaining, etc. (Johansen and Fossen, 2013), and can also be generated offline for all possible failures. In case of systems with a small number of actuators, the rules might also be generated using expert's knowledge about the system.

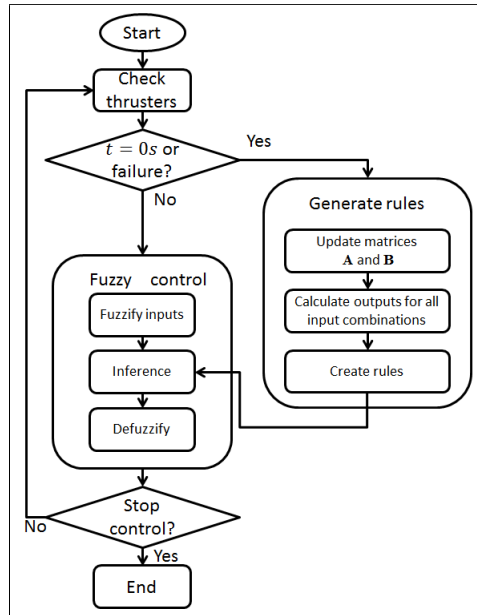


Figure 5.2: Algorithm of the proposed hybrid fuzzy control allocation method.

The fuzzification of the inputs can be done with any type and number of membership functions, however, if one is concerned about computational cost then it is recommended to keep the number of membership functions as low as possible to reduce the number of rules. The fuzzy inference method (Mamdani or Takagi-Sugeno) and the defuzzification method can be any method that best suits the process.

The proposed approach can be applied to any control allocation problem and it is specially recommended for applications with limited computational resources. In the following section, we present the application of the proposed approach to the control allocation of thrusters on-board of a spacecraft.

## 5.4. SIMULATION SETTINGS AND ANALYSIS

The proposed approach has been applied to the control allocation of thrusters on-board of a spacecraft for active space debris removal. The thrusters are used to compensate disturbances generated during the deployment of a net that is used to capture space debris. A Monte Carlo simulation for two configurations with four and six thrusters has been performed to assess the performance of the controller with different input parameters. Table 5.1 shows the parameters used in the simulations and Table 5.2 shows the parameters used in the Monte Carlo simulation.

Figure 5.3 shows a diagram of the satellite with arrows indicating the position and direction of each thruster (blue) as well as the information of the bullets (red). The thrusters are slightly tilted with respect to the  $z$ -axis to provide rotational capabilities in that axis and positioned at the corners of the structure to provide maximum torque.

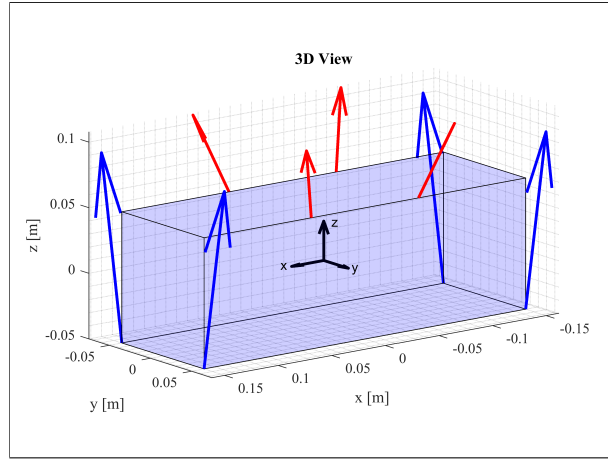


Figure 5.3: Representation of the 3U CubeSat considered in the simulations (case with four thrusters). The dotted red arrows represent the direction in which the bullets are fired and the dashed blue arrows represent the thrusters.

#### 5.4.1. CONTROLLER DESIGN

The fuzzy controller has been designed with four inputs: the first three are the components of the target torque vector to be generated by the thrusters and the fourth is the component of the target net force to be generated by the thrusters in the direction opposite to the net deployment direction. The target torque and force are calculated using a simple control law given by [Wie and Barba \(1985\)](#) (the same control law has been used in Chapter 4):

$$T_i = k_{p_T} \hat{q}_{e_i} + k_{r_T} \omega_i \quad (5.5)$$

$$F_i = k_{p_F} x_i + k_{r_F} v_i \quad (5.6)$$

where  $i \in \{x, y, z\}$  indicates the vector component,  $k_p$  is the position gain,  $k_r$  is the rate gain, and  $\hat{q}_e$  are the vectorial components of the error quaternion defined by  $q_e = q^{-1} \otimes q_t$  where  $q_t$  represents the target attitude,  $\otimes$  is the multiplication of two quaternions and the index  $-1$  indicates the inverse of a quaternion. In the case approached here, the position gains are set to zero as the goal is to reduce the linear and angular velocities only.

The first three inputs were designed to have triangular/trapezoidal membership functions with three levels: negative (represented by '-'), zero (represented by '0') and positive (represented by '+'). Figure 5.4-a shows the three functions for one of the inputs ( $\omega$ ) where the values are defined in Table 5.1. The fourth input, the force, is defined with only two levels negative and zero as this input is expected to be always in this range due to the characteristics of the application. Figure 5.4-b shows the membership functions of this input where the values are defined in Table 5.1. The number of levels for each input was defined as three and two in order to keep the number of rules to a minimum. The

shape of the membership functions, i.e., triangular/trapezoidal, was selected in order to generate a sharper output surface.

As the position and orientation of each thruster is constant with respect to the spacecraft body we can assume that matrices **A** and **B** in (5.2) are constant from the beginning. Therefore, the rules of the fuzzy controller stay the same as long as no thruster fails, in which case the matrices must be adjusted to exclude the faulty thruster resulting in a different set of rules.

Table 5.1: Parameters used in the simulations. The gains and the values of the membership functions have been empirically selected by trial and error in order to achieve a reasonable performance.

	Parameter	Value	Description
Spacecraft	$m$	4 kg	Mass
	$l$	0.1 m	Length
	$h$	0.1 m	Height
	$w$	0.3 m	Width
Bullets	$m_b$	30 g	Mass
	$v_{max}$	1.8 m/s	Speed
	$\beta$	25°	Shooting angle
Controller	$k_{pT}$	0	Torque position gain
	$k_{rT}$	-100	Torque rate gain
	$k_{pF}$	0	Force position gain
	$k_{rF}$	-200	Force rate gain
Fuzzy	$[T_1, \dots, T_7]$	$[-1.0, -0.005, -0.001, 0.0, 0.001, 0.005, 1.0]$	See Fig. 5.4
	$[F_1, F_2, F_3, F_4]$	$[-1.0, -0.001, 0.0, 0.0]$	See Fig. 5.4

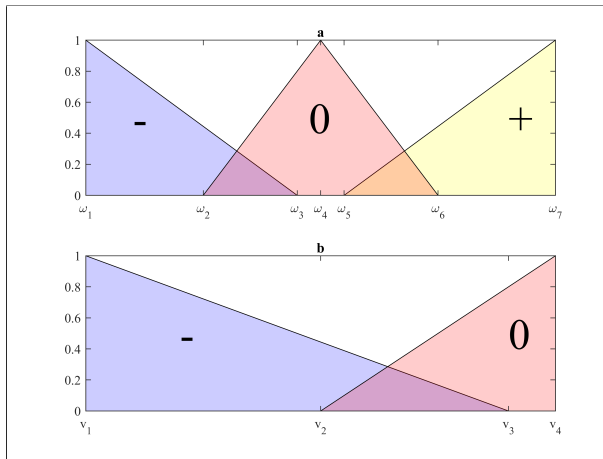


Figure 5.4: Membership functions for the angular velocity (a) and linear velocity in the  $z$ -axis (b).

The fuzzy inference method chosen is the Takagi-Sugeno method that implies that the output is either a constant value or a linear function of the inputs. The outputs are the levels of thrust from 0 to 1 (scaled to the maximum thrust possible) for each of the thrusters installed in the spacecraft. The “and” method was set to the minimum of the

fuzzified inputs and the defuzzification method was set to weighted average of all the rule outputs. Other options related to the controller were kept as the default values implemented in the MATLAB® toolbox for the Takagi-Sugeno type of controller.

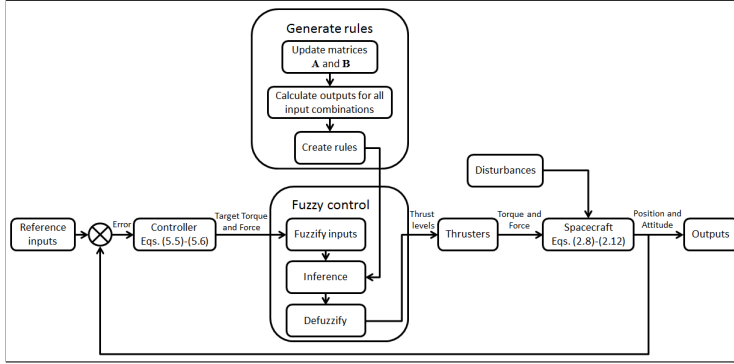


Figure 5.5: Diagram of the complete system including the controller and the spacecraft.

5

Finally, the control allocation part of the rule generation step was done using the re-distributed pseudo-inverse method which is a constrained linear method, i.e., it provides a solution considering the constraints of the actuators. However, it does not guarantee that an optimal solution is always found (Johansen and Fossen, 2013). The method starts solving 5.1 to obtain  $\mathbf{u}$  without constraints and if the outputs are within the bounds (not saturated) then it found a feasible solution. In case one or more outputs are saturated, then the corresponding elements of the output are kept constant at the saturated values and the non-saturated elements are re-calculated using a reduced control effectiveness matrix.

#### 5.4.2. SIMULATION CASES

The algorithm of the system was implemented in MATLAB® (The MathWorks, Inc., Natick, MA, USA) version R2016b based on the equations shown in sections 2 and 3 using a standard ordinary-differential-equation solver. In all simulations, each thruster  $i$  is bounded by a lower and an upper limit defined by  $0\text{mN} \leq F_i \leq 1.0\text{mN}$ . Three test cases have been simulated to assess the performance of the controller:

1. 4 thrusters, no failures and ideal shooting of the bullets (no torque generated)
2. 4 thrusters, no failures and bullets data from the experiment reported by Shan et al. (2017c)
3. 6 thrusters, failure in one thruster during the operation and and bullets data from the experiment

Given the two configurations with four and six thrusters, we can calculate the analytical solution for the time to stabilize the spacecraft, i.e. bring the relative angular and linear velocities back to zero. The solution for the linear motion is calculated considering the ideal case when all bullets are fired with the same velocity and angle. In such case,

all thrusters are switched on with maximum thrust. Similarly, the solution for the angular motion is calculated considering a hypothetical case when two bullets are fired with double the velocity of the other two. In the case with four thrusters, the time to stop the linear motion is  $t_l = 49.7\text{s}$  and to stop the angular motion is  $t_a = 14.2\text{s}$ . In the case with six thrusters  $t_l = 33.2\text{s}$  and  $t_a = 18.4\text{s}$ . The difference in the time to stabilize the angular motion is due to the fact that the placement of the thrusters in case 1 and 2 is optimized for torque generation whereas in case 3 the placement of the thrusters is optimized to allow failures to occur.

### 5.4.3. CASE 1: 4 THRUSTERS WITH IDEAL SHOOTING

The thrusters are ideally positioned in such a way to provide the maximum torques around the  $x$ - and  $y$ - axes, i.e., in the corners of the satellite, and they are all tilted by  $\alpha = 10^\circ$  with respect to  $z$ -axis in order to provide torque also in that direction. With this configuration the controller can compensate torque disturbances in all directions and a force in the  $z$ - direction. It is also possible to compensate forces in other directions but for this application they are considered negligible.

The matrices  $\mathbf{A}$  and  $\mathbf{B}$  are defined based on the position and orientation vectors  $\vec{d}$  and  $\vec{e}$  of each thruster with respect to the body reference frame positioned at the geometric center of the cuboid:

$$\begin{bmatrix} \vec{d}_1 & \vec{d}_2 & \vec{d}_3 & \vec{d}_4 \end{bmatrix} = \begin{bmatrix} -0.1500 & -0.1500 & 0.1500 & 0.1500 \\ 0.0500 & -0.0500 & -0.0500 & 0.0500 \\ -0.0500 & -0.0500 & -0.0500 & -0.0500 \end{bmatrix} \text{ m}$$

$$\begin{bmatrix} \vec{e}_1 & \vec{e}_2 & \vec{e}_3 & \vec{e}_4 \end{bmatrix} = \begin{bmatrix} 0 & 0 & 0 & 0 \\ \sin(\alpha) & -\sin(\alpha) & -\sin(\alpha) & \sin(\alpha) \\ \cos(\alpha) & \cos(\alpha) & \cos(\alpha) & \cos(\alpha) \end{bmatrix}$$

$$\mathbf{A} = \begin{bmatrix} 0.0579 & -0.0579 & -0.0579 & 0.0579 \\ 0.1477 & 0.1477 & -0.1477 & -0.1477 \\ -0.0260 & 0.0260 & -0.0260 & 0.0260 \end{bmatrix} \text{ m} \quad (5.7)$$

$$\mathbf{B} = \begin{bmatrix} 0 & 0 & 0 & 0 \\ 0.1736 & -0.1736 & -0.1736 & 0.1736 \\ 0.9848 & 0.9848 & 0.9848 & 0.9848 \end{bmatrix} \quad (5.8)$$

Figure 5.6 shows the linear velocity of the spacecraft with respect to the body axis. As it is seen the spacecraft moves in only one direction and it is braked by the thrusters which are fired with the same levels. In Fig. 5.7 we see the levels of the thrusters that are fired together with the same thrust level in order to brake the satellite without producing torques.

Figure 5.6 shows the total linear displacement of the spacecraft with respect to the inertial frame due to the applied forces which is  $-1.029\text{ m}$ . As the bullets are ideally fired, there is no angular displacement but the total linear displacement might influence the post-capturing phase. However, the displacement during the time expected for the net to reach the target, which is around  $1\text{ s}$  as indicated in [Shan et al. \(2017b\)](#), is less than  $-5\text{ cm}$ .

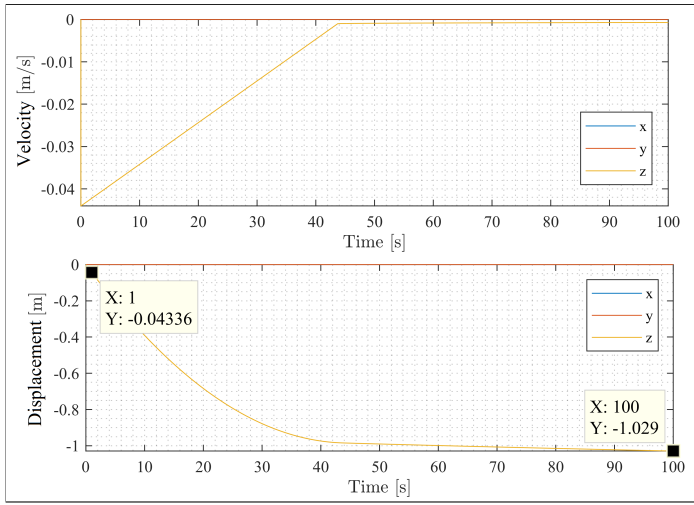


Figure 5.6: Linear velocities of the spacecraft with respect to the body frame (top) and displacement (bottom) in the case with four thrusters and ideal shooting of the bullets.

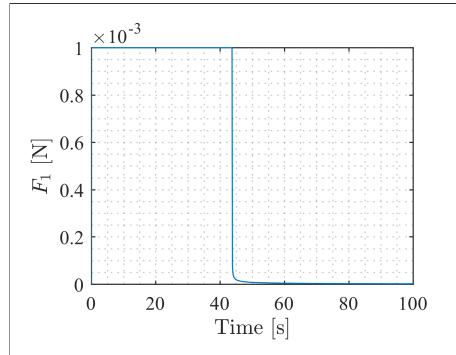


Figure 5.7: Thruster actuation level in the case with four thrusters and ideal shooting of the bullets. All thrusters have the same activation profile.

#### 5.4.4. CASE 2: 4 THRUSTERS WITH EXPERIMENTAL DATA

In this case the data presented in [Shan et al. \(2017c\)](#) has been used to estimate the initial magnitude and direction of the velocities of each bullet. The data was collected during a test campaign of a prototype net deployment mechanism done in zero gravity environment. The velocities are:

$$\begin{bmatrix} \vec{v}_1 \\ \vec{v}_2 \\ \vec{v}_3 \\ \vec{v}_4 \end{bmatrix} = \begin{bmatrix} -0.5316 & -0.5358 & 1.6090 \\ 0.4663 & -0.6725 & 1.6937 \\ -0.3567 & 0.3382 & 1.4783 \\ 0.4714 & 0.2851 & 1.6974 \end{bmatrix} \text{ m/s} \quad (5.9)$$

where the indices identify the corners where the bullets are. The norm of the four velocities is  $\bar{v} = [1.5579 \ 1.7773 \ 1.8811 \ 1.7846]^T$  m/s. As they differ from each other, the satellite

will be subject to not only forces but also torques causing it to rotate while moving backwards. The controller has to be able to compensate both disturbance in order to keep the stability of the spacecraft.

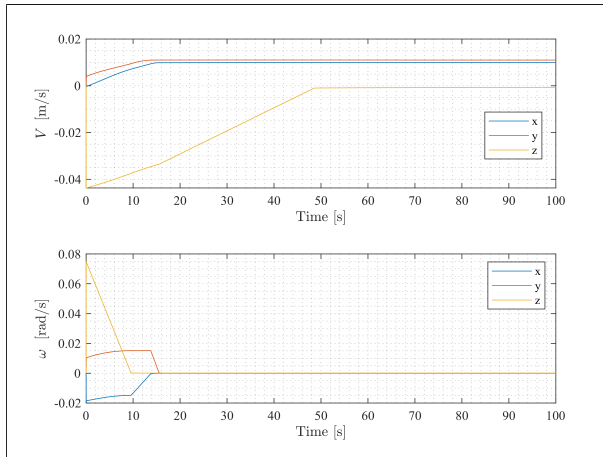


Figure 5.8: Linear velocities of the spacecraft with respect to the body frame, and angular velocity in the case with four thrusters and experimental data.

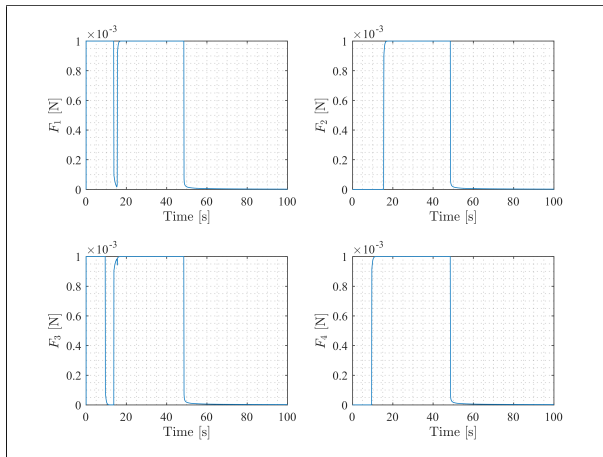


Figure 5.9: Thrusters actuation levels in the case with four thrusters and experimental data.

As we can see in Fig. 5.8 the satellite's rotation is significantly reduced while it is braked by the thrusters. Figure 5.10 shows that the displacement in the  $z$ -axis is up to  $-1.5$  m, however, as Fig. 5.9 shows, the controller reduces the actuation effort at around 50 s as the velocity is approaching zero. We can also see the changes in the actuators between 10 s and 20 s which coincide with the moments when the rotation rates of different axes approach zero. The attitude change is at most  $20^\circ$  and might be further reduced in

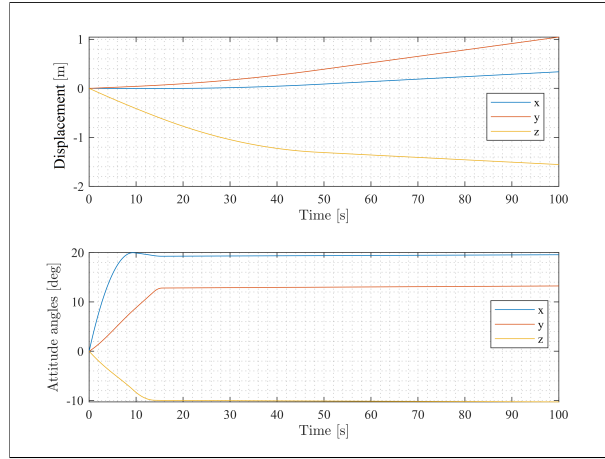


Figure 5.10: Linear and angular displacement during the deployment of the net in the case with four thrusters and experimental data.

5

a post-capture phase using the attitude control system.

#### 5.4.5. CASE 3: 6 THRUSTERS WITH EXPERIMENTAL DATA AND FAILURE

The thrusters for this case are positioned in a similar manner as suggested in [Pena et al. \(2000\)](#) which allows for the failure of one thruster. The failure considered is of zero response type meaning that the thruster cannot provide any thrust. In this case, the satellite is stabilized even when one thruster stops working during the operation. For this configuration, the matrices defining the position and orientation of the thrusters are:

$$[\vec{d}_1 \vec{d}_2 \vec{d}_3 \vec{d}_4 \vec{d}_5 \vec{d}_6] = \begin{bmatrix} 0.0400 & -0.0454 & 0.0500 & 0.0100 & -0.0454 & -0.0100 \\ -0.0500 & -0.0100 & -0.0400 & 0.0454 & 0.0100 & 0.0454 \\ -0.0500 & -0.0500 & -0.0500 & -0.0500 & -0.0500 & -0.0500 \end{bmatrix} \text{ m}$$

$$[\vec{e}_1 \vec{e}_2 \vec{e}_3 \vec{e}_4 \vec{e}_5 \vec{e}_6] = \begin{bmatrix} 0.0990 & 0.0000 & -0.0990 & -0.1961 & 0.0000 & 0.1961 \\ 0.0990 & 0.1961 & -0.0990 & 0.0000 & -0.1961 & 0.0000 \\ 0.9901 & 0.9806 & 0.9901 & 0.9806 & 0.9806 & 0.9806 \end{bmatrix}$$

$$\mathbf{A} = \begin{bmatrix} -0.0446 & 0.0000 & -0.0446 & 0.0446 & 0.0000 & 0.0446 \\ -0.0446 & 0.0446 & -0.0446 & 0.0000 & 0.0446 & 0.0000 \\ 0.0089 & -0.0089 & -0.0089 & 0.0089 & 0.0089 & -0.0089 \end{bmatrix} \text{ m} \quad (5.10)$$

$$\mathbf{B} = \begin{bmatrix} 0.0400 & -0.0454 & 0.0500 & 0.0100 & -0.0454 & -0.0100 \\ -0.0500 & -0.0100 & -0.0400 & 0.0454 & 0.0100 & 0.0454 \\ -0.0500 & -0.0500 & -0.0500 & -0.0500 & -0.0500 & -0.0500 \end{bmatrix} \quad (5.11)$$

which represent six thrusters pointing mainly in the  $z$ -axis direction and tilted to an angle either in  $x$  or  $y$ -axis or both as shown in Fig. 5.11.

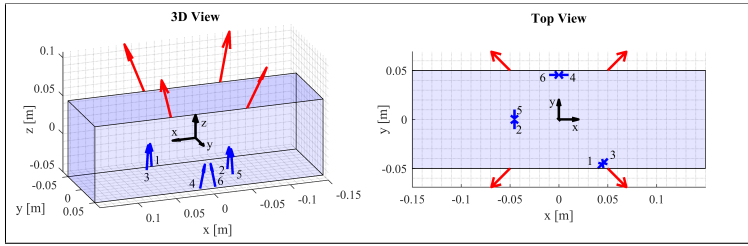


Figure 5.11: Views of the satellite model indicating the position and orientation of the six thrusters (blue arrows) and the bullets (red arrows).

The failure is injected in time  $t = 3\text{s}$  as highlighted in Fig. 5.13. As we can see, thruster 1 is suddenly at  $0\text{ mN}$  and the other thrusters are rearranged in order to compensate the failure of the former.

Figure 5.12 shows that the controller is able to compensate the disturbances in rotation and linear velocity even after a failure occurs during the operation.

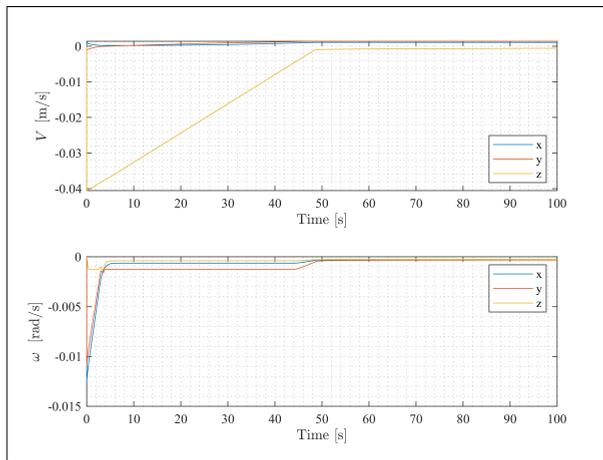


Figure 5.12: Linear velocities of the spacecraft with respect to the body frame, and angular velocity in the case with six thrusters and experimental data.

#### 5.4.6. MONTE CARLO ANALYSIS

The input parameters for the simulation of the controller that have been analyzed are summarized in Table 5.2. The velocities of the bullets were randomly generated with uniform distribution in the range  $1.44\text{--}2.16\text{ m/s}$  (corresponding to  $1.80 \pm 20\% \text{m/s}$ ). The integration time corresponds to the time to fire the bullets and it is used to calculate the force of each bullet. The failure instant is the moment when one of the thrusters fails. The output of the simulation is the time necessary to stabilize the rotation ( $t_a$ ) and to

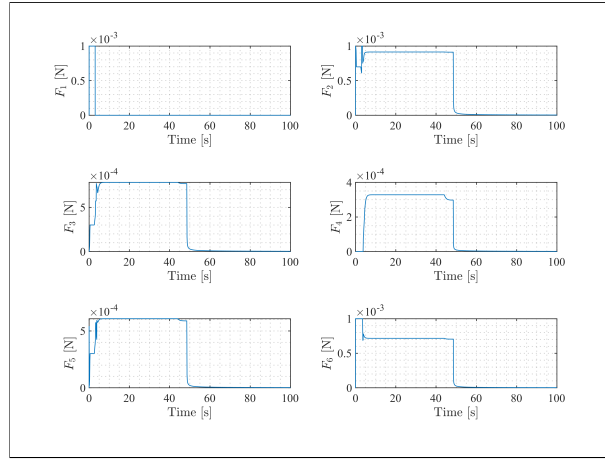


Figure 5.13: Thrusters actuation levels in the case with six thrusters and experimental data.

5

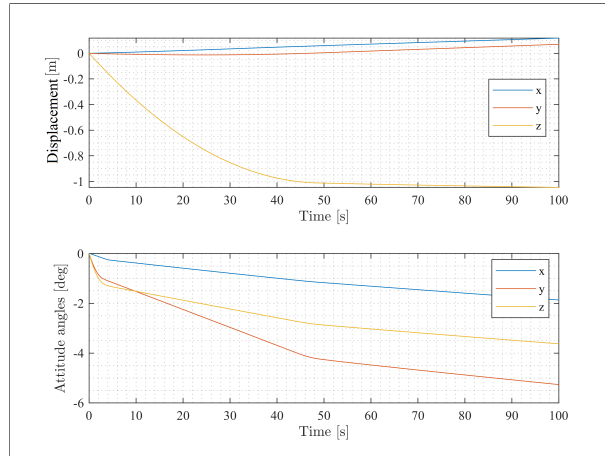


Figure 5.14: Linear and angular displacement during the deployment of the net in the case with six thrusters and experimental data.

stabilize the linear velocity ( $t_l$ ). The threshold for stabilization is considered when the total angular velocity is below  $0.01$   $^\circ/s$  and the linear velocity in the  $z$  direction is below  $0.003$   $m/s$ . These values were empirically selected based on the actuation levels of the thrusters and when they all approach zero. These two times have been measured for cases 2 and 3. A total of 15 runs were performed for the first case and 120 for the second. In all runs the controller was able to compensate the angular and linear disturbances generated by the bullets.

The average time and corresponding standard deviation to stabilize the spacecraft using the four thrusters configuration was  $t_l = 48.6 \pm 4.1$  s and  $t_a = 7.9 \pm 2.3$  s. With the six thrusters configuration average time and standard deviation was  $t_l = 48.7 \pm 11.9$  s and

$$t_a = 3.8 \pm 2.5 \text{ s.}$$

The results of the analysis of variance (ANOVA)<sup>1</sup> are used to assess the influence of the parameters of the Monte Carlo simulation in the time necessary to stabilize the spacecraft, i.e., correct the angular and linear disturbances.

In case 1, with four thrusters, the  $p$ -value 0.0477 corresponding to the bullets' velocities indicates that the response for different velocities is significantly different, i.e., the bullets' velocities significantly affect the time to stabilize the spacecraft. However, the integration time for the calculation of the momentum produced by the bullets, with corresponding  $p$ -value = 0.5738, does not interfere in the correction of the angular disturbance. Therefore in the simulations with six thrusters the minimum value for this parameter, i.e. 0.01 s, was used.

In case 2, with six thrusters, we can see similar results, the  $p$ -value corresponding to the velocities of the bullets is zero, meaning that the velocities influence the time to stabilize the satellite. The time in which the failure occurs also significantly affects the time to correct the disturbances in the linear momentum but not the angular momentum as the corresponding  $p$ -values indicate, 0.5784 and 0.0000 respectively. The specific thruster that fails, with corresponding  $p$ -values 0.0359 and 0.2332 for angular and linear disturbances, does not significantly influence the time to correct the linear disturbance, however, it does affect the time to correct the angular disturbance.

Table 5.2: Input parameters used in the Monte Carlo simulation.

4 Thrusters			
Parameter	Type	Count	Note
Bullets velocities	Random	5	1.44–2.16 m/s
Integration time	Fixed	3	{0.01s, 0.05s, 0.1s}
Total runs		15	
6 Thrusters			
Parameter	Type	Count	Note
Bullets velocities	Random	5	1.44–2.16 m/s
Integration time	Fixed	1	Selected 0.01 s
Failure instant	Fixed	4	{0s, 3s, 10s, 50s}
Failure thruster	Fixed	6	{1, 2, 3, 4, 5, 6}
Total runs		120	

## 5.5. CONCLUSIONS

This chapter presented a hybrid approach combining a fuzzy controller with a traditional control allocation method (redistributed pseudo inverse) applied to the problem of controlling a spacecraft during a space debris removal mission. The control allocation method is used to generate the rules used in the inference system of the fuzzy controller that calculates the necessary control effort for each of the actuators, in this case

<sup>1</sup>The interested reader can refer to [Rumsey \(2009\)](#) for a detailed explanation of the analysis of variance and  $p$ -value.

Vaporizing Liquid Microthrusters. The hybrid system has successfully performed in different simulation scenarios considering two configurations with four and six thrusters on-board the CubeSat including a scenario with experimental data and failure in one thruster. In the latter case the controller was able to control the satellite even after one of the thrusters failed.

A Monte Carlo simulation was performed to assess the influence of different input parameters in the time necessary to stabilize the spacecraft. In the case with four thrusters, the average time to stabilize the rotation and the translation over 15 runs were  $t_l = 48.6 \pm 4.1$  s and  $t_a = 7.9 \pm 2.3$  s respectively. In the case with six thrusters the times were  $t_l = 48.7 \pm 11.9$  s and  $t_a = 3.8 \pm 2.5$  s over 120 runs.

The proposed approach is expected to reduce the computational effort during the operation of the controller as it reduces the calculations to simple rules used by the fuzzy controller. The more complex calculations involving matrix inversions can be restricted to an offline phase or to when a failure occurs. Although this is also possible to be done with traditional approaches the presented approach is specially useful in cases with many actuators.

The controller shown in this chapter has been tested in the situation of rejecting the disturbances generated when firing the bullets of the net, however, it can be also applied to other stages of the mission that still need a robust approach due to high levels of uncertainties as, for example, the rendezvous phase when the chaser satellite needs to approach the target or during the post-capture phase to control the spacecraft with the connecting tether attached to the target during de-orbiting.

# 6

## APPLICATIONS AND SCENARIOS OF VLM SYSTEMS

*Ik kan surfen  
Mits de juiste baai  
Mits de juiste tijd, maanstand, windrichting en de onderstroom*  
From the song *Surfen* by Typhoon <sup>1</sup>

*This chapter presents an analysis on the possible applications of VLM systems. The analysis considers realistic scenarios of nano- and pico-satellites and the specific characteristics of a VLM system with one or more thrusters. An example orbit is selected to further analyse the details concerning possible missions.*

---

<sup>1</sup>*I can surf, provided the right bay, provided the right time, moon phase, wind direction, and underflow*

Table 6.1: Parameters considered in the analysis.

Type	Propulsion system				Spacecraft		
	Num. thrusters	Mass %	Nozzle throat (1e-9 m <sup>2</sup> )	Nozzle exit (1e-8 m <sup>2</sup> )	Area ratio	Mass (kg)	Max. Power (W)
3U CubeSat	[1, 4, 6]	10–50 %	1–5	5	10–50	4	6
3U PocketQube	[1, 4, 6]	10–50 %	1–5	5	10–50	0.5	1.5

## 6.1. INTRODUCTION

Chapter 2 discussed some general applications of micropropulsion systems for CubeSats and PocketQubes. In this Chapter, the focus is on the application of VLM systems and on the specific implementation of such systems.

## 6.2. SPACECRAFT AND MICROPROPULSION REQUIREMENTS

In order to assess the different scenarios and missions where VLM systems can be used, we need to define the basic requirements for the spacecraft and for the micropropulsion system. These requirements are used to calculate the performance of the system and to evaluate what can be achieved with such scenario.

Two types of spacecraft are considered: a 3U CubeSat with a propulsion system that has either one, four or six thrusters and a 3U PocketQube with the same number of thrusters. Table 6.1 shows the values considered for the propulsion systems and the spacecraft.

The available power for the micropropulsion system is the limiting factor of VLM systems. It constraints the maximum mass flow rate that the system can use which limits other factors such as pressure and thrust. The range 0.5–10 W can be defined as the operating range of VLMs (see Chapter 2) in terms of power then we can calculate the maximum mass of water that can be vaporized per unit time, i.e. the maximum mass flow rate, as follows:

$$\dot{m}_{\max} = \frac{P}{\Delta H(p)} \quad (6.1)$$

where  $P$  is the available power,  $\Delta H(p)$  in J/kg is the enthalpy of vaporization of water (assuming an initial temperature of 20 °C and without further heating the fluid after it is vaporized) and it is a function of the pressure  $p$ . This maximum mass flow rate is shared by all the thrusters on-board of the spacecraft and is used to calculate the maximum pressure using 4.5 which is re-written here for convenience with the pressure as a function of the mass flow rate and  $N$  being the number of thrusters:

$$p_{\max} = \left( \frac{\frac{\dot{m}_{\max}}{N}}{A_t \sqrt{\frac{\gamma}{R_s} \left( \frac{2}{\gamma+1} \right)^{\frac{\gamma+1}{\gamma-1}}}} - \beta_1 \right) \frac{1}{\alpha_1} \quad (6.2)$$

The following algorithm is used to calculate the values of thrust and specific impulse for a given power and nozzle geometry:

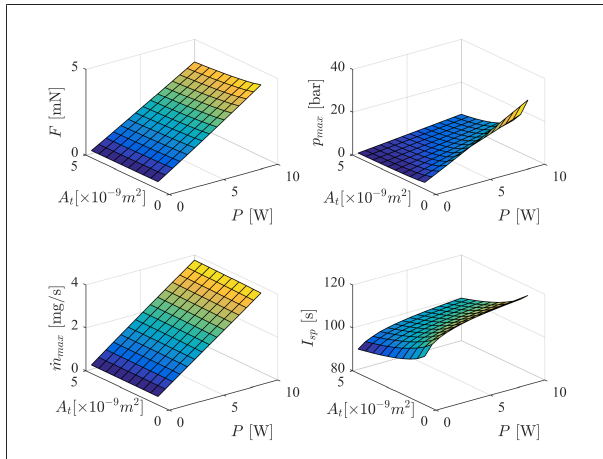


Figure 6.1: Performance parameters of the thruster as functions of the power and the nozzle area ratio.

```

k = 1
p_max[k] = initial value
for P = 0.5W to 10W do
  while p_1[k + 1] = p_max[k] do
    Calculate enthalpy for p_max[k]
    Calculate m_dot_max using (6.1)
    Calculate p_max[k + 1] using (6.2)
    k = k + 1
  end while
  Calculate F and I_sp using (2.1) and (2.7)
end for

```

The same algorithm is used to calculate thrust and specific impulse with all the nozzle geometries shown in Table 6.1. The initial values for the pressure were set to 5 bar, however, the algorithm converges with any value close to the expected ones.

Figure 6.1 shows the values of thrust, specific impulse, maximum mass flow rate and maximum pressure as functions of the power and the nozzle area ratio considering only one thruster.

Figure 6.2 shows the values of thrust and specific impulse for two area ratios. In case of multiple thrusters, the specific impulse is the same for all thrusters whereas the thrust shown is the sum of the thrust of all thrusters considering that they are all pointing in the same direction. It is interesting to note the “turning point” in the curves of specific impulse at around 2.8 W for an area ratio of 50 and at around 1.6 W for an area ratio of 10. This point is where the curves cross each other indicating that there is a change in the number of thrusters for which the best results are achieved. This turning point suggests that a configuration with less thrusters is preferred when the available power is below that point as in the case of PocketQubes.

Figure 6.3 shows the maximum values of pressure (a), mass flow rate (b), thrust (c), and specific impulse (d) as a function of the power for two different nozzles with area

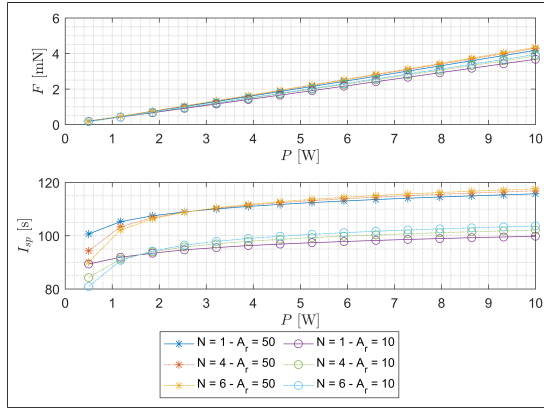


Figure 6.2: Thrust and specific impulse as functions of the power for configurations with one, four, or six thrusters and two area ratios.

ratios equal to  $A_r = 10$  and  $A_r = 50$ . We can clearly see the linear correlation between thrust and power which is characteristic to resistojets. The maximum pressure is significantly reduced with the reduction of the area ratio.

These values might be used to set the performance requirements of the micropropulsion system. In the case of a 3U PocketQube, considering the maximum power of 1.5 W, the maximum thrust that can be produced is about 0.6 mN and maximum specific impulse of 106.4 s with a nozzle with an area ratio of  $A_r = 50$ . In the case of a 3U CubeSat with maximum power of 6 W, the maximum thrust is then 2.6 mN and the maximum specific impulse 114.5 s. These maximum values can be increased by increasing the area ratio of the nozzle.

Some applications might be considered and defining other important limits to the micropropulsion system such as number of thrusters and mass percentage of propellant. These values are used in the following section to draw some conclusions regarding applications of VLM systems. Note, however, that these values can be higher or lower depending on the specific mission for which the spacecraft is designed.

### 6.3. VLM APPLICATIONS

The velocity change of the spacecraft is calculated as follows:

$$\Delta v = I_{sp} g_0 \ln \frac{m_0}{m_f} \quad (6.3)$$

where  $m_0$  is the total (wet) mass of the spacecraft and  $m_f$  is the final (dry) mass after using all of the propellant. The propellant mass percentage  $\zeta$  is defined as:

$$\zeta = \frac{m_p}{m_0} \quad (6.4)$$

where  $m_p = m_0 - m_f$  is the mass of propellant. Table 6.2 shows the performance in term of thrust, specific impulse, and  $\Delta v$  for different configurations of the propulsion system

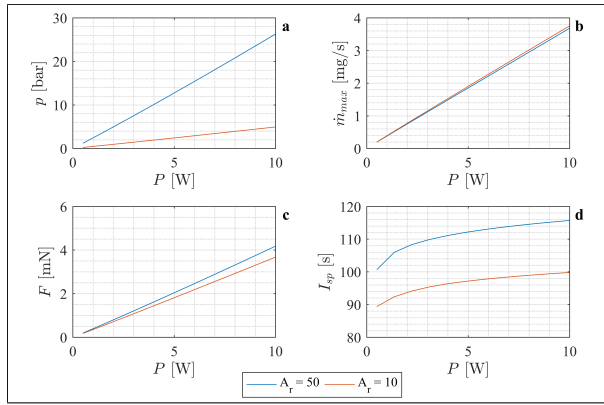


Figure 6.3: Values of pressure (a), mass flow rate (b), thrust (c) and specific impulse (d) as a function of the power considering only one thruster and different nozzle area ratios. The exit area is the same in both configurations as given in Table 6.1.

Table 6.2: Comparison of performance values for different configurations of thrusters. The velocity change is given for mass percentages of 1 %, 10 % and 20 % (see (6.4)). The thrust is the total amount of thrust generated regardless of the orientation of the thrusters. The nozzle exit area is the same in all cases.

Num. Thrusters	3U CubeSat						3U PocketQube					
	1		4		6		1		4		6	
Area ratio	10	50	10	50	10	50	10	50	10	50	10	50
Total thrust [mN]	2.18	2.46	2.28	2.53	2.33	2.56	0.53	0.59	0.54	0.60	0.54	0.60
$I_{sp}$ [s]	97.8	113.1	99.9	113.9	101.2	114.5	92.7	106.4	92.7	105.3	92.7	104.5
$\Delta v$ [m/s] - $\zeta = 1\%$	9.6	11.1	9.8	11.2	10.0	11.3	9.1	10.5	9.1	10.4	9.1	10.3
$\Delta v$ [m/s] - $\zeta = 10\%$	101.1	116.8	103.2	117.7	104.5	118.3	95.7	110.0	95.7	108.8	95.7	107.9
$\Delta v$ [m/s] - $\zeta = 20\%$	214.1	247.5	218.5	249.3	221.4	250.5	202.8	232.9	202.8	230.3	202.8	228.6

for CubeSats and PocketQubes. As we can see, the total amount of thrust generated increases with a larger number of thrusters in both cases (CubeSats and PocketQubes), however, efficiency in terms of specific impulse and velocity change decreases in the PocketQube case.

Considering as an example a near-circular orbit with around 550 km of altitude, and the performance values given in Table 6.2, the following applications are considered <sup>2</sup>:

- **Orbital maneuvering:** This can be either a change in altitude or in orbital plane. The former requires a velocity change of 0.55 m/s per kilometer (Wertz et al., 2011) whereas the latter requires 132.38 m/s per degree. Considering the maximum and minimum values of  $\Delta v$  given in Table 6.2, the altitude change can be approximately in the range from 17 km to 423 km in the PocketQube Case and from 18 km to 455 km in the CubeSat case. Similarly, orbital plane change maneuvers might be in the range from 0.1° to 1.8° for PocketQubes and from 0.1° to 1.9° for CubeSats. It is important to note that these values are calculated considering an ideal scenario in which losses and efficiency are optimal.

<sup>2</sup>The data presented here can be found in Table I-1 of Wertz et al. (2011).

- Drag compensation: This depends strongly on the geometry and attitude of the spacecraft. The velocity change required to keep the altitude for one year might be more than 19 m/s per year depending on the mass and surface area of the spacecraft (Wertz et al., 2011). At this rate, the lifetime of the spacecraft could be extended around 6 months to more than 13 years. As usually miniaturized spacecraft have a short operational lifetime and are required to decay naturally after 25 years, a configuration with low propellant mass percentage can be used to keep the altitude for a certain time and then used to deorbit the spacecraft.
- Deorbiting: A velocity change of around 143 m/s is required to deorbit a spacecraft from an altitude of 550 km (Wertz et al., 2011). Thus, any configuration of the propulsion system with more than 10% of propellant mass is sufficient to deorbit the spacecraft. A higher percentage might be used in order to perform other maneuvers, such as drag compensation, and make sure that there is enough propellant for the deorbit phase.
- Formation flying: A wide range of possibilities depending on the specific mission can be considered for this kind of applications. Velocity changes ranging from a couple of meters per second to tens of meters per second might be necessary for a single maneuver or for the entire mission. Therefore, depending on the type, frequency, and length of the maneuvers a different configuration of the micropropulsion system must be selected.
- Space debris removal: this requires different types of maneuvers (Shan et al., 2018) in different phases. In the initial phase, an approaching maneuver similar to those used in formation flying is necessary to reach the target. Then a series corrections might be necessary during the capturing phase which depends on the capturing method used (e.g. deployable net or a harpoon) and requires velocity changes of at most around 10 m/s (see Chapter 5). The last phase is similar to deorbiting a single spacecraft but with a larger mass (mass of chaser and target). Velocity changes required during the last phase are around 143 m/s. A propellant mass fraction of around 24% would be required for a CubeSat to deorbit another spacecraft of the same size, and around 25% for a PocketQube.

#### 6.4. CONCLUDING REMARKS

This chapter analyzed the possible applications of VLM systems considering CubeSats and PocketQubes. A more general analysis was done assuming a standard orbit in order to assess the different scenarios with different goals. VLM systems might be used in a variety of applications which require different amounts of propellant.

The space debris removal case is very interesting as VLM systems are suitable for all the phases of the mission (approaching, capturing, and deorbiting). However, a large propellant mass percentage is required for the last phase in order to deorbit debris heavier than the spacecraft. Another possible solution, would be increasing the available power, e.g. with larger solar panels or pre-charged batteries, which increases the maximum achievable specific impulse thus increasing the velocity change.

# 7

## CONCLUSIONS

*When you're dead, you're dead.  
But you're not quite so dead  
if you contribute something – Jim Lahey*

From the series *Trailer Park Boys*

*This chapter concludes this thesis presenting a summary of the research presented, the most relevant research findings related to the research questions proposed in the beginning, the innovations of this thesis regarding research and engineering, and a brief outlook on the research and development of MEMS micropropulsion systems.*

## 7.1. SUMMARY

As presented in the Introduction, the objective of this thesis was to investigate concepts of thrust control in micropropulsion systems that use green propellants. The research presented here embraced general aspects of MEMS micropropulsion systems comparing the different types of devices that have been developed over the past few decades. MEMS micropropulsion systems might be used in a wide range of applications and they are specially interesting for miniaturized spacecraft in the nano- and pico-satellite classes, however, they might very well be applied to larger spacecraft or even smaller ones. The advance of MEMS manufacturing techniques might push even further the boundaries of such systems to include extremely miniaturized satellites that are just a small board or even a single chip.

A focus was given to Vaporizing Liquid Microthruster (VLM) systems that use water as the propellant. The aim was to develop modeling and control concepts for VLM systems in order to allow the execution of position and attitude maneuvers by the spacecraft. The major effort was put on the thrust control problem, i.e. controlling the magnitude and direction of the thrust-vector, considering the constraints imposed by the size of the satellites.

Part of the research presented in this thesis was focused on the characterization and modeling of VLM systems. The characterization is intended to support the modeling by introducing experimental data to some parts of the models. A complete model of a VLM system was developed using theoretical and experimental relations. This model mathematically represents the system containing all components of a VLM system. All the empirical parts of the model are sufficient for the type of analysis presented here. However, a more accurate model might be achieved by using theoretical relations empirically adjusted to the conditions of the test. For example, a discharge coefficient can be applied to the nozzle model in order to account for losses. A more sophisticated vaporization model might be used to replace the volumetric change of the gas, however, as most of the models found in literature are empirical relations derived for specific cases depending on the two-phase flow regime, a more detailed empirical model for the flow inside a resistojet might be a good choice. The model of the volume of gas inside the thruster might be improved with the use of a more sophisticated test setup including high speed cameras to capture the motion of the fluid more precisely. Future work will be focused on the extension of the modeling to address the points mentioned and to improve the accuracy of the model by considering a broader range of operational parameters. The comparison of the model with experimental data might further improve the validation of model which has been done only numerically. A more advanced application scenario will also be considered in order to investigate other characteristics of thrust control in micropropulsion applications.

Another part of the research focused on the development of approaches for the control of VLM systems. Control schemes were developed for the individual control of the thrusters and for the control allocation in cases where multiple thrusters are used. The individual control is achieved by regulating flow of propellant inside the system which allows the fine regulation of performance parameters such as thrust and specific impulse. The fine regulation of thrust is an important feature of micropropulsion systems that allows the use of the thrusters in accurate attitude control maneuvers or to compensate

small unbalances generated while using multiple thrusters at the same time. Controlling a set of redundant thrusters is done using a control allocation approach that allocates the necessary actuation efforts to the appropriate thrusters. This thesis presented a novel control allocation approach combining an artificial intelligence method (Fuzzy control) with a traditional control allocation algorithm. The proposed approach reduces the computational effort of the control system which might significantly decrease the demand on the on-board computer. Future work will be focused on the control with variable angle thrusters that might improve the robustness of the controller and flexibility of the spacecraft.

The last part of the research concerned the possible applications of VLM systems. A scenario considering a common polar orbit has been used in order to assess the capabilities of a VLM system on-board of a CubeSat or a PocketQube. The versatility of VLM systems is significantly increased by controlling the thrust therefore allowing it to execute short and small maneuvers, such as rejecting disturbances, as well as long and large maneuvers, such as orbital maneuvers. The specific case of disturbance rejection while deploying a net in a space debris removal mission was presented demonstrating the effectiveness of the control allocation method developed and the individual controllers. A more complex scenario including the approaching and de-orbiting phases of the mission will be studied in order to get more insights into the problem.

## 7.2. RESEARCH FINDINGS

As presented in Chapter 1, some research questions were formulated in order to guide the research and give it an objective. In the next paragraphs, those questions are revisited in a general manner highlighting the most important findings.

**What are the aspects that bound the state-of-the-art MEMS micropropulsion systems?** As shown in Chapter 2 most of the MEMS micropropulsion systems are still under development and many of them are TRL 3 or lower. However, more advanced systems that are suitable for spacecraft in the classes nano- and pico-satellites have been identified. Cold-gas thrusters, for example, are very attractive for their simplicity and low power consumption. Some devices have already flown and demonstrated in-flight operation. As the level of development of propulsion systems for nano- and pico-satellites is in general at an early stage, each specific system lacks some particular feature that prevents it from flying in a real mission. Power consumption, for example, is one of the issues of some devices whereas for others is the safety of the propellant that brings problems. In some cases, as solid propellant microthrusters for example, the limited control in the operation is a key factor reducing the applicability of the thruster. The efficiency level of most MEMS micropropulsion systems still needs major improvements. Here, two key aspects have been identified. First the power consumption needs to be further reduced. This could be achieved, for example, by reducing thermal losses. Second, the propellant use can be optimized, for example, by reducing friction losses in the fluidic channels.

Concerning MEMS micropropulsion in general, there is room for improvements in all the types of propulsion systems assessed in Chapter 2. In some cases, only performance characteristics are available while a specific system design is lacking. The use of MEMS fabrication technologies is a great advantage in the sense that this is a very active

research field and its processes are well developed and it is very interesting for the fabrication of very small structures and channels with integrated components such as sensors and actuators. However, other components of the system, such as propellant tanks and electronic circuits, have to be produced using conventional manufacturing techniques. Regarding the specific design concerns of the VLM system used in this thesis, there are many points to improve specially in the manufacturing process of the thruster chip and interfacing with other components of the system.

**What is the best way of controlling the mass flow of a microthruster?** Mass flow rate control in VLM systems can be achieved by controlling a valve in the line between the propellant tank and the thruster. Two types of valves might be used: on-off valve or proportional valve, depending on the application and the mission requirements. A proportional valve allows the continuous regulation of the flow resulting in a more smooth operation whereas an on-off valve needs to be operated using pulse modulation in order to achieve flow rates at different levels. The pulse modulation is either in the width of the input signal (PWM) or in both width and frequency (PWPFM). Both methods produce similar results.

**How can we describe the dynamic behavior of a Vaporizing Liquid Microthruster?** The dynamics of VLM systems is a result of the coupling of the different dynamics of each component, i.e., tank, valve, and thruster, with different time constants. The tank is the slowest part of the system and behaves as a charged capacitor discharging as the propellant is used. The pressure inside the tank decreases with time affecting the pressure drop over the valve, which affect the flow rate, and reducing the maximum pressure at which the thruster can work. The tank can be considered a passive component as it does not have a control variable. The valve, used to regulate the flow, changes the rate at which the pressure in the tank decreases and directly controls the pressure inside the thruster. Therefore, the valve is an active component and the main contributor to the overall changes in the process in terms of pressure and mass flow rate. The thruster is the critical part of the system since it is required to completely vaporize the propellant to make sure that no liquid is expelled through the nozzle in which case the performance is degraded. Its control variable is the power applied to the heaters to vaporize the propellant. This power needs to be sufficient to heat up the thruster to a certain temperature and completely vaporize the propellant which is at a certain initial temperature. A percentage of the power is lost to the environment. The vaporization process is affected by several factors. Any changes in the pressure inside the thruster change the boiling point of the liquid and the enthalpy of vaporization whereas changes in the power affect the temperature of the thruster and the heat transfer to the fluid. The heat transfer to the fluid in turn affects the boiling process and the position inside the thruster chamber where boiling occurs. If boiling happens in a place close to the nozzle, some droplets might be ejected and on the contrary if occurs far from the nozzle a more complete vaporization can be guaranteed. Other important factors are the initial temperature of the thruster and the changes in the temperature caused by the flow. In the beginning of operation, the thruster is cooled down by the liquid affecting the vaporization process. Therefore, controlling the temperature of the thruster is crucial to a smooth operation of VLM systems. The target temperature of the thruster has to be chosen based on the operating pressure which is at most the same as the pressure in the propellant tank.

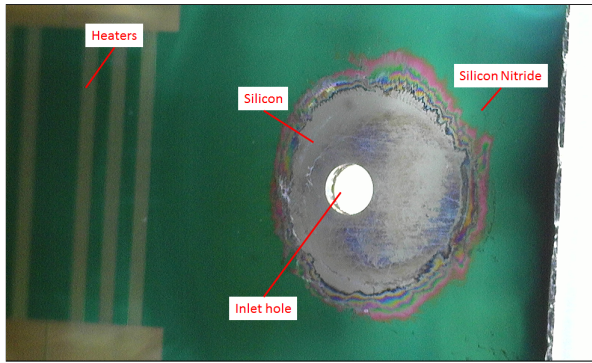


Figure 7.1: Picture of a device showing the area surrounding the inlet hole where the layer of silicon nitride has been removed.

### What are the characteristics of controlling the thrust direction of microthrusters?

There are two different manners of controlling the direction of the thrust vector: one is by actively deflecting the flow in the nozzle exit either by using deflectors or by redirecting the complete nozzle. In this way, the thrust vector is adjusted to generate torques that are used to control the attitude of the spacecraft together with its position. The second is by controlling a set of thrusters that are positioned in such a way to generate torques and forces on the spacecraft's body allowing the combined attitude and position control. The main drawback of the first approach, in the context of MEMS micropropulsion systems, is in achieving a feasible and reliable design that is more advantageous either in terms of performance or applicability than using a normal thruster and relying on the attitude control system to reject disturbances. The second approach, which consists of controlling a set of thrusters, is more promising in terms of feasibility and reliability than the first one. However, it increases the overall system complexity as it adds more components (e.g. valves, fittings, etc.) and also the computational complexity increases as a control allocation algorithm is necessary.

Other important aspects encountered during the research were related to MEMS technologies and manufacturing. The fact that molybdenum (the material used in the heaters of the thrusters) oxidizes faster in the presence of water in high temperatures, as discussed in Chapter 3, poses a great threat to the operation of the thrusters as the heaters are easily damaged by droplets of water. Another interesting effect that had not been foreseen was the removal (etching) of silicon nitride (SiNx) around the inlet hole. A thin layer of silicon nitride is deposited on top of the silicon substrate to insulate the heaters. This layer of silicon nitride was partially or totally removed around the inlet hole of some devices that went through an extensive testing campaign. This effect might be related to the subcritical water boiling around the hole. The device shown in Fig. 7.1 has gone through several hours of testing and the layer of silicon nitride has been removed almost completely. Although this is not expected to influence the performance of the thruster, this effect needs to be better understood.

### 7.3. INNOVATIONS

Several innovations have been introduced in this thesis and this section aims at summarizing the main points.

In Chapter 2, an extensive review of MEMS micropropulsion systems was presented. Reviews focused only on MEMS devices are very few despite the importance of such technologies. A complexity parameter was introduced to compare the suitability of the different devices taking into account the philosophy behind the development of CubeSats and PocketQubes which requires simplicity. Furthermore, the devices were analyzed based on the data in scientific literature, rather than coarse analytical considerations. This makes the analysis much more realistic and reliable.

In Chapter 3, an extensive test campaign was performed with the thrusters with the aim of characterizing the devices. A large dataset was built including videos and multiple types of tests. Regarding the design, several improvements with respect to the original design have been proposed, developed and successfully tested. A simple and robust interface has been developed for the tests. This interface provides a reliable way to integrate electrical, mechanical and fluidic parts of the thruster while including sensors and the possibility of visualizing the boiling inside the thruster chamber. This interface solved many issues in previous ideas that prevented the successful testing of thrusters and allowed the tests using water. Many software interfaces were created to allow the data acquisition for further analysis. Regarding the thruster chip, two important design choices were made: the use of metal heaters, in this case molybdenum, which are more stable in the temperature ranges needed and can achieve very high temperatures. Second is the use of a glass wafer to cover the thruster while providing a way to visualize the flow inside of it. Finally, the manufacturing process as well as the mask design have been improved to facilitate the fabrication by reducing process steps and also to reduce differences between the designed and the manufactured devices. The mask shown in Fig. 7.2 has recently been designed to overcome some of the issues faced in the previous design, for example, a protection for the heaters to avoid oxidation.

In Chapter 4, the complete model of a VLM system was presented for the first time including analytical and empirical relations and allowing the complete simulation of the system. The reduction of the nozzle model to a linear relation between mass flow rate and pressure as a result of the saturation conditions inside the chamber helped to achieve a simple model that represents the behavior of the system. The characterization of volumetric changes inside the chamber opens the path to further analyze the vaporization and characterization of the heat transfer coefficient.

In Chapter 5, a novel hybrid control allocation approach was developed for cases in which redundant thrusters are used to either propel the spacecraft or to control its attitude providing velocity changes and/or torques. This hybrid approach combining a fuzzy system with a control allocation algorithm reduces the on-board computational effort by solving the allocation problem using a set of rules instead of complex large matrices calculations.

In Chapter 6, many application scenarios have been considered for a VLM system and actual performance figures, such as thrust and specific impulse, have been calculated for a specific type of orbit and considering power constraints that limit the operation of the thrusters. The case of active space debris removal has been deeply analyzed

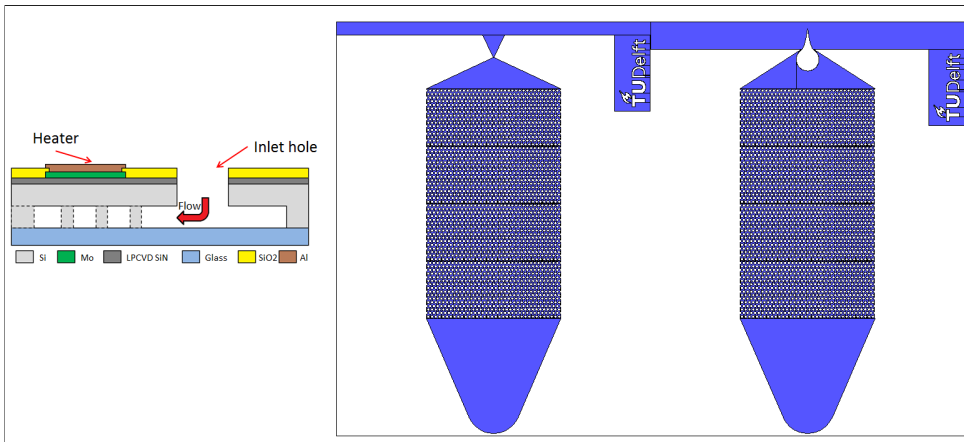


Figure 7.2: Details of the newly designed mask. Two types of nozzles can be produced and have the same area ratio. Only four heaters are used instead of seven as in the current design and the heaters are protected by a layer of silicon dioxide and an aluminum pad for wire bonding.

and the results show that a VLM system is a very interesting choice as it can be used in all the different phases of the mission.

## 7.4. FUTURE RESEARCH

Regarding the design of the VLM chip, future research might be focused on the optimization of the channels in the heating chamber in order to improve the heat transfer and reduce power consumption. The integration of other MEMS components, such as valves and sensors, as well as electronics for the power control of the heaters is currently under investigation. This will represent a large step towards a fully integrated device. The interface for the thrusters also need improvement to reduce size and increase thermal insulation. The manufacturing process might be improved by reducing the number of steps, specially in the etching of the cavities, and by including a protection in the heaters to reduce problems with oxidation at high temperatures. The measurements of initial resistance and temperature need to be improved in favor of the electrical characterization as well as the measurement of resistance during operation to reduce noise in the estimated temperature. In this case, the calibration process could be done by testing the heaters in a hot plate in vacuum. This is expected to increase the precision of the measurements since a more homogeneous distribution of temperature can be achieved. To this purpose, a new interface is needed to facilitate these measurements. More tests in vacuum are needed to reduce the heat losses and also using a thrust measurement bench to measure the actual thrust and specific impulse of the devices.

An interesting alternative to the current design of the system is a self pressuring system that uses the pressure generated by the boiling to push the propellant in the feeding lines. The concept is shown in Fig. 7.3. In this concept, the liquid part is pushed by the vapor generated during the boiling. A fixed geometry passive check-valve with a high diodicity can be used to make sure that the flow goes only in one direction. The boiling

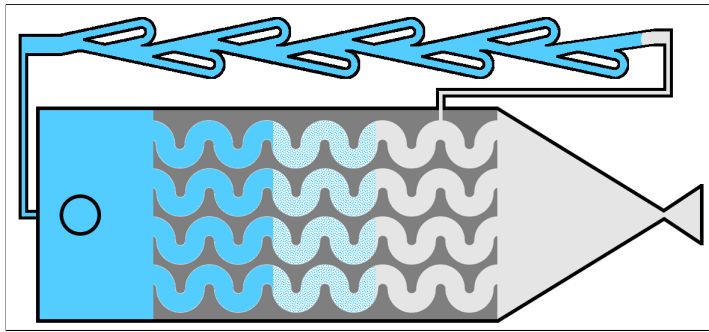


Figure 7.3: Design concept of a self-pressuring thruster. A fixed geometry passive check-valve prevents the flow from going backwards in the channels. The propellant can be stored in the narrow channels between the valve and the thruster.

produces high-frequency pressure changes that together with the “diode like” structure of the channels produces a one-way flow. The nozzle exit has to be closed before the operation to avoid losses of propellant. This concept might be very useful to extremely miniaturized systems as it reduces the number of components needed.

In the context of modeling and control, future work might be focused on the extension of the modeling to improve the accuracy of the model by considering a broader range of operational parameters. The comparison of the model with more experimental data might further improve the validation of model which has been done only numerically.

A more advanced application scenario might also be considered in order to investigate other characteristics of thrust control in micropropulsion applications. The control with variable angle thrusters might be an interesting approach that might improve the robustness of the controller and flexibility of the spacecraft.

Regarding the manufacturing, other fabrication methods have to be analyzed considering costs of fabrication since MEMS can be highly expensive in a small-scale production which is the case for nano- and pico-satellites. In addition, other unconventional approaches of propellantless propulsion (solar sail for example) or the ejection of solid particles can be interesting alternatives and have to be further investigated. The integration of electronics for the power control of the heaters is very promising. This will represent a large step towards a fully integrated device.

Finally, regarding applications, the pre- and post-capture phases in a active space-debris removal mission might be investigated as well as the effects of measurement noise and biases in the sensor and actuators. Other applications and scenarios should also be considered in order further assess the applicability of VLM systems.

## REFERENCES

- Ahmed, Z., Gimelshein, S. F., and Ketsdever, A. D. (2006). Numerical analysis of free-molecule microresistorjet performance. *Journal of Propulsion and Power*, 22(4):749–756.
- Anz-Meador, P. (2018). Orbital debris quarterly news. In *NASA Orbital Debris Program Office, Volume 22, Issue 2, May*.
- Arestie, S., Lightsey, E. G., and Hudson, B. (2012). Development of a modular, cold gas propulsion system for small satellite applications. *Journal of Small Satellites*, 1(2):63–74.
- Berg, S. P. and Rovey, J. L. (2016). Decomposition of a double salt ionic liquid monopropellant on heated metallic surfaces. In *52nd AIAA/SAE/ASEE Joint Propulsion Conference*.
- Berg, S. P., Rovey, J. L., Prince, B. D., Miller, S. W., and Bemish, R. J. (2015). Electro spray of an energetic ionic liquid monopropellant for multi-mode micropropulsion applications. In *51st AIAA/SAE/ASEE Joint Propulsion Conference*.
- Bidabadi, M., Heidari, M., and Rahbari, A. (2010). A novel analytical model of a MEMS vaporizing liquid micro thruster. In *2010 The 2nd International Conference on Computer and Automation Engineering (ICCAE)*, volume 5, pages 321–325.
- Blanco, A. and Roy, S. (2013). Numerical simulation of a free molecular electro jet (fmej) for in-space propulsion. In *51st AIAA Aerospace Sciences Meeting including the New Horizons Forum and Aerospace Exposition*, page 208.
- Briand, D., Guillot, L., Bley, U., Danninger, S., Gass, V., De Rooij, N., and Ammotec, R. (2008). Digital micro-thrusters with simplified architecture and reliable ignition and combustion. In *Proceedings Power MEMS 2008 (Sendai, Japan, 9-12 November 2008)*, pages 157–160.
- Cai, Y., Liu, Z., and Shi, Z. (2017). Effects of dimensional size and surface roughness on service performance for a micro laval nozzle. *Journal of Micromechanics and Microengineering*, 27(5):055001.
- Candini, G. P., Piergentili, F., and Santoni, F. (2012). Miniaturized attitude control system for nanosatellites. *Acta Astronautica*, 81(1):325 – 334.
- Carroll, D., Cardin, J., Burton, R., Benavides, G., Hejmanowski, N., Woodruff, C., Bassett, K., King, D., Laystrom-Woodard, J., Richardson, L., Day, C., Hageman, K., and Bhandari, R. (2015). Propulsion unit for cubesats (puc). In *Proceedings of the 62nd JANNAF Propulsion Meet. (7th Spacecr. Propulsion)*.

- Cen, J. and Xu, J. (2010). Performance evaluation and flow visualization of a MEMS based vaporizing liquid micro-thruster. *Acta Astronautica*, 67(3–4):468 – 482.
- Cervone, A., Mancas, A., and Zandbergen, B. (2015). Conceptual design of a low-pressure micro-resistojet based on a sublimating solid propellant. *Acta Astronautica*, 108(0):30 – 39.
- Cervone, A., Pallichadath, V., Silva, M. A. C., Guerrieri, D., Silvestrini, S., Mestry, S., Maxence, D., Zandbergen, B., and Zeijl, H. V. (2017). MEMS water micro-resistojets for cubesats and pocketqubes. In *MPCS 2017 - International Workshop on Micropropulsion and CubeSats*.
- Cervone, A., Zandbergen, B., Guerrieri, D. C., Silva, M. A. C., Krusharev, I., and van Zeijl, H. (2016). Green micro-resistojet research at delft university of technology: new options for cubesat propulsion. *CEAS Space Journal*, Online first:1–15.
- Chaalane, A., Chemam, R., Houabes, M., Yahiaoui, R., Metatla, A., Ouari, B., Metatla, N., Mahi, D., Dkhissi, A., and Esteve, D. (2015). A MEMS-based solid propellant microthruster array for space and military applications. In *Journal of Physics: Conference Series*, volume 660, page 012137. IOP Publishing.
- Chang, Y., Yuan, R., Tan, X., and Yi, J. (2016). Observer-based adaptive sliding mode control and fuzzy allocation for aero and reaction jets' missile. *Proceedings of the Institution of Mechanical Engineers, Part I: Journal of Systems and Control Engineering*, 230(6):498–511.
- Cheah, K. and Chin, J. (2011). Performance improvement on MEMS micropropulsion system through a novel two-depth micronozzle design. *Acta Astronautica*, 69(1–2):59 – 70.
- Cheah, K. H. and Low, K.-S. (2015). Fabrication and performance evaluation of a high temperature co-fired ceramic vaporizing liquid microthruster. *Journal of Micromechanics and Microengineering*, 25(1):015013.
- Chen, C.-C., Kan, H.-C., Lee, M.-H., and Liu, C.-W. (2012). Computational study on vaporizing liquid micro-thruster. In *Microsystems, Packaging, Assembly and Circuits Technology Conference (IMPACT), 2012 7th International*, pages 68–71.
- Chen, C.-C., Liu, C.-W., Kan, H.-C., Hu, L.-H., Chang, G.-S., Cheng, M.-C., and Dai, B.-T. (2010). Simulation and experiment research on vaporizing liquid micro-thruster. *Sensors and Actuators A: Physical*, 157(1):140 – 149.
- Cheung, N. C., Lim, K. W., and Rahman, M. F. (1993). Modelling a linear and limited travel solenoid. In *Industrial Electronics, Control, and Instrumentation, 1993. Proceedings of the IECON '93., International Conference on*, pages 1567–1572 vol.3.
- Ciaralli, S., Coletti, M., and Gabriel, S. (2015). Performance and lifetime testing of a pulsed plasma thruster for cubesat applications. *Aerospace Science and Technology*, 47:291 – 298.

- Ciaralli, S., Coletti, M., and Gabriel, S. (2016). Results of the qualification test campaign of a pulsed plasma thruster for cubesat propulsion (pptcup). *Acta Astronautica*, 121:314 – 322.
- Coletti, M., Ciaralli, S., and Gabriel, S. (2015). Ppt development for nanosatellite applications: Experimental results. *IEEE Transactions on Plasma Science*, 43(1):218–225.
- Coletti, M., Guarducci, E., and Gabriel, S. (2011). A micro {PPT} for cubesat application: Design and preliminary experimental results. *Acta Astronautica*, 69(3–4):200 – 208.
- Coletti, M., Marques, R., and Gabriel, S. (2009). Design of a two-stage ppt for cubesat application. In *Proceedings of the 31st International Electric Propulsion Conference, Electric Rocket Propulsion Society, Ann Arbor, USA*.
- Courtney, D., Dandavino, S., and Shea, H. (2015). Performance and applications of ionic electrospray micro-propulsion prototypes. In *AIAA SPACE 2015 Conference and Exposition*, page 4672.
- Courtney, D., Dandavino, S., and Shea, H. (2016). Comparing direct and indirect thrust measurements from passively fed ionic electrospray thrusters. *Journal of Propulsion and Power*, 32:392–407.
- CubeSatShop.com (2017). Cubesatshop. In *www.cubesatshop.com*. Accessed in 22/03/2017.
- Dandavino, S., Ataman, C., Ryan, C., Chakraborty, S., Courtney, D., Stark, J., and Shea, H. (2014). Microfabricated electrospray emitter arrays with integrated extractor and accelerator electrodes for the propulsion of small spacecraft. *Journal of Micromechanics and Microengineering*, 24(7):075011(13pp).
- DDBST, G. (2018). Dortmund data bank. In *www.ddbst.com*. Accessed in 08/11/2018.
- Fan, Y., Meng, X., Yang, X., Liu, K., and Zhu, J. (2011). Control allocation for a v/stol aircraft based on robust fuzzy control. *Science China Information Sciences*, 54(6):1321–1326.
- Gad-el Hak, M. (2001). *The MEMS handbook*. CRC press.
- Gohardani, A. S., Stanojev, J., Demairé, A., Anflo, K., Persson, M., Wingborg, N., and Nilsson, C. (2014). Green space propulsion: Opportunities and prospects. *Progress in Aerospace Sciences*, 71:128 – 149.
- Guerrieri, D. C., Cervone, A., and Gill, E. (2016a). Analysis of nonisothermal rarefied gas flow in diverging microchannels for low-pressure microresistojets. *Journal of Heat Transfer*, 138 (11)(11):112403–112403–11.
- Guerrieri, D. C., Silva, M. A. C., Cervone, A., and Gill, E. (2017). Selection and characterization of green propellants for micro-resistojets. *ASME Journal of Heat Transfer*, 139(10):9.

- Guerrieri, D. C., Silva, M. A. C., Zandbergen, B., and Cervone, A. (2016b). Heater chip with different microchannels geometries for a low pressure free molecular micro-resistojet. In *Space Propulsion 2016*.
- Haris, P. and Ramesh, T. (2014). Numerical simulation of superheated steam flow in a micronozzle. In *Applied Mechanics and Materials*, volume 592, pages 1677–1681. Trans Tech Publ.
- Hejmanowski, N. J., Woodruff, C., Burton, R., and Carroll, D. L. (2015). Cubesat high impulse propulsion system (chips). In *Proceedings of the 62nd JANNAF Propulsion Meet. (7th Spacecr. Propulsion)*.
- Hitt, D. L., Zakrzewski, C. M., and Thomas, M. A. (2001). MEMS-based satellite micro-propulsion via catalyzed hydrogen peroxide decomposition. *Smart Materials and Structures*, 10(6):1163.
- Imken, T., Stevenson, T., and Lightsey, G. (2015). Design and testing of a cold gas thruster for an interplanetary cubesat mission. *Journal of Small Satellites*, 4:371–386.
- Ivanov, M., Markelov, G., Ketsdever, A., and Wadsworth, D. (1999). Numerical study of cold gas micronozzle flows. In *37th Aerospace Sciences Meeting and Exhibit*, Aerospace Sciences Meetings. American Institute of Aeronautics and Astronautics.
- Janson, S., Helvajian, H., and Breuer, K. (1999). MEMS, microengineering and aerospace systems. In *30th Fluid Dynamics Conference*, page 3802.
- Johansen, T. A. and Fossen, T. I. (2013). Control allocation—a survey. *Automatica*, 49(5):1087 – 1103.
- Karayiannis, T. and Mahmoud, M. (2017). Flow boiling in microchannels: Fundamentals and applications. *Applied Thermal Engineering*, 115:1372 – 1397.
- Karthikeyan, K., Chou, S., Khoong, L., Tan, Y., Lu, C., and Yang, W. (2012). Low temperature co-fired ceramic vaporizing liquid microthruster for microspacecraft applications. *Applied Energy*, 97(0):577 – 583. Energy Solutions for a Sustainable World - Proceedings of the Third International Conference on Applied Energy, May 16-18, 2011 - Perugia, Italy.
- Kelso, T. S. (2018). Satcat boxscore. In <http://www.celestrak.com/satcat/boxscore.asp>, accessed in July 2018.
- Ketsdever, A., Lee, R., and Lilly, T. (2005). Performance testing of a microfabricated propulsion system for nanosatellite applications. *Journal of Micromechanics and Microengineering*, 15(12):2254–2263.
- Ketsdever, A. D., Wadsworth, D. C., Vargo, S., and Muntz, E. P. (1998). The free molecule micro-resistojet: An interesting alternative to nozzle expansion. In *34th AIAA/ASME/SAE/ASEE Joint Propulsion Conference and Exhibit*.

- Khaji, Z., Klintberg, L., Barbade, D., Palmer, K., and Thornell, G. (2016). Alumina-based monopropellant microthruster with integrated heater, catalytic bed and temperature sensors. In *Journal of Physics: Conference Series*, volume 757.
- Kisaki, S., Muraoka, R., Huanjun, C., Tanaka, M., Tahara, H., and Wakizono, T. (2013). Research and development of electrothermal pulsed plasma thruster systems onboard Osaka Institute of Technology PROITERES nano-satellites. In *33rd International Electric Propulsion Conference*.
- Kohler, J., Bejhed, J., Kratz, H., Bruhn, F., Lindberg, U., Hjort, K., and Stenmark, L. (2002). A hybrid cold gas microthruster system for spacecraft. *Sensors and Actuators A: Physical*, 97–98(0):587 – 598. Selected papers from Eurosensors {XV}.
- Koninck, D., Briand, D., Guillot, L., Bley, U., Gass, V., and de Rooij, N. (2011). Ignition and combustion behavior in solid propellant microsystems using joule-effect igniters. *Journal of Microelectromechanical Systems*, 20(6):1259–1268.
- Korczyk, P. M., Cybulski, O., Makulska, S., and Garstecki, P. (2011). Effects of unsteadiness of the rates of flow on the dynamics of formation of droplets in microfluidic systems. *Lab Chip*, 11:173–175.
- Krejci, D., Mier-Hicks, E., Thomas, R., Haag, T., and Lozano, P. (2017). Emission Characteristics of Passively Fed Electrospray Microthrusters with Propellant Reservoirs. *Journal of Spacecraft and Rockets*, Online first:1–12.
- Krpoun, R. and Shea, H. (2009). Integrated out-of-plane nanoelectrospray thruster arrays for spacecraft propulsion. *Journal of Micromechanics and Microengineering*, 19(4):045019(10pp).
- Kundu, P., Bhattacharyya, T., and Das, S. (2014). Electro-thermal analysis of an embedded boron diffused microheater for thruster applications. *Microsystem Technologies*, 20(1):23–33.
- Kundu, P., Bhattacharyya, T. K., and Das, S. (2012). Design, fabrication and performance evaluation of a vaporizing liquid microthruster. *Journal of Micromechanics and Microengineering*, 22(2):025016.
- Kundu, P., Sinha, A., Bhattacharyya, T., and Das, S. (2013).  $MnO_2$  nanowire embedded hydrogen peroxide monopropellant MEMS thruster. *Journal of Microelectromechanical Systems*, 22(2):406–417.
- Kvell, U., Puusepp, M., Kaminski, E., Past, J.-E., Palmer, K., Grönland, T.-A., and Noorma, M. (2014). Nanosatellite orbit control using MEMS cold gas thrusters. *Proceedings of the Estonian Academy of Sciences*, 63(2S):279–285.
- La Torre, F., Kenjeres, S., Kleijn, C. R., and Moerel, J.-L. P. (2010). Effects of wavy surface roughness on the performance of micronozzles. *Journal of Propulsion and Power*, 26(4):655–662.

- Lee, J., Kim, K., and Kwon, S. (2010). Design, fabrication, and testing of MEMS solid propellant thruster array chip on glass wafer. *Sensors and Actuators A: Physical*, 157(1):126 – 134.
- Lee, J. and Kim, T. (2013). MEMS solid propellant thruster array with micro membrane igniter. *Sensors and Actuators A: Physical*, 190:52 – 60.
- Lee, R. H., Lilly, T. C., Killingsworth, M. D., Duncan, J. A., Ketsdever, A. D., and Bauer, A. (2008). Free-molecule-microresistojet performance using water propellant for nanosatellite applications. *Journal of Spacecraft and Rockets*, 45(2):264–269.
- Leiter, H., Lotz, B., Feili, D., Tartz, M., Neumann, H., and Di Cara, D. M. (2009). Design development and test of the rit-ák mini ion engine system. In *31st International Electric Propulsion Conference*.
- Lewis, D. H., Janson, S. W., Cohen, R. B., and Antonsson, E. K. (2000). Digital micro-propulsion. *Sensors and Actuators A: Physical*, 80(2):143 – 154.
- Liu, X., Li, T., Li, Z., Ma, H., and Fang, S. (2015). Design, fabrication and test of a solid propellant microthruster array by conventional precision machining. *Sensors and Actuators A: Physical*, 236:214 – 227.
- London, A., Epstein, A., and Kerrebrock, J. (2001). High-pressure bipropellant micro-rocket engine. *Journal of Propulsion and Power*, 17(4):780–787.
- Louwerse, M. C. (2009). *Cold Gas Micro Propulsion, Ph.D. Thesis, University of Twente, Enschede, The Netherlands*. Phd thesis, University of Twente.
- Maurya, D., Das, S., and Lahiri, S. (2005a). An analytical model of a silicon MEMS vaporizing liquid microthruster and some experimental studies. *Sensors and Actuators A: Physical*, 122(1):159 – 166.
- Maurya, D. K., Das, S., and Lahiri, S. K. (2005b). Silicon MEMS vaporizing liquid microthruster with internal microheater. *Journal of Micromechanics and Microengineering*, 15(5):966.
- Mele, L., Santagata, E., Iervolino, E., Mihailovic, M., Rossi, T., Tran, A., Schellevis, H., Creemer, J., and Sarro, P. (2012). A molybdenum MEMS microhotplate for high-temperature operation. *Sensors and Actuators A: Physical*, 188:173 – 180.
- Mihailovic, M., Mathew, T., Creemer, J., Zandbergen, B., and Sarro, P. (2011). MEMS silicon-based resistojet micro-thruster for attitude control of nano-satellites. In *Solid-State Sensors, Actuators and Microsystems Conference (TRANSDUCERS), 2011 16th International*, pages 262–265.
- Mitterauer, J. (2004). Micropropulsion for small spacecraft: a new challenge for field effect electric propulsion and microstructured liquid metal ion sources. *Surface and Interface Analysis*, 36(5-6):380–386.

- Miyakawa, N., Legner, W., Ziemann, T., Telitschkin, D., Fecht, H.-J., and Friedberger, A. (2012). MEMS-based microthruster with integrated platinum thin film resistance temperature detector (rtd), heater meander and thermal insulation for operation up to 1,000°C. *Microsystem Technologies*, 18(7-8):1077–1087.
- Mukerjee, E., Wallace, A., Yan, K., Howard, D., Smith, R., and Collins, S. (2000). Vaporizing liquid microthruster. *Sensors and Actuators A: Physical*, 83(1–3):231 – 236.
- Oh, H.-U., Kim, T.-G., Han, S.-H., and Lee, J. (2017). Verification of MEMS fabrication process for the application of MEMS solid propellant thruster arrays in space through launch and on-orbit environment tests. *Acta Astronautica*, 131:28 – 35.
- Oppenheimer, M. W. (2011). Control allocation. In Levine, W. S., editor, *The Control Handbook - Control Systems Applications*, chapter 8. Taylor and Francis Group, LLC. Second Edition.
- Palmer, K., Nguyen, H., and Thornell, G. (2013). Fabrication and evaluation of a free molecule micro-resistojet with thick silicon dioxide insulation and suspension. *Journal of Micromechanics and Microengineering*, 23(6):065006.
- Passino, K. M., Yurkovich, S., and Reinfrank, M. (1998). *Fuzzy control*. Addison-Wesley Longman. First Edition.
- Passino, K. W. (2011). Intelligent control. In Levine, W. S., editor, *The Control Handbook - Control Systems Advanced Methods*, chapter 54. Taylor and Francis Group, LLC. Second Edition.
- Patel, K. D., Bartsch, M. S., McCrink, M. H., Olsen, J. S., Mosier, B. P., and Crocker, R. W. (2008). Electrokinetic pumping of liquid propellants for small satellite microthruster applications. *Sensors and Actuators B: Chemical*, 132(2):461 – 470.
- Pena, R. S. S., Alonso, R., and Anigstein, P. A. (2000). Robust optimal solution to the attitude/force control problem. *IEEE Transactions on Aerospace and Electronic Systems*, 36(3):784–792.
- Polzin, K. A., Markusic, T. E., Stanojev, B. J., Dehoyos, A., Raitses, Y., Smirnov, A., and Fisch, N. J. (2007). Performance of a low-power cylindrical hall thruster. *Journal of Propulsion and Power*, 23(4):886–888.
- Poyck, R., Krusharev, I., Bellini, Q., Zandbergen, B., and Cervone, A. (2014). A water-fed micro-resistojet for the delfi formation flying mission. In *International Astronautical Congress*.
- Rangsten, P., Palmer, K., Bejhed, J., Zaldivar Salaverri, A., Jonsson, K., and Grönland, T.-A. (2013). Closed-loop thrust control in a MEMS-based micro propulsion module for cubesats. In *Small Satellite Conference*.
- Rossi, C., Conto, T. D., Estève, D., and Larangot, B. (2001). Design, fabrication and modelling of MEMS-based microthrusters for space application. *Smart Materials and Structures*, 10(6):1156.

- Rossi, C., Larangot, B., Lagrange, D., and Chaalane, A. (2005). Final characterizations of MEMS-based pyrotechnical microthrusters. *Sensors and Actuators A: Physical*, 121(2):508 – 514.
- Rossi, C., Orioux, S., Larangot, B., Conto, T. D., and Estève, D. (2002). Design, fabrication and modeling of solid propellant microrocket-application to micropropulsion. *Sensors and Actuators A: Physical*, 99(1–2):125 – 133.
- Ru, C., Wang, F., Xu, J., Dai, J., Shen, Y., Ye, Y., Zhu, P., and Shen, R. (2016). Superior performance of a MEMS-based solid propellant microthruster (spm) array with nanothermites. *Microsystem Technologies*, Online first:1–14.
- Rudenauer, F. G. (2007). Field emission devices for space applications. *Surface and Interface Analysis*, 39(2-3):116–122.
- Rumsey, D. (2009). *Statistics II for Dummies*. Wiley.
- Sathiyathan, K., Lee, R., Chesser, H., Dubois, C., Stowe, R., Farinaccio, R., and Ringuette, S. (2011). Solid propellant microthruster design for nanosatellite applications. *Journal of Propulsion and Power*, 27:1288–1294.
- Seo, D., Lee, J., and Kwon, S. (2012). The development of the micro-solid propellant thruster array with improved repeatability. *Journal of Micromechanics and Microengineering*, 22(9):094004.
- Servidia, P. A. and Pena, R. S. (2005). Spacecraft thruster control allocation problems. *IEEE Transactions on Automatic Control*, 50(2):245–249.
- Servidia, P. A. and Pena, R. S. S. (2002). Thruster design for position/attitude control of spacecraft. *IEEE Transactions on Aerospace and Electronic Systems*, 38(4):1172–1180.
- Shan, M., Guo, J., and Gill, E. (2016). Review and comparison of active space debris capturing and removal methods. *Progress in Aerospace Sciences*, 80:18 – 32.
- Shan, M., Guo, J., and Gill, E. (2017a). Contact dynamic models of space debris capturing using a net. *Acta Astronautica*.
- Shan, M., Guo, J., and Gill, E. (2017b). Deployment dynamics of tethered-net for space debris removal. *Acta Astronautica*, 132:293 – 302.
- Shan, M., Guo, J., and Gill, E. (2018). Contact dynamics on net capturing of tumbling space debris. *Journal of Guidance, Control, and Dynamics*, online first:1–10.
- Shan, M., Guo, J., Gill, E., and Gołębowski, W. (2017c). Validation of space net deployment modeling methods using parabolic flight experiment. *Journal of Guidance, Control, and Dynamics*, 40:3319–3327.
- Shoji, S. and Esashi, M. (1994). Microflow devices and systems. *Journal of Micromechanics and Microengineering*, 4(4):157.

- Silva, M. A. C. (2017). Vaporizing liquid microthruster. In <https://youtu.be/LawZseC6ffQ>. Accessed in: 01-03-2017.
- Silva, M. A. C., Guerrieri, D. C., and Cervone, A. (2015). Investigation of innovative thrust-vector control techniques for micro propulsion systems. In *IAF 66th International Astronautical Congress*, page 8.
- Silva, M. A. C., Guerrieri, D. C., Cervone, A., and Gill, E. (2018). A review of MEMS micro-propulsion technologies for cubesats and pocketqubes. *Acta Astronautica*, 143:234 – 243.
- Silva, M. A. C., Guerrieri, D. C., van Zeijl, H., Cervone, A., and Gill, E. (2017). Vaporizing liquid microthrusters with integrated heaters and temperature measurement. *Sensors and Actuators A: Physical*, 265:261 – 274.
- Silvestrini, S. (2017). Closed-loop thrust magnitude control system for nano- and pico-satellite applications. Master's thesis, Faculty of Aerospace Engineering - TU Delft.
- Smirnov, A., Raitses, Y., and Fisch, N. (2002). Performance studies of miniaturized cylindrical and annular hall thrusters. In *38th AIAA/ASME/SAE/ASEE Joint Propulsion Conference and Exhibit, Indianapolis, IN*.
- Stenmark, L. and Eriksson, A. (2002). Cold gas micro thrusters. In *NanoTech 2002 - "At the Edge of Revolution"*, NanoTech Conferences. American Institute of Aeronautics and Astronautics.
- Stevenson, T. and Lightsey, G. (2016). Design and characterization of a 3d-printed attitude control thruster for an interplanetary 6u cubesat. In *30th Annual AIAA/USU Conference on Small Satellites*.
- Sutton, G. P. and Biblarz, O. (2010). *Rocket propulsion elements*. John Wiley & Sons, 8th edition.
- Szelecka, A., Kurzyna, J., Daniłko, D., and Barral, S. (2015). Liquid micro pulsed plasma thruster. *Nukleonika*, 60(2):257–261.
- Tajmar, M., Genovese, A., and Steiger, W. (2004). Indium field emission electric propulsion microthruster experimental characterization. *Journal of Propulsion and Power*, 20(2):211–218.
- Tanaka, M., Kisaki, S., Ikeda, T., and Tahara, H. (2012). Research and development of pulsed plasma thruster systems for nano-satellites at osaka institute of technology. In *Vehicle Power and Propulsion Conference (VPPC), 2012 IEEE*, pages 517–522.
- Taylor, G. (1964). Disintegration of water drops in an electric field. *Proceedings of the Royal Society of London A: Mathematical, Physical and Engineering Sciences*, 280(1382):383–397.
- Thome, J. R. (2004). Boiling in microchannels: a review of experiment and theory. *International Journal of Heat and Fluid Flow*, 25(2):128 – 139.

- Tohid, S. and Sedigh, A. K. (2013). Fault tolerant fuzzy control allocation for overactuated systems. In *2013 13th Iranian Conference on Fuzzy Systems (IFSC)*, pages 1–5.
- Tsay, M., Frongillo, J., and Zwahlen, J. (2016a). Maturation of iodine fueled bit-3 rf ion thruster and rf neutralizer. In *52nd AIAA/SAE/ASEE Joint Propulsion Conference, AIAA Propulsion and Energy Forum*.
- Tsay, M., Zwahlen, J., Lafko, D., Feng, C., and Robin, M. (2016b). Complete em system development for busek's 1u cubesat green propulsion module. In *52nd AIAA/SAE/ASEE Joint Propulsion Conference, AIAA Propulsion and Energy Forum*.
- Wertz, J. R., Everett, D. F., and Puschell, J. J. (2011). *Space mission engineering: the new SMAD*. Microcosm Press.
- Wie, B. and Barba, P. M. (1985). Quaternion feedback for spacecraft large angle maneuvers. *Journal of Guidance, Control, and Dynamics*, 8(3):360–365.
- Wu, M.-H. and Lin, P.-S. (2010). Design, fabrication and characterization of a low-temperature co-fired ceramic gaseous bi-propellant microthruster. *Journal of Micromechanics and Microengineering*, 20(8):085026.
- Wu, X., Dong, P., Li, Z., Li, S., Liu, Q., Xu, C., and Wan, H. (2009). Design, fabrication and characterization of a solid propellant micro-thruster. In *2009 4th IEEE International Conference on Nano/Micro Engineered and Molecular Systems*, pages 476–479.
- Xiong, J., Zhou, Z., Sun, D., and Ye, X. (2005). Development of a MEMS based colloid thruster with sandwich structure. *Sensors and Actuators A: Physical*, 117(1):168 – 172.
- Ye, X., Tang, F., Ding, H., and Zhou, Z. (2001). Study of a vaporizing water micro-thruster. *Sensors and Actuators A: Physical*, 89(1–2):159 – 165.
- Zeng, W., Jacobi, I., Beck, D. J., Li, S., and Stone, H. A. (2015a). Characterization of syringe-pump-driven induced pressure fluctuations in elastic microchannels. *Lab Chip*, 15:1110–1115.
- Zeng, W., Jacobi, I., Li, S., and Stone, H. A. (2015b). Variation in polydispersity in pump- and pressure-driven micro-droplet generators. *Journal of Micromechanics and Microengineering*, 25(11):115015.
- Zhang, K., Chou, S., Ang, S., and Tang, X. (2005). A MEMS-based solid propellant microthruster with au/ti igniter. *Sensors and Actuators A: Physical*, 122(1):113 – 123.
- Zhang, K., Chou, S. K., and Ang, S. (2007). Investigation on the ignition of a MEMS solid propellant microthruster before propellant combustion. *Journal of Micromechanics and Microengineering*, 17:322–332.
- Zolghadri, A. (2018). The challenge of advanced model-based fdir for real-world flight-critical applications. *Engineering Applications of Artificial Intelligence*, 68:249 – 259.

# ACKNOWLEDGEMENTS

I am lucky, lucky for being born in a place where I could enjoy freedom to pursue my goals, lucky for being born to parents that valued education more than anything, lucky for meeting all the right people in the right times, and lucky for always having the health and strength to carry on.

“Um dia a gente chega e no outro vai embora”<sup>1</sup> So many people contributed and helped me to get to here that listing all of their names would require a separate book. I want to thank all of you for being part of this in one way or another.

I want to thank my dad Salvador, my mom Edi Marli, my brother Anselmo and my sister Edisa for your unconditional support.

My girlfriend Carina, thank you for being with me and supporting me through these years.

All the friends I made during this journey, thank you so much for all the good and bad times we shared. Fernanda, Zoé, Yuxin, Mao, Sebastian, Sebastian, Tatiana, Samiksha, Stephanie, Ramon, Tiago, Fabrício, Bianca, Stefan, Ehsan, Mahboubeh, Roberto, Saullo, Haiyang, thank you everyone. Elbard, thank you so much for helping me with Dutch and all the drinks. Stefano Silvestrini, thank you very much for your help, it was a pleasure to work with you.

My fellow PhDs Linyu, Fiona, Daduí, Jing, Dennis, Zixuan, Minghe, Johan, Adolfo, Victor, Mario, Stefano, Lorenzo, and Prem, thank you all and good luck with your ongoing projects.

A special thank you to the SpE and EKL staff, in particular Vidhya, Barry, Kevin, Henk, Silvana, Silvana, and Sevet.

Finally, I want to thank my supervisors Angelo and Eberhard for their support. My extended family and friends in Brazil, thank you all.

Thank you everyone, I love you all!

---

<sup>1</sup>“One day we come the other we go” from the song *Tocando em Frente* by Almir Sater and Renato Teixeira.



# A

## THRUST DIRECTION CONTROL USING MEMS ACTUATORS

### A.1. DESCRIPTION

This Appendix presents the partial results of an initial investigation into the problem of controlling the thrust vector of micropropulsion systems. Three approaches have been analyzed and are presented in the next section. For the details, the reader can refer to the original publication [Silva et al. \(2015\)](#).

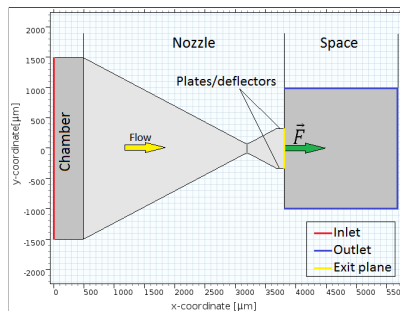


Figure A.1: Baseline geometry used in the simulations.

**Setting 1 – electric field:** in this case, an electric field is applied around the nozzle exit to steer the flow (considered charged). Figure A.2 shows the results for different voltages applied to the plates and the deflection and magnitude for different inputs.

**Settings 2 and 3 – movable deflector:** in these cases, the plates at the nozzle exit move to steer the flow. Figure A.3 shows the different angles of the thrust vector due to the rotation of the deflectors. Figure A.4 shows the results when translating the deflectors.

Parts of this Appendix have been published in [Silva et al. \(2015\)](#).

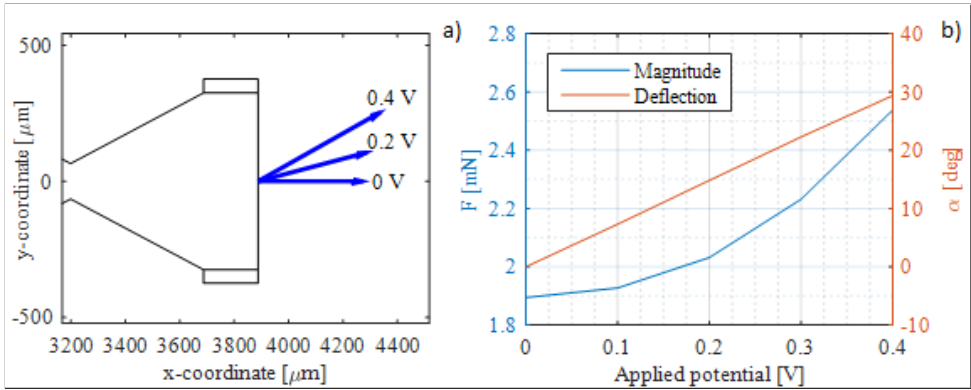


Figure A.2: a) - Thrust vector for three levels of potential applied. b) - Deflection and magnitude of the thrust vector with different levels of potential.

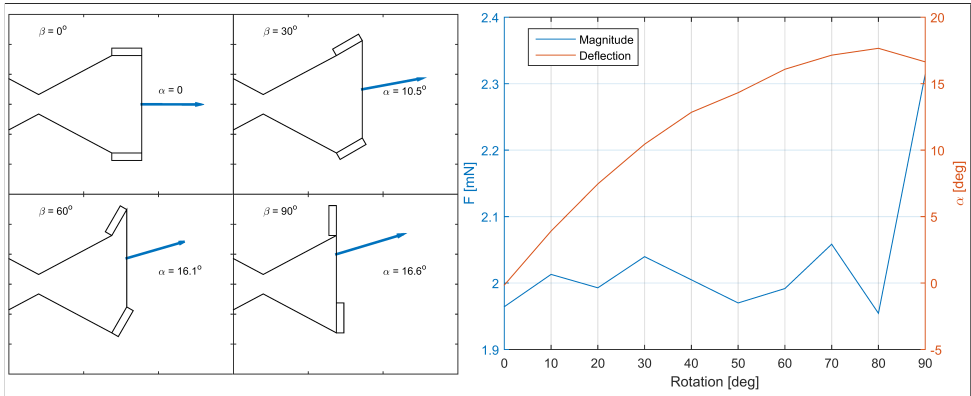


Figure A.3: a) - Sequence of images of the rotating deflector. The blue arrow represents the thrust vector. b) - Deflection and magnitude of the thrust vector for different rotation angles of the rotating deflector.

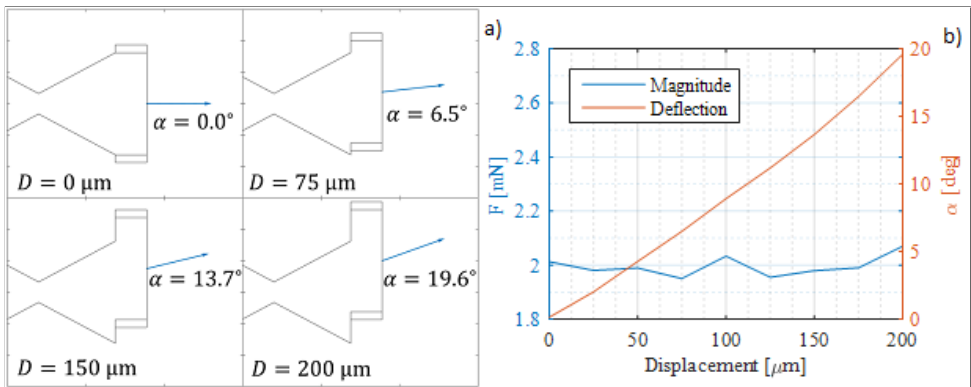


Figure A.4: a) - Sequence of images of the sliding deflector. The blue arrow represents the thrust vector. b) - Deflection and magnitude of the thrust vector for different displacements of the sliding deflector.

# LIST OF PUBLICATIONS

## *Journal Papers*

1. **Silva, M. A. C.**, Shan, M., Cervone, A., Gill, E., *Hybrid fuzzy control allocation of microthrusters for space debris removal using CubeSats*, submitted to Engineering Applications of Artificial Intelligence in 2018.
2. **Silva, M. A. C.**, Silvestrini, S., Guerrieri, D. C., Cervone, A., Gill, E., *A Comprehensive Model for Control of Vaporizing Liquid Microthrusters*, [IEEE Transactions on Control Systems Technology](#), manuscript accepted.
3. Guerrieri, D. C., **Silva, M. A. C.**, Cervone, A., Gill, E., *An Analytical Model for Characterizing the Thrust Performance of a Low-Pressure Micro-Resistojet*, [Acta Astronautica 152](#), November 2018, 719-726, 2018.
4. **Silva, M. A. C.**, Guerrieri, D. C., Cervone, A., Gill, E., *A review of MEMS micropropulsion technologies for CubeSats and PocketQubes*, [Acta Astronautica 143 \(February 2018\)](#), 234-243, 2017.
5. Guerrieri, D. C., **Silva, M. A. C.**, van Zeijl, H., Cervone, A., Gill, E., *Fabrication and Characterization of Low Pressure Micro-Resistojets with Integrated Heater and Temperature Measurement*, [Journal of Micromechanics and Microengineering](#), 14, 2017.
6. **Silva, M. A. C.**, Guerrieri, D. C., van Zeijl, H., Cervone, A., Gill, E., *Vaporizing Liquid Microthrusters with integrated heaters and temperature measurement*, [Sensors and Actuators A: Physical 265](#), Pages 261-27, 2017.
7. Guerrieri, D. C., **Silva, M. A. C.**, Cervone, A., Gill, E., *Selection and Characterization of Green Propellants for Micro-Resistojets*, [Journal of Heat Transfer 139 \(10\)](#), 102001-102010, 2, 2017.
8. Cervone, A., Zandbergen, B., Guerrieri, D. C., **Silva, M. A. C.**, Krusharev, I., van Zeijl, H., *Green micro-resistojet research at Delft University of Technology: new options for Cubesat propulsion*, [CEAS Space Journal](#), 1-15, 5, 2016.
9. **Silva, M. A. C.**, Figueiredo, H. V., Boglietti, B. G. N., Saotome, O., Villani, E., Kienitz, K. H., *A Framework for Development of Satellite Attitude Control Algorithms*, [Journal of Control, Automation and Electrical Systems](#), Volume 25, Issue 6, pp 657-667, 2014.
10. Coelho, L. S., Mariani, V. C., **Silva, M. A. C.**, Batistela, N. J., Leite, J. V., *Hysteresis parameters estimation using a modified harmony search*, [COMPEL: The International Journal for Computation and Mathematics in Electrical and Electronic Engineering](#), Vol. 32 Issue: 6, pp.1974-1985, 2013.
11. **Silva, M. A. C.**, Klein, C. E., Mariani, V. C., Coelho, L. S., *Multiobjective scatter search approach with new combination scheme applied to solve environmental/economic dispatch problem*, [Energy 53](#), 14-21, 2013.

12. **Silva, M. A. C.**, Coelho, L. S., Lebensztajn, L., *Multiobjective biogeography-based optimization based on predator-prey approach*, *IEEE Transactions on Magnetics* 48 (2), 951-954, 2012.

#### Patents

1. **Silva, M. A. C.**, Guerrieri, D. C., *Capillary tank for micropropulsion.*, Application filed in 2017.

#### Selected Conference Papers

1. Pallichadath, V., Radu, S., **Silva, M. A. C.**, Guerrieri, D. C., Cervone, A., *Integration and Miniaturization Challenges in the Design of Micro-Propulsion Systems for Picosatellite Platforms*, Space Propulsion, 2018.
2. **Silva, M. A. C.**, Guerrieri, D. C., Cervone, A., Gill, E., *Topology Optimization of Heating Chamber of Vaporizing Liquid Microthruster*, Space Propulsion, 2018.
3. Pallichadath, V., **Silva, M. A. C.**, Guerrieri, D. C., Uludag, M. S., Zandbergen, B., Cervone, A., *In-orbit micro-propulsion demonstrator for pico-satellite applications*, IAF 69th International Astronautical Congress, 2018.
4. Leveratto, S., van de Poel, M., **Silva, M. A. C.**, Guerrieri, D. C., Cervone, A., *Characterisation of a Thrust Stand to Assess Micro-Thruster Performance*, IAF 68th International Astronautical Congress 2017.
5. Pallichadath, V., Silvestrini, S., **Silva, M. A. C.**, Maxence, D., Guerrieri, D. C., Mestry, S., Soriano, T. P., Bacaro, M., van Zeijl, H., Zandbergen, B., Cervone, A., *MEMS Based Micro-Propulsion System for CubeSats and PocketQubes*, IAF 68th International Astronautical Congress, 2017.
6. Silvestrini, S., **Silva, M. A. C.**, Cervone, A., *Closed-Loop Thrust Control for Micropropulsion Systems*, IAF 68th International Astronautical Congress, 2017.
7. **Silva, M. A. C.**, Guerrieri, D. C., Cervone, A., *State space modeling of fluid flow for thrust control in mems-based micropropulsion*, Proceedings of the Space propulsion 2016.
8. Guerrieri, D. C., **Silva, M. A. C.**, Zandbergen, B., Cervone, A., *Heater Chip with Different Microchannels Geometries for a Low Pressure Free Molecular Micro-Resistojet*, Space Propulsion 2016.
9. **Silva, M. A. C.**, Guerrieri, D. C., Cervone, A., *State space modeling of fluid flow for thrust control in mems-based micropropulsion*, Space Propulsion 2016.
10. **Silva, M. A. C.**, Guerrieri, D. C., Cervone, A., *Investigation of Innovative Thrust-Vector Control Techniques for Micro Propulsion Systems*, IAF 66th International Astronautical Congress, 2015.
11. Rodrigues, L. O., **Silva, M. A. C.**, Januzi, R. B., Oliveira, N. M. F., Villani, E., *A hardware-in-the-loop simulation approach for testing control systems of small satellites*, 22nd International Congress of Mechanical Engineering (COBEM), 2013.
12. **Silva, M. A. C.**, Coelho, L. S., Freire, R. Z., *Biogeography-based Optimization approach based on Predator-Prey concepts applied to path planning of 3-DOF robot manipulator*, *IEEE 15th Conference on Emerging Technologies and Factory Automation (ETFA)*, 2010.